2

NUREG/CR-3163
SAND83-0245
R4
Printed March 1983

RELAP5 Assessment: LOFT Small-Break L3-6/L8-1

Lubomyra N. Kmetyk

Prepared by
Sandia National Laboratories
Albuquerque, New Mexico 87185 and Livermore, California 94550
for the United States Department of Energy
under Contract DE-AC04-76DP00789

Prepared for
U. S. NUCLEAR REGULATORY COMMISSION

Available from
GPO Sales Program
Division of Technical Information and Document Control
U.S. Nuclear Regulatory Commission
Washington, D.C. 20555

and

National Technical Information Service
Springfield, Virginia 22161

DISCLAIMER

NUREG/CR--3163

SAND83-0245
NUREG/CR-3163

DE83 013481

R-4

RELAP5 ASSESSMENT: LOFT SMALL-BREAK L3-6/L8-1

L. N. Kmetyk

Date Published: March 1983

Sandia National Laboratories
Albuquerque, NM 87185
Operated by
Sandia Corporation
U. S. Department of Energy

Prepared for
Analytical Models Branch
Division of Accident Evaluation
Office of Nuclear Regulatory Research
U. S. Nuclear Regulatory Commission
Washington, DC 20555
Under Memorandum of Understanding DOE 40-550-75
NRC FIN No. A-1205

DISCLAIMER

ABSTRACT

The RELAP5 independent assessment project at Sandia National Laboratories is part of an overall effort funded by the NRC to determine the ability of various systems codes to predict the detailed thermal/ hydraulic response of LWR's during accident and off-normal conditions. The RELAP5 code is being assessed at SNLA against test data from various integral and separate effects test facilities. As part of this assessment matrix, a small break transient and subsequent partial core uncovery transient performed at the LOFT facility have been analyzed.

The results show that RELAP5/MOD1 does very well on predicting the qualitative behavior for this small break experiment, although there are a number of quantitative disagreements. The primary mass inventory and core clad response during the first transient are in excellent agreement with data; however, the calculated break flow is ~25% high at early times and the overall primary side depressurization is ~18% overestimated. (The primary depressurization rate is very sensitive to small errors in break flow, decay heat, environmental heat loss and steam generator heat transfer.) The steam generator response during reverse heat transfer is not predicted accurately. After delayed pump trip, the core does experience a sustained dryout, but the predicted peak clad temperature (561 K) is lower than was observed experimentally (637 K) in the second transient, largely because the decay power then is ~20% low compared to data and because of premature core quench, but also because pump coastdown is significantly slower than was measured. A subsequent rapid core quench is observed after substantial ECC injection. Some difficulties were encountered in obtaining a good steady state which matched all the experimental initial conditions, and the transient calculations were very slow-running, precluding any sensitivity studies on the results obtained.

TABLE OF CONTENTS

LIST OF ILLUSTRATIONS

LIST OF TABLES

ACKNOWLEDGMENTS

We would like to express our appreciation for the effort of other Sandia staff involved in the RELAP5 assessment project: John Orman for modifying and maintaining RELAP5 on the Sandia computer system, Katherine McFadden for graphics support, Jan Frey for construction of the reports and Larry Buxton for many helpful discussions.

1.0 INTRODUCTION

The RELAP5 independent assessment project at Sandia National Laboratories in Albuquerque (SNLA) is part of an overall effort funded by the U. S. Nuclear Regulatory Commission (NRC) to determine the ability of various systems codes to predict the detailed thermal/hydraulic response of LWR's during accident and off-normal conditions. The RELAP5 code [1] is based on a nonhomogeneous and nonequilibrium one-dimensional model for two-phase systems, and has been under development at the Idaho National Engineering Laboratory (INEL) for an extended period, with the first version released in May 1979. The version being used for this assessment project is RELAP5/MOD1/CYCLE14, the latest publicly released version available at the time the project started. According to current INEL program plans, only error correction is projected for MOD1; major developmental efforts are being directed toward MOD2, which should be released in 1983.

The RELAP5 code is being assessed at SNLA against test data from various integral and separate effects test facilities. The assessment test matrix includes several transients performed at the Loss-of-Fluid Test (LOFT) facility [2] at INEL. One of these assigned transients was LOFT nuclear experiment L3-6/L8-1, which consisted of two parts completed sequentially. The L3-6 transient simulates a 2.5% cold leg break that, together with L3-5, is part of a pumps on/pumps off study. The pumps in L3-6 are tripped late in the transient, initiating L8-1, the first intentional partial core uncovery experiment. [3,4,5]

This report summarizes the RELAP5 analyses of the L3-6/L8-1 set of LOFT transients. The RELAP5 model used for the analyses is described in Section 2, and the calculational results are presented in Section 3. The overall conclusions and their possible relevance to future RELAP5 code development are discussed in Section 4. The appendices provide a brief description of the test facility, and an input listing for the transient, for reference.

2.0 NODALIZATION

The Loss-of-Fluid Test (LOFT) facility (shown in Figure 2.1) is located at the Idaho National Engineering Laboratory and supported by the NRC. The facility [2] is a 50 MWt pressurized water reactor (PWR) with instrumentation to measure and provide data on the thermal/hydraulic conditions during a postulated accident. The general philosophy in scaling coolant volumes and flow areas was to use the ratio of the LOFT core power (50 MWt) to a typical PWR core (3000 MWt). The experimental assembly includes five major subsystems: the reactor vessel, the intact loop (scaled to represent three operational loops), the broken loop, the blowdown suppression system and the emergency core cooling system. A more detailed description of the test facility is provided in Appendix I.

The RELAP5 nodalization we developed for LOFT test L3-6/L8-1 is shown in Figure 2.2. The intact loop is shown on the left while the broken loop is on the right; the vessel is in the middle. A complete input listing for this nodalization is given in Appendix II.

There are a total of 202 volumes, 217 junctions and 167 heat slabs in this nodalization. In the intact loop, 2 volumes are used for the two parallel primary coolant pumps and 34 volumes are used to model the piping. The steam generator contains a total of 61 volumes -- 10 for the primary side plena and U-tubes, 17 in the secondary side, 3 for the steam outflow and 31 in the feedwater train. The pressurizer and its surge line are modelled with 20 volumes, 9 of which are in the pressurizer itself and 1 which represents the spray cooling line. The broken loop contains 37 volumes. The vessel itself is modelled with 45 volumes -- 9 in the main annular downcomer, 3 in the lower plenum, 4 in the core, 4 in the upper plenum, and 25 representing various secondary and bypass flow paths. The ECCS is modelled by 3 volumes, one for the scaled HPIS flow in L3-6 and late in L8-1, another representing the unscaled HPIS flow (from both pumps A and B) early in L8-1, and the third modelling the unscaled accumulator injection early in L8-1. Heat slabs for most of the piping and major structural mass are included, as well as for the core fuel rods and steam generator U-tubes. Most of the heat slabs contain five nodes, although the fuel rods are modelled with ten.

The vessel nodalization is shown in more detail in Figure 2.3. The relative elevations of the cell boundaries are given, as are either cell flow areas or volumes. Most of the vessel flow areas were taken from a careful study of the flow area data given in Table A-5 of reference [2]. We attempted to model most

area changes explicitly (e.g., small flow area changes in the downcomer). However, we modelled a rapid series of area changes (such as in the lower core support structure) as a typical area with a geometrically-derived loss coefficient. The bypass controlling junctions are indicated (with the number corresponding to the bypass identifiers used in the description given in Appendix I). Besides the fuel rods themselves, heat slabs have been included for the outer vessel, the filler blocks, the core barrel, the upper and lower core support structures, and the upper closure plate. These heat slabs account for ~89,000 kg of vessel structural mass (as compared to ~93,000 kg of vessel structural mass shown in Table AI.8).

The steam generator nodalization is shown in Figure 2.4, with the relative elevations of the cell boundaries. All the U-tubes are lumped into a single flow path. Besides the U-tubes themselves, heat slabs representing the tube sheet, the shroud and the external wall are included in the model. Because of the limited amount of information on the steam generator secondary side in the facility description [2], we had to estimate the secondary volume distribution, given the global secondary volumes and dimensions in Tables AI.4 and AI.5. The nodalization of the feedwater train is taken almost in toto from an INEL RELAP5 LOFT nodalization [7], since again very little was available in the facility description. A few changes were made to insure consistency with the available facility description information.

All area changes and elbows are carefully modelled in the loop piping. Figure 2.5 shows the loss coefficients used in the calculations. These loss coefficients can be either user-input, as for elbow losses, or code-calculated using abrupt area change models. The user-input numbers are given first; two values are given for the forward and reverse loss coefficients respectively, if they are different. The code-calculated numbers, which are shown in parentheses, are single-phase values (in the direction of normal steady-state flow) which may change in two-phase flow. The resulting pressure drops are in good agreement with the differential pressure measurements for steady-state conditions.

The pump homologous curves used were those handed out at the LOFT/Semiscale modelling workshop [7]. Also taken from the data made available at that workshop were the nominal values of the various bypass flows and the estimated environmental heat loss magnitude and distribution. In our nodalization, we used average heat transfer coefficients for natural convection for the appropriate component sizes and temperatures [8], and assumed containment temperature to be 300 K. Heat transfer coefficients were approximated by linear functions of surface temperature.

Three functions were used -- one for all of the piping, another for the vessel cylinder and a third, artificially lowered, function for the pressurizer and steam generator walls. These yield a steady-state heat loss of ~204 kW -- 30 kW from the steam generator secondary, 104 kW from the vessel, 28 kW and 31 kW from the intact and broken loop piping respectively, and 12 kW from the pressurizer.

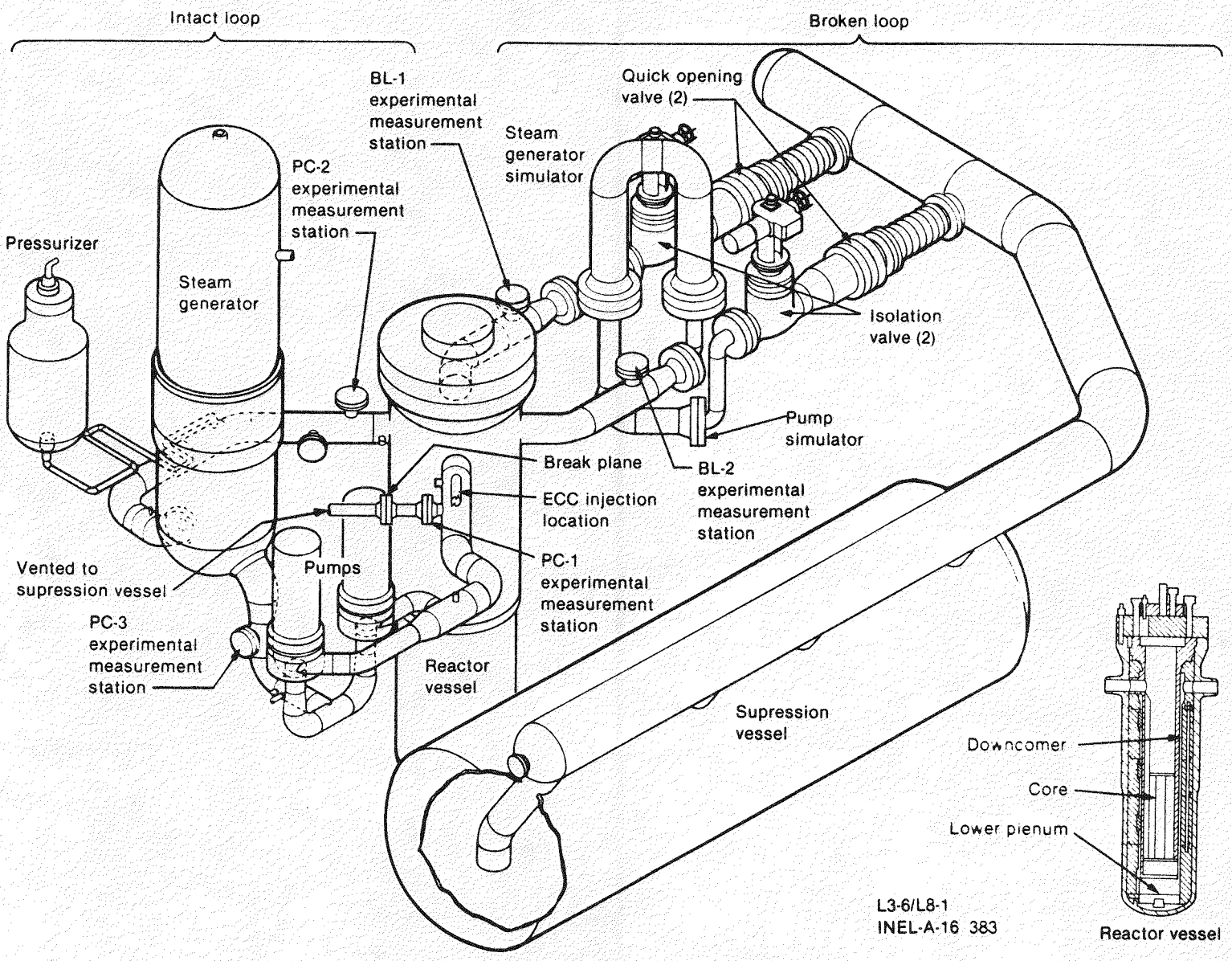

Figure 2.1 LOFT Configuration for L3-6/L8-1

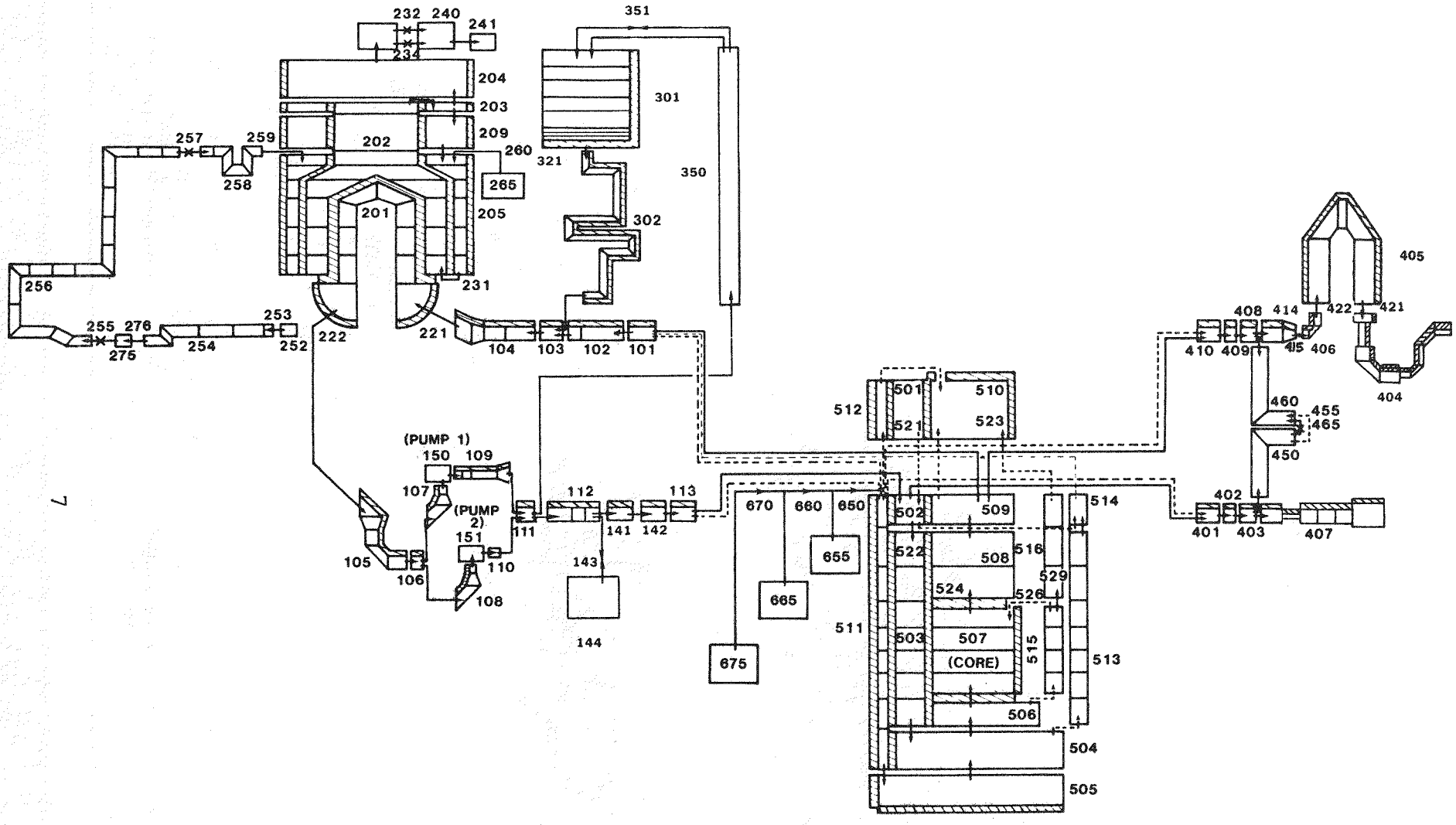

Figure 2.2 LOFT L3-6/L8-1 Nodalization

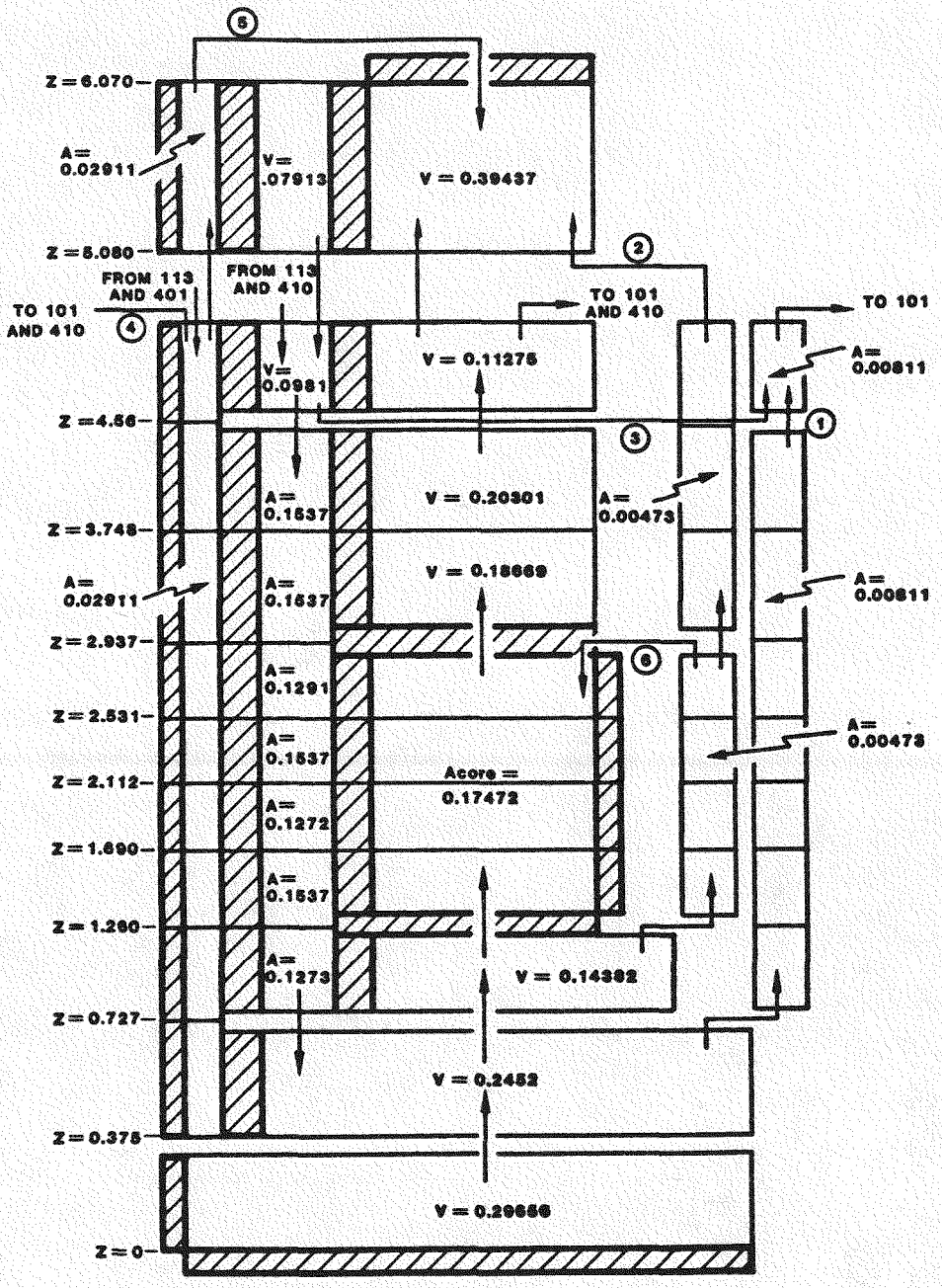

Figure 2.3 LOFT Vessel Nodalization

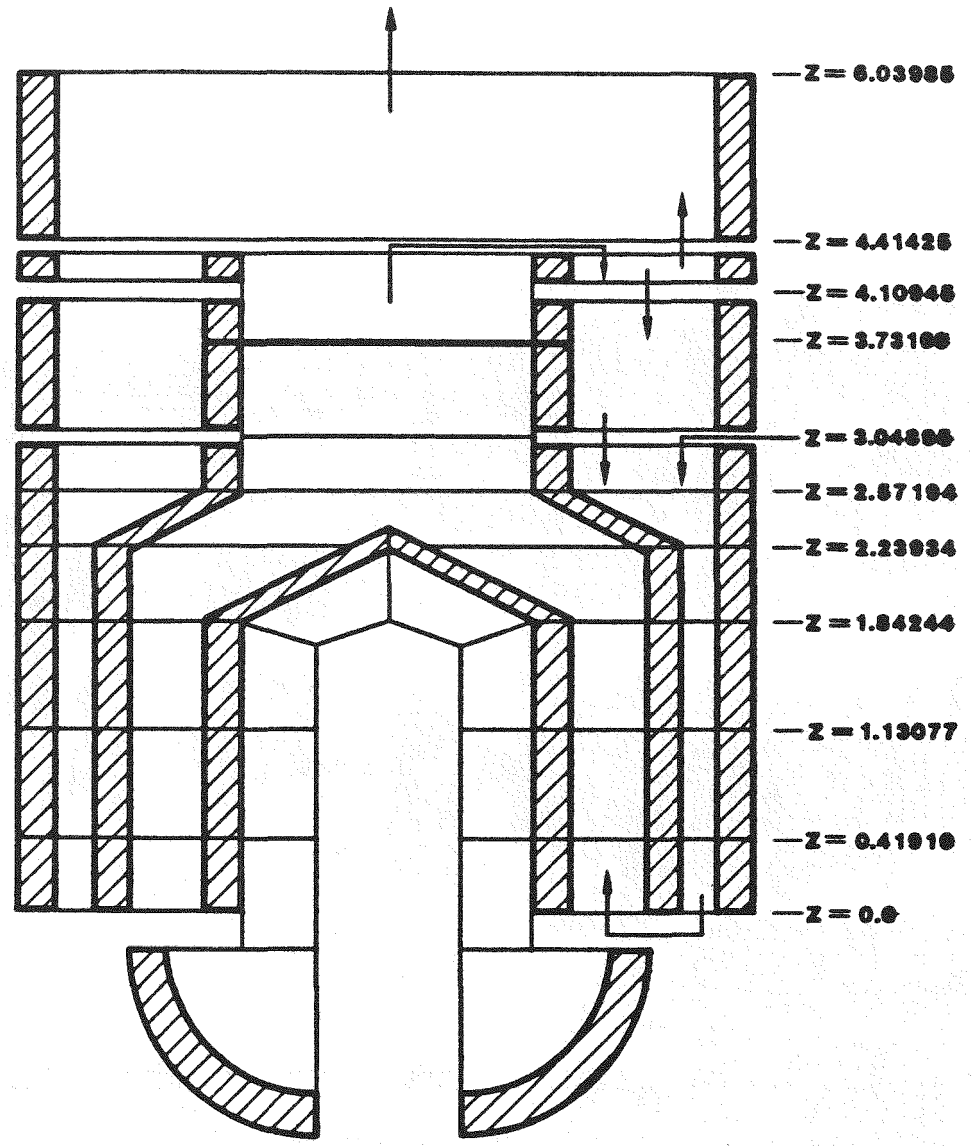

Figure 2.4 LOFT Steam Generator Nodalization

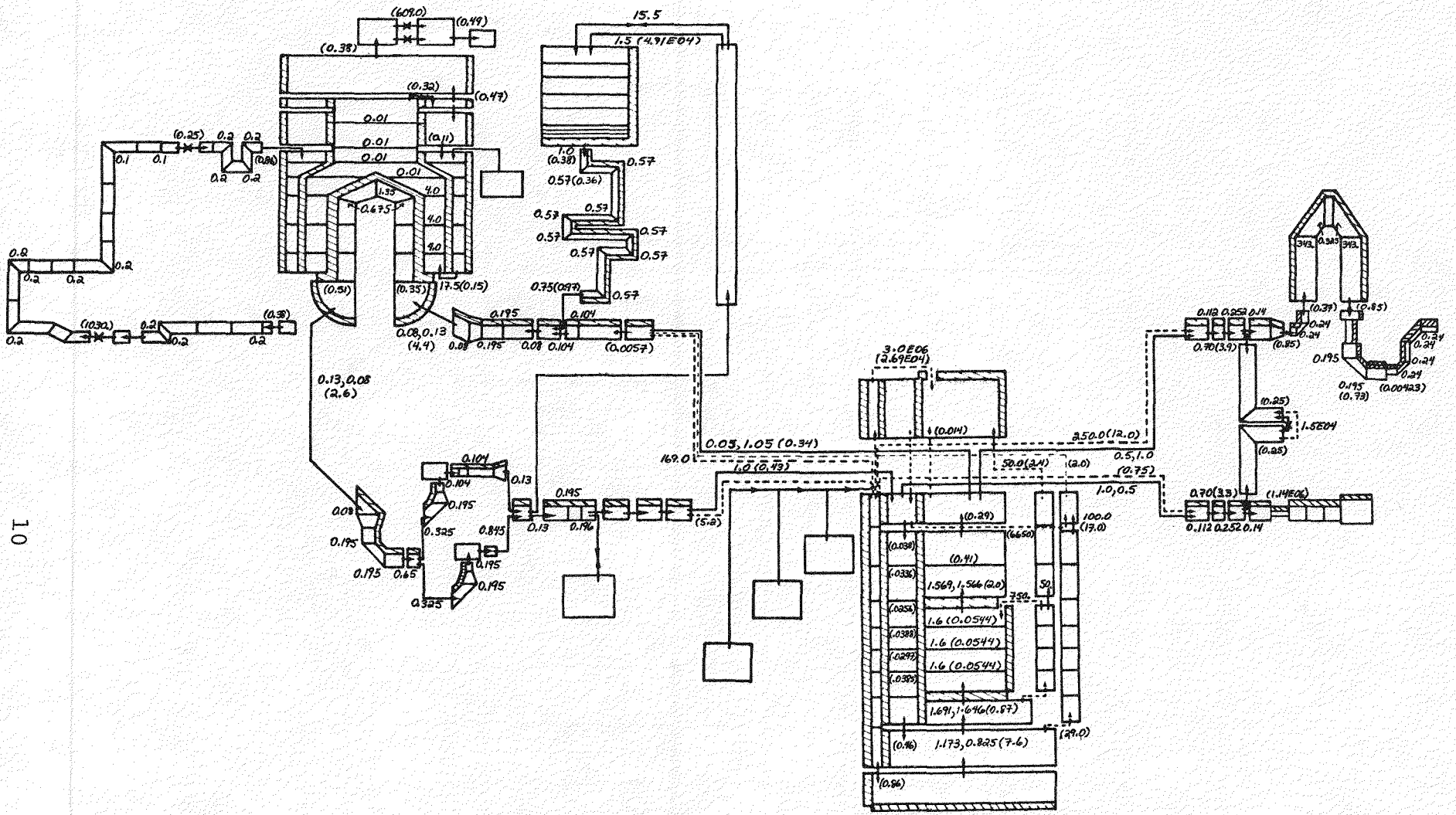

Figure 2.5 Loss Coefficients Used in LOFT L3-6/L8-1 Nodalization

3.0 ANALYSES

LOFT experiment L3-6/L8-1, successfully completed on December 10, 1980, consisted of two parts, each addressing specific reactor safety issues. The first part (L3-6) simulated a 4-in. (2.5%) pipe break in a PWR, and, together with the previously conducted L3-5, provided data to study the thermal/hydraulic behavior in a PWR caused by operating (L3-6) and/or not operating (L3-5) the primary coolant pumps during small break LOCAs. The second part (L8-1) was initiated at the end of L3-6; it was the first intentional partial core uncovery experiment and provided information on in-core heat transfer and fuel cladding heatup rates during core uncovery at low decay heat levels. [3,4,5]

L3-6 was initiated from operating conditions representative of a commercial PWR. At 5.8 seconds prior to the official transient start (break initiation is defined as "time zero"), the reactor was scrammed manually. The primary coolant pumps were left running after scram. HPIS "A" tripped on system pressure at 3.6 seconds. The pressurizer emptied by 20.2 seconds, followed by fluid saturation in the upper plenum. The break flow saturated at 44.2 seconds. Steam generator auxiliary feed was begun at 73.4 seconds, followed by the main steam flow control valve cycling open 15.4 seconds later, at 88.8 seconds, and closing again at 99.6 seconds, after which primary and secondary depressurization continued. The steam generator was a system heat sink until 930 seconds, when the primary system pressure dropped below the secondary, and then was a potential heat source for the rest of the transient. At 1856 seconds the steam generator secondary auxiliary feed pump was manually shut down. The primary coolant pumps were tripped off at 2371 seconds, when the intact loop hot leg pressure had dropped to 2.15 MPa, followed by manual HPIS termination 56.8 seconds later, which nominally ended L3-6.

The fluid in the primary system appeared to be distributed uniformly throughout the system by the pumps, which operated normally all during L3-6. Just prior to the scheduled pump trip, the core was not liquid-full because of the low system mass inventory. The fuel cladding, however, was being cooled by pump forced flow with an average system void fraction of approximately 90%. Liquid level measurements, inferred from thermocouples and conductivity probes in the reactor vessel, showed no systematic decrease in reactor vessel liquid level as the system depressurized, confirming that the pumps were maintaining a two-phase mixture in the vessel and preventing dryout.

The L8-1 part of the experiment effectively began approximately 25 seconds after the start of pump coastdown. At this time (2396 seconds), the fuel cladding temperatures began to increase and reached a maximum recorded temperature of 637 K within 70 seconds. Pump coastdown was completed at 2458 seconds and the break was isolated at 2460 seconds, at which time the system reached a minimum inventory of 650±50 kg. ECC injection was initiated manually when the clad temperature reached 589 K; the accumulator and HPIS flows were not scaled down from reactor values to LOFT dimensions (as was the HPIS in L3-6), but were both as large as was possible. This full-scale ECC flow, begun about 3 seconds before peak clad temperature occurred, quenched the core from the top down 10 seconds after initiation. The top-down quench was probably caused by ECC-induced condensation in the downcomer and lower plenum, which drew upper plenum liquid down through the core. Continued ECC injection cooled the fuel cladding below fluid saturation temperature for a short period, with decreased liquid subcooling observed at increasing core elevations. The accumulator was shut off 34 seconds after clad quench, followed by HPIS "B" shutoff 65.6 seconds later. At 2574.6 seconds HPIS "A" was reduced from full flow to its normal scaled value and long-term primary refill was initiated. Primary system pressure again became greater than secondary system pressure at 4981 seconds, and the primary system upper plenum reached a subcooled condition 753 seconds later. Pressurizer refill began at 7123 seconds; subsequently, the experiment was terminated at 7469 seconds when the liquid temperature in the intact loop hot leg decreased to 28 K subcooling.

3.1 Steady State Calculation

Ideally it should be possible to calculate all of the experimental initial conditions for the primary and secondary sides simultaneously with RELAP5, within the given experimental uncertainties. We were able to achieve such a starting condition for L3-6/L8-1, shown in Table 3.1.1, but a substantial effort was required. The starting point was the L6-7/L9-2 steady state [9]. Many of the same difficulties encountered during that calculation and others [10,11] reoccurred during the L3-6/L8-1 initialization. As before, the primary pump speed controller and the pressurizer heaters and sprays worked very well, while the secondary side proved to be a problem.

The steam flow valve was controlled to match the steam dome pressure using an exponential relaxation scheme. The desired secondary pressure had to be reduced to its lowest possible experimental value to yield good primary side temperature agreement, and that was only after manipulation of the secondary side heated equivalent diameter (which helps control the

temperature gradient across the U-tubes). Using the strict geometric definition of heated equivalent diameter, the primary side temperature would be ~5 K too high for a given secondary side pressure and saturation temperature. Lowering the equivalent diameter by about an order of magnitude (a number based on the U-tube wall-to-wall spacing) resulted in cold leg temperatures within the high side of the experimental uncertainty when the secondary pressure was specified at the low end of its uncertainty.

The feedwater valve was controlled by both the liquid level and feedwater flow. The controller first brings the liquid level to the desired value and then attempts to bring the feedwater mass flow to its specified value. If the liquid level drifts outside of the allowed limits, then control is returned to the level controller until the desired level is reestablished. We could not match the secondary feedwater flow and downcomer liquid level values simultaneously for L3-6/L8-1. (This was not in general true for the other LOFT transients analyzed in this assessment project. [9,10]) Since the secondary was to be isolated at the beginning of the transient, we decided that the liquid level was the more important parameter, in order to insure the correct secondary side inventory.

3.2 L3-6 Transient Calculation

The RELAP5 calculation for L3-6 predicted the important phenomena occurring during the transient in the proper sequence, as shown in Table 3.2.1, although the transient was calculated to end earlier than actually occurred. Figure 3.2.1 compares the calculated and measured primary system pressure. (The uncertainty on the measured pressure is $\pm$0.25 MPa.) The agreement of analysis with data is excellent at early times but there is growing disagreement later in the transient, as the system depressurizes more slowly than calculated. (Since L3-6 ends on a pressure trip, the transient is thus calculated to end earlier than occurred.) Potential causes of the discrepancy between calculated and measured depressurization would include overprediction of steam generator heat transfer, overestimating break flow, overestimating environmental heat loss, and underestimating the core decay power. Small errors in any or all of the above could lead to small errors in depressurization rate, and to a significant cumulative error in primary pressure at late times.

The calculated primary side temperatures exhibit the same overall behavior as the system pressure, as shown by the hot leg temperature (whose experimental uncertainty is $\pm$3 K) in Figure 3.2.2, since after the first ~50 seconds the primary system is at saturation conditions. The underprediction of primary system

pressure at late times leads to a slight overprediction of the HPIS injection rate, as shown in Figure 3.2.3, because it is specified as a well-known (uncertainty of $\pm$0.02 kg/s) flow-vs-pressure boundary condition. (Although the HPIS is overestimated at later times, the total amount of water injected during L3-6 is less than in the experiment, because of the premature termination.)

Figure 3.2.4 shows the calculated and measured secondary side pressures in the steam generator dome. (The experimental uncertainty on the secondary side pressure is $\pm$0.12 MPa.) The calculation shows the relief valve cycling far too early (~10 seconds) and the secondary later repressurizing to too low a value. (This is responsible for the qualitative disagreement in primary side pressure around 100 seconds.) The calculated depressurization rate is then in excellent agreement with data for hundreds of seconds, until the system enters a reverse heat transfer mode and the measured and calculated pressures then diverge rapidly. There are a few periods late in the transient (~1100, ~1300 and ~1900 seconds), however, where the calculated depressurization rate agrees with the experimentally observed value; a closer look at these periods helps provide an explanation of the overall discrepancy, as shown in Figure 3.2.5.

The temperatures calculated for the top and bottom of the steam generator downcomer are given in Figure 3.2.5, together with the measured temperature (known to within $\pm$3 K) near the downcomer bottom. The periods during which the correct depressurization rate is being calculated correspond closely to periods in which some temperature gradient is seen on the secondary side. The cold auxiliary feedwater injected during most of L3-6 should collect at the bottom of the steam generator, forming a subcooled layer under a region of hot saturated water, with steam in the dome; thus, with forward heat transfer in the subcooled layer and reverse heat transfer in the saturated layer, the net heat exchange with the primary should be greatly reduced. The experimental data shown in Figures 3.2.4 and 3.2.5 confirm this scenario, since after ~600 seconds the downcomer temperature shown is progressively less than the saturation temperature associated with the steam dome pressure given. On the other hand, the calculation, except for the short periods already mentioned, shows the steam generator secondary at saturation conditions throughout. The subcooled auxiliary feedwater is in effect completely mixed with the saturated liquid inventory, necessitating a simultaneous condensation of steam in order to maintain saturation conditions; the auxiliary feed thus has an overall depressurizing effect on the secondary side, contrary to data.

(Similar behavior has been observed in other assessment calculations. [10,12] In particular, the results of a FLECHT SEASET steam generator separate effects test analysis using RELAP5/MOD1 [12] confirms the above argument, and suggests that the nonequilibrium behavior on the secondary side of a steam generator in reverse heat transfer cannot be correctly calculated with MOD1. The presence of such a subcooled layer on the tube sheet is closely associated with the propagation of a "quench front" up the insides of the U-tubes. This quench front cannot be calculated without a reflood model containing a nonequilibrium heat transfer correlation package together with a moving fine-mesh temperature grid, which will not be available in RELAP5 until MOD1.5 and MOD2 are released.)

The L3-6 calculation correctly demonstrates the availability of adequate core cooling as long as the pumps are running, even when a major portion of the primary fluid and the steam generator heat sink have been lost in a small break, as shown by the core clad temperatures shown in Figure 3.2.6. Two experimental temperature plots are given; each represents an average of all the given thermocouple measurements at a given core elevation, in this case at 0.533 m and at 1.14 m. Both calculated and measured clad temperatures closely follow the system saturation temperature throughout the transient, even though the vessel does not retain enough liquid to completely cover the core (as shown in Figure 3.2.7). The lower saturation temperature due to the lower primary system pressure calculated produces correspondingly lower clad temperatures than were experimentally observed. One level in the core experiences a brief dryout in the calculation, when the void fraction in that cell momentarily rises above α-crit=0.96. The adjacent cells reach void fractions as high as 0.95, but that does not trigger dryout.

After the primary coolant pumps are finally tripped, the ability of the system to continue to provide adequate core cooling depends in large part on the primary coolant mass inventory remaining in the system at the time of pump trip. Our calculation predicts a final mass inventory at the end of L3-6 of 890 kg, which at first appears quite high when compared to the quoted experimental final inventory of 650 kg. However, comparison of calculated and measured primary mass inventories throughout L3-6, given in Figure 3.2.8, shows overall excellent agreement. (The data could not be found on the data tape or in the Experimental Data Report [5]; the experimental results shown were digitized from a small plot in the Quick-Look Report [4]. The oscillations in that plot do not seem to support the claimed experimental uncertainty of $\pm$50 kg.) The mass inventory is slightly underpredicted during the first ~500 seconds, and slightly overpredicted during the last ~400 seconds but lies

well within the oscillations recorded. The discrepancy in final inventory is probably due to slight overprediction of the HPIS injection (Figure 3.2.3) and the slight underprediction of break flow (Figure 3.2.9) at late times. Since the HPIS flow and the break flow are almost equal at these late times, as shown by the flattening out of the primary mass inventory, we do not think that the earlier termination of L3-6 in the calculation significantly affects the final inventory present.

Figure 3.2.9 shows the calculated and measured break flows during L3-6. Break flow measurements are not available during the first 50 seconds of the test, so the accuracy of the calculated subcooled break flow can only be checked indirectly by comparing primary side pressure (Figure 3.2.1) and mass inventory (Figure 3.2.8) agreement. The saturated break flow during the first several hundred seconds appears significantly higher than what was observed experimentally, and the break flow out at late times may be a bit low compared to the data. Such a discrepancy at late times could be expected, since the too-rapid primary depressurization during the latter part of the transient reduces the driving head slightly. The impact of these discrepancies on the overall transient behavior seems slight, based on the pressure and inventory behavior observed. Discharge coefficients of 0.85 were used for both subcooled and saturated break flow. No sensitivity studies were done, since experimental subcooled break flow data was not available and long runs would be required to evaluate the effects of varying the saturated break flow. (The break flow is not well-known experimentally. The uncertainty is $\pm$15% for 50 to 1435 seconds, and $\pm$0.75 kg/sec for 1435 to 2400 seconds.)

One possible source of the discrepancy observed in primary system depressurization that was not identified until late in the analysis is the core decay power, shown in Figure 3.2.10. (The decay power was not found on the data tape; the experimental plot shown was digitized from a graph given in the Experimental Data Report.) The underprediction of decay power would have the same effect as overestimating environmental heat loss. In fact, the error in decay heat (~150 kW) is comparable to the total environmental heat loss (~200 kW). The reason for the disagreement between calculation and experiment is not known. All the reactor kinetics input was taken from INEL sources; there is not enough published information to allow independent verification.

This L3-6 calculation was so slow-running (more than 16 hours of CPU time, as discussed in Section 3.4) that sensitivity studies on the effects of discharge coefficients, environmental heat loss, etc. were not economically feasible. It does appear likely that small variations in total environmental heat loss

could easily affect the primary depressurization rate. One sensitivity calculation for part of the transient was done, however, in an effort to resolve the early-time anomalous steam generator secondary behavior and thus perhaps improve the long-term steam generator response, since the probable misestimate of the reverse heat transfer late in the transient could also significantly affect the primary side depressurization rate.

Following a suggestion made by LASL [13], the transient was rerun with a small delay on the turbine trip. As shown in Figure 3.2.11, a delay of 2 seconds prevents the relief valve from opening at very early times, as occurred in the reference calculation discussed above, and results in a calculated secondary pressure in better agreement with data during the first ~600 seconds. However, at later times the secondary pressure drops much more rapidly than in the experiment, remaining closely coupled to the primary side pressure, just as in the reference calculation.

Closer comparison between the two calculations shows that, although the original calculation does not perhaps agree as well quantitatively with experimental data throughout most of the transient, it did exhibit the "correct" depressurization rate for short times during the period of reverse heat transfer, which this delayed turbine trip calculation failed to do. The reason for this is shown in Figure 3.2.12, where the experimental temperature data from the bottom of the steam generator downcomer is plotted with temperatures at the downcomer top and bottom for the delayed turbine trip calculation. Just as in Figure 3.2.4, the experimental temperature shown is substantially below the saturation temperature corresponding to the secondary pressure in the latter part of the transient. The calculation on the other hand shows the steam generator at saturated conditions (except for a much shorter and smaller amount of subcooling than in the reference calculation), confirming that the correct secondary depressurization rate cannot be calculated during the reverse heat transfer period without the development of a subcooled layer at the tube sheet.

3.3 L8-1 Transient Calculation

The second half of this small break experiment studied both the rapid (within ~200 seconds) loss of core cooling and subsequent rod dryout after pump trip and the long-term (~5000 seconds) refill of the primary system after the break is isolated. Due largely to the long run times required and the lack of any particularly interesting phenomena during the system refill, only the first portion (~10%) of the L8-1 transient has

been analyzed. Various events in L8-1 were specified in the input to occur on time since pump trip in the transient analysis, due to the earlier noted discrepancy in the time that L3-6 was calculated to end. The comparison plots given in this section have all been shifted in time so that time "zero" corresponds to the time of pump trip (and thus the start of L8-1). However, the various discrepancies between calculation and experiment at the "end" of L3-6 preclude any significant quantitative comparison between calculation and experiment for L8-1.

There also exists a serious lack of documented facility and experimental data required for a complete analysis of L8-1. There is no information readily available on the accumulator surge line configuration and resistance for direct downcomer injection and "unscaled" flow. There is also no data given in the tables of experimental initial conditions in the Quick-Look Report or the Experimental Data Report on the accumulator initial liquid level (although this piece of information is available as a data plot). There is furthermore no data given in the reports or on the data tape on the actual accumulator flow rate for use as a boundary condition, although the appropriate instrumentation is listed as present. We estimated the required accumulator flow rate data by differentiating the accumulator liquid level data which was given, multiplying by an area estimated from the volume vs level plots given in the facility description and then multiplying by the subcooled water density. The result was applied to the vessel downcomer as a user-specified boundary condition. (We have not been able to obtain copies of either INEL's pre-test or post-test reports to see if any of the missing information is available there.)

The accumulator injection thus backed out of the available data is shown in Figure 3.3.1. While this flow appears quite high at first glance, comparison of the calculated and experimental primary mass inventory (shown in Figure 3.3.2) indicates that the injection rate used is probably very close to the correct test value. The effects of both break isolation and the onset of unscaled ECC injection at ~90 seconds is clearly seen as a sudden increase in primary inventory. The accumulator shutoff at ~135 seconds shows up as a sharp change in the refill rate, and the subsequent cutback from unscaled to scaled HPIS flow at ~200 seconds causes another visible decrease in refill rate. The slightly higher mass inventory late in the calculation is probably a direct consequence of the higher calculated mass inventory at the end of L3-6 (890 kg vs 650 kg), although the digitized mass inventory data is not as reliable as if it could have been obtained directly from the data tape.

After the pump trip which begins L8-1, the pump-driven forced flow is no longer available to entrain liquid in the core, and the liquid then collapses to below the lower core elevation (as shown in Figure 3.3.3); this exposes the core, which is covered with a draining and drying liquid film, to a steam environment. As the liquid film dries out, temperature excursions begin throughout the core, as shown in Figure 3.3.4. The rod heatup is followed by operator-initiated unscaled accumulator and HPIS injection, and the core is completely quenched within a few seconds after the maximum rod temperature is observed. The code calculates the correct qualitative behavior but the quantitative experimental behavior is not reproduced, as shown in the individual core clad temperature plots in Figures 3.3.5 and 3.3.6.

These two plots compare the calculated clad temperature in a single core node with measured data. Each of the experimental data curves is an average of all the thermocouple readings at a given elevation; three such elevations, bracketing each calculational core node, are given for comparison. Thus the core clad temperature calculated at 0.64 m core elevation is plotted with average measured clad temperatures at 0.533, 0.660 and 0.762 m, and the core clad temperature calculated at 1.06 m is given with average clad temperature data from 0.991, 1.040 and 1.14 m core elevations. The experimental elevations were chosen as either closest to the core node location (within 2 cm), or almost equally above and below it. Each elevation chosen contains between ten and twenty thermocouples used in the averaging; thus although the single thermocouple peak clad temperature of 637 K is observed at the ~0.7 m core elevation, the average peak clad temperature at ~0.7 m is only ~601 K (still substantially higher than calculated).

Several factors contribute to the lower clad temperatures calculated. The temperature rise starts from a lower (by ~10 K) value, the heatup is slower due to the lower (by ~20%) decay heat calculated, and the quench is comparatively early (all events in the L8-1 calculation were tripped on time since pump trip, but in the experiment ECC injection was initiated manually when an observed clad temperature reached 589 K). The primary mass inventory may be higher than in the experiment, resulting in a little more residual core cooling, and the calculated pump coastdown (shown in Figure 3.3.7) is slower than occurred, which might also contribute a small amount of residual cooling.

Rod quenching occurred in the experiment from the top down, caused by the injection of subcooled accumulator and HPIS water directly into the downcomer. The downflow of this subcooled liquid created a heat sink in the lower plenum; condensation of steam in the downcomer and lower plenum then caused a

low-pressure region which drew liquid from the intact loop hot leg, upper plenum and broken loop hot leg down through the core. Rapid core quench is observed in the calculation at the correct time, but it is not clear whether top-down quench is occurring as in the test. There is no significant downward flow of liquid visible in the calculation during the quench time. The calculation does show decreasing liquid subcooling with increasing core elevation after quench, indicating establishment of positive core flow, although the maximum subcooling occurs slightly later than observed in the test data.

3.4 Computational Speed

The L3-6 calculation, run with RELAP5/MOD1/CYCLE14, required 16.24 hours of CPU time on a CDC CYBER76 computer to run a total of 2077 seconds of problem time (which includes 100 seconds of steady state for plot purposes), as shown in Figure 3.4.1. Although the average speed was ~28:1, the plot shows two distinct regions; during the steady state calculation and the first ~700 seconds of the transient the ratio of CPU time to problem time was ~14:1, while during the later stages of the transient the ratio averaged ~37:1.

Out of a total of 196,146 time steps attempted, the code decided to repeat 55,549 of them. Thus more than 28% of the time steps, and hence of the total calculational time, were thrown away. Of the two regions mentioned above, twice as many time steps were repeated in the second part of the transient (32%) than in the first part (16%).

At first glance, no single dominating location or phenomenon can be seen in the deciding time step limits. The intact loop piping controls the time step 16.7% of the time, through Courant limits around the pump inlets and outlets. The steam generator secondary, and the pressurizer and surge line, control 8.8% and 3.5% of the time, respectively, primarily through the static quality criterion in the steam generator and Courant limit in the pressurizer system. The broken loop piping dominates 44.9% of the time step selection, mostly through the static quality check but also through significant thermodynamic property problems. The vessel controls 26.1% of the time, through mass error and also through the static quality error check. (We were surprised to see the supposedly inactive broken loop controlling the time step almost half the time.)

A closer examination of the vessel and broken loop, however, shows that while these two subsystems together control the time step 71% of the time they in turn are dominated by just a few cells (parts of components 406, 409 and 414 in the broken loop, and components 501, 512 and 514 in the vessel). These cells are

all in the immediate vicinity of various bypass paths in the vessel or the RABV leakage in the broken loop. Problems in modelling these small flow paths have been encountered in other LOFT analyses. [9,10] In both our L6-7/L9-2 and L9-1/L3-3 assessment calculations, rapid oscillations were observed in these bypass flow paths which resulted in significant mass and energy conservation errors, when the abrupt area change model was used with very small junction areas for such pinhole leaks. (The developers have since come up with a user guideline that larger fictitious junction areas with user-specified loss coefficients should be used for area changes greater than 0.1 to 0.01, to avoid such oscillations.) The "pinhole leak" modelling in L3-6 was not changed appropriately, however, because no ill effects could be seen in the overall calculated results. These time step studies indicate that oscillations in the various bypass junctions did adversely affect the calculation, albeit indirectly (although the magnitude of the effect is not known).

During the steady state calculation and early parts of the transient calculation, which are more Courant-limit dominated, some efforts were made to improve the run time by renodalizing the pump inlets and outlets (the source of the Courant limits). If the limiting region was renoded with smaller cells combined into somewhat larger cells, the Courant limit obviously moved elsewhere. (In this case, it did tend to remain in the intact loop piping.) However, a 10% or 20% increase in the Courant time step limit did not usually result in an equivalent decrease in run time, since the code can only halve or double the time step. In order to double the Courant limit at any given time, very extensive renodalization would be necessary. Because of this halving/doubling of the time step, the calculation is usually not running as efficiently as possible. (Renodalizations cannot be effectively undertaken during the course of a long transient since most cells in our model have associated heat slabs, and heat slab input cannot be changed on restart in MOD1.)

The L8-1 calculation, also run with RELAP5/MOD1/CYCLE14, required 3.2 hours of CPU time on a CDC CYBER76 computer to run a total of 430 seconds of problem time, as shown in Figure 3.4.2. The average speed was ~27:1, quite similar to the average run time for L3-6, and the time step control pattern is quite similar to that seen in L3-6. Although the effects of ECC injection startup and later reduction can be seen in the run time, there do not appear to be different behavioral regions such as the two visible in Figure 3.4.1. The time step actually used by the code during the L8-1 calculation is shown in Figure 3.4.3, and the discrete time step values available to the code are readily visible.

The average grind time (CPU seconds/number of volumes x number of cycles) for the entire calculation was 0.0015.

3.5 Code Errors and Modifications

In order to correctly model a flywheel clutch on the LOFT primary pumps, INEL recommended that the following update be made to RELAP5:

```
*I PUMP.84
      IF (PMPOLD(I).GT.78.53982)
      PINVAR=((-542.47*S+640.95)*S+136.32)*0.04215
```

This update is used if a new input card (180) has the word LOFTPUMP on it; if card 180 is not input, or if it is input with something other than LOFTPUMP on it, the LOFT pump update is not used. This new input card was added to avoid separate versions of the code being used for the various assessment projects.

In several instances during the L3-6 analysis, we had calculations aborted by the code sending a negative argument to the square root function. We traced this to a sequence treating horizontally stratified flow at a junction prescribed to have a smooth area change and a flow area larger than the adjacent volume areas. Apart from the obvious restriction on the square root's argument, the treatment was intended for abrupt area changes only. INEL personnel suggested a code modification to bypass the calculation for junction areas larger than 90% of the minimum adjacent volume area, and for smooth area changes. No significant differences were observed in the results, other than the obvious one of being able to continue computing.

The code error resulting in the negative argument to the square root function is in subroutine JPROP. This subroutine computes the hydrodynamic properties of liquid and vapor in junctions. The INEL update to avoid the square root calculation for smooth area changes is:

```
*I JPROP.89
      IF (SHIFT(JC(I),2).GE.0) GO TO 900
```

The INEL update to avoid the square root calculation for junction areas larger than 90% of the minimum adjacent volume flow area is:

```
*I JPROP.94
      IF (AJ.GT.0.9) GO TO 900
```

Table 3.1.1

L3-6 INITIAL CONDITIONS

PARAMETER	DATA	RELAP5
MASS FLOW (KG/SEC)	483.0±2.6	483.7
HOT LEG PRESSURE (MPA)	14.87±0.14	14.85
HOT LEG TEMPERATURE (K)	577.1±1.8	577.8
COLD LEG TEMPERATURE (K)	557.9±1.1	558.4
CORE POWER (MW)	50±1	50.0
PRESSURIZER LIQUID LEVEL (M)	1.18±0.11	1.22
SECONDARY LIQUID LEVEL (M)	3.17±0.03	3.15
SECONDARY MASS FLOW (KG/SEC)	27.8±0.1	25.75
SECONDARY PRESSURE (MPA)	5.57±0.06	5.51

Table 3.2.1

L3-6 CHRONOLOGY

EVENT	TIME (S)	
	DATA	RELAP5
REACTOR SCRAMMED	-5.8±0.2	-5.8
BREAK STARTED	0.0	0.0
HPIS INITIATED	3.6±0.2	4.85
PRESSURIZER EMPTIED	20.2±0.2	~24
UPPER PLENUM SATURATED	28.5±0.2	~30
SUBCOOLED BREAK FLOW ENDED	44.2±0.2	~58
SCS AUX FEED STARTED	73.4±0.2	73.44
SCS PRESSURE>PCS PRESSURE	930.0±30.0	~1100
SCS AUX FEED ENDED	1856.0±5.0	1856.0
PUMPS TRIPPED (P<2.15 MPA)	2371.4±0.2	1976.7

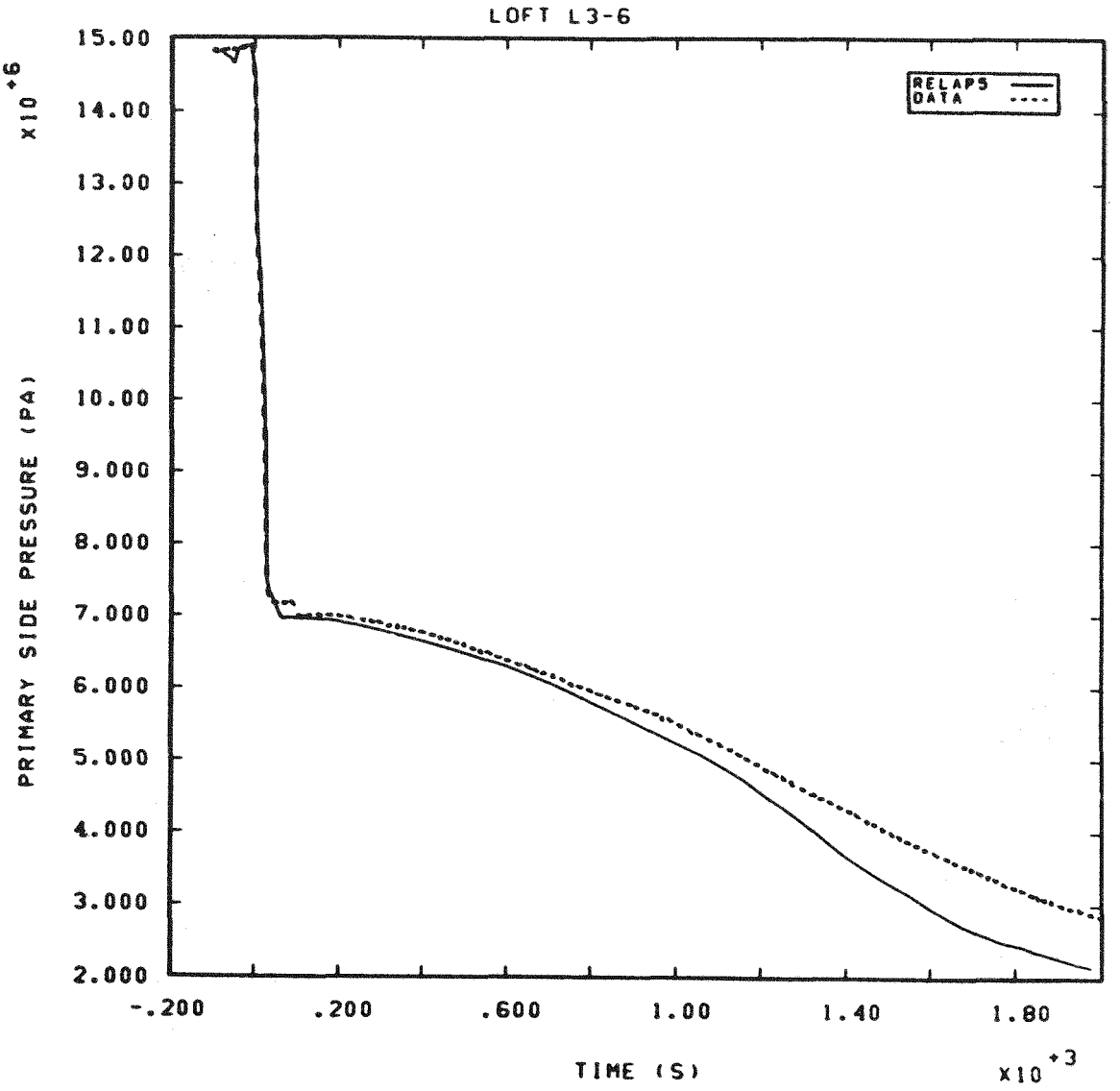

Figure 3.2.1 Calculated vs. Measured Primary Side Pressure for L3-6

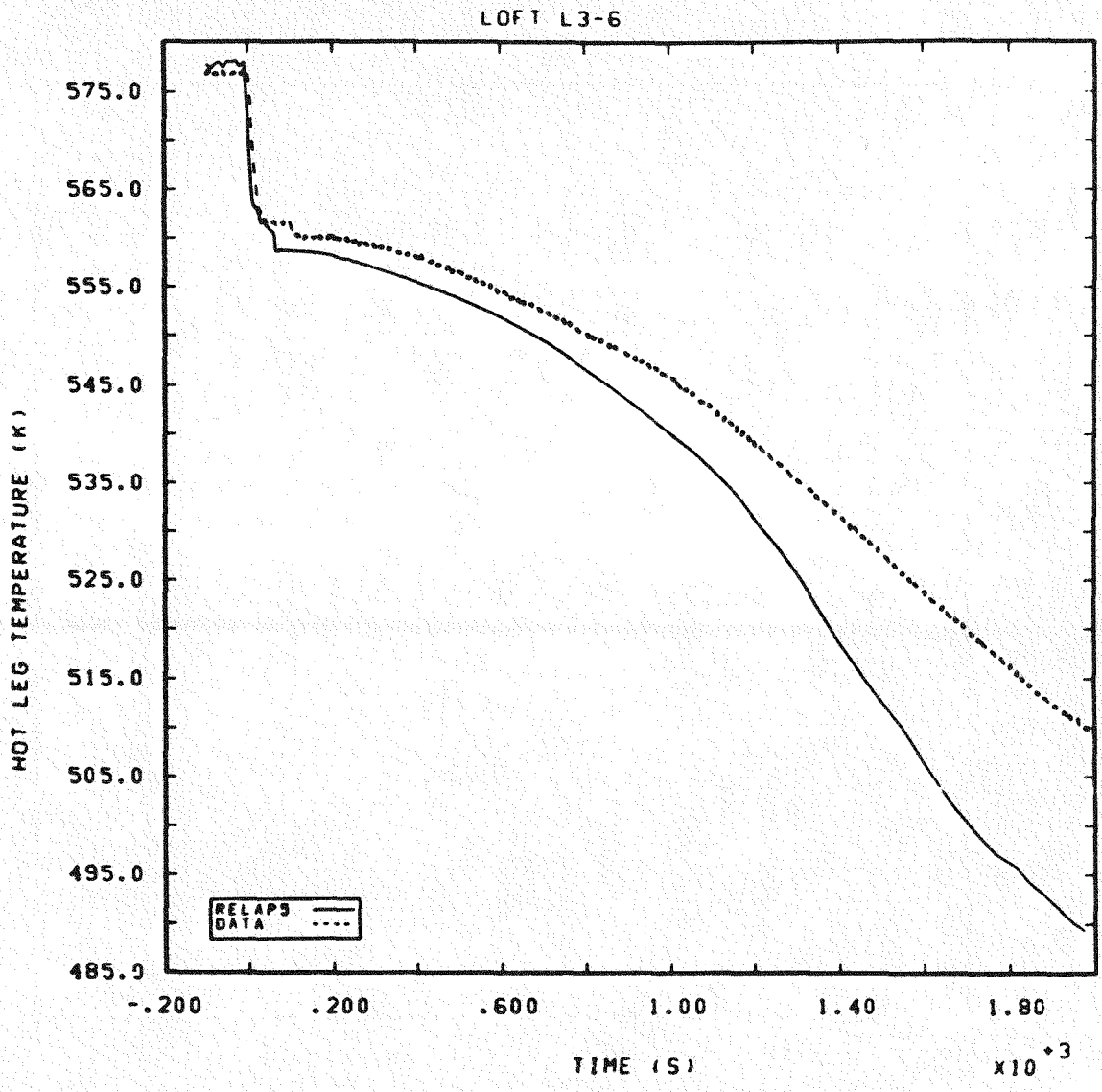

Figure 3.2.2 Calculated vs. Measured Hot Leg Temperature for L3-6

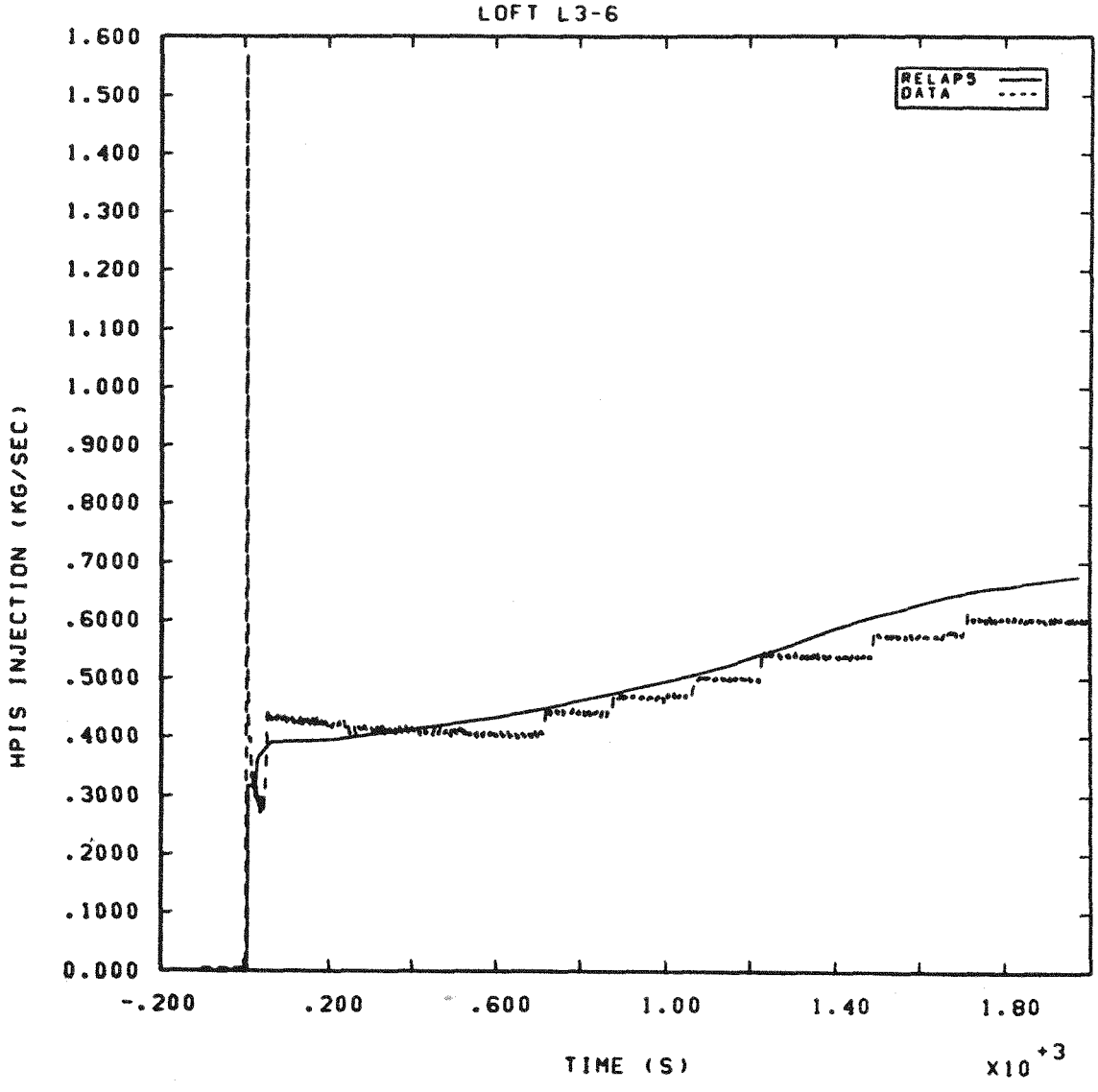

Figure 3.2.3 Calculated vs. Measured HPIS Flow for L3-6

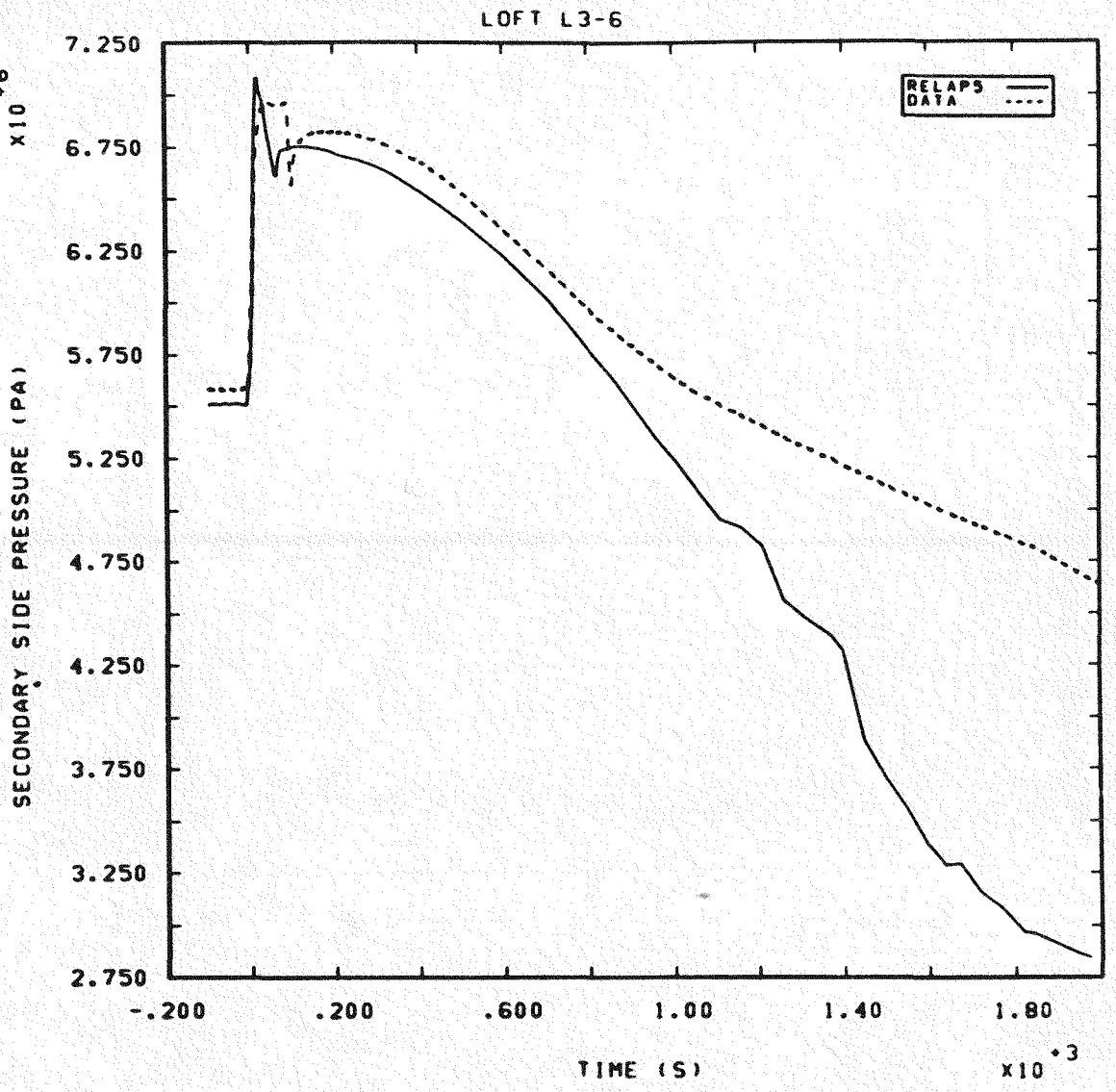

Figure 3.2.4 Calculated vs. Measured Secondary Side Pressure L3-6

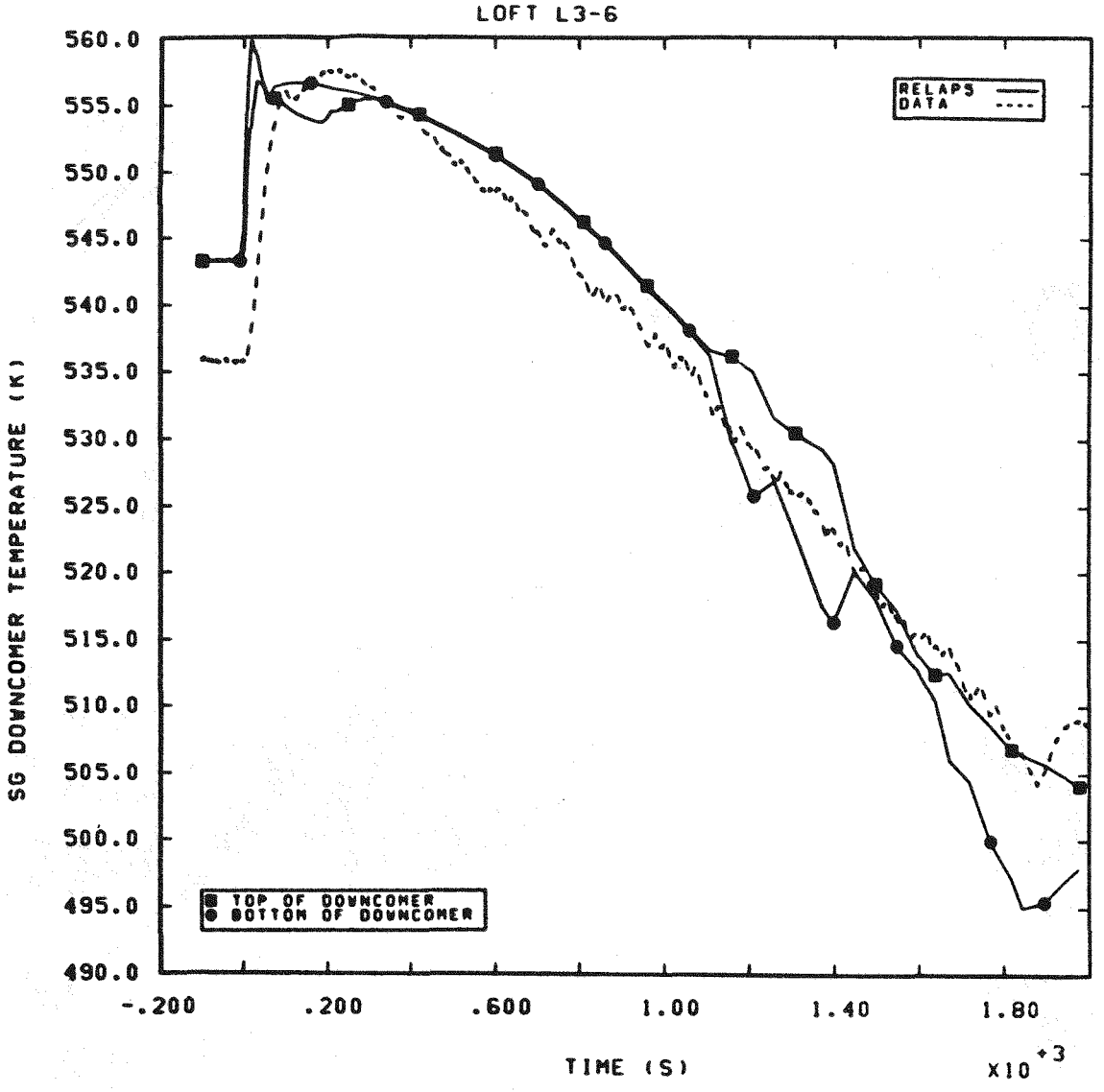

Figure 3.2.5 Calculated vs. Measured SG Downcomer Temperatures for L3-6

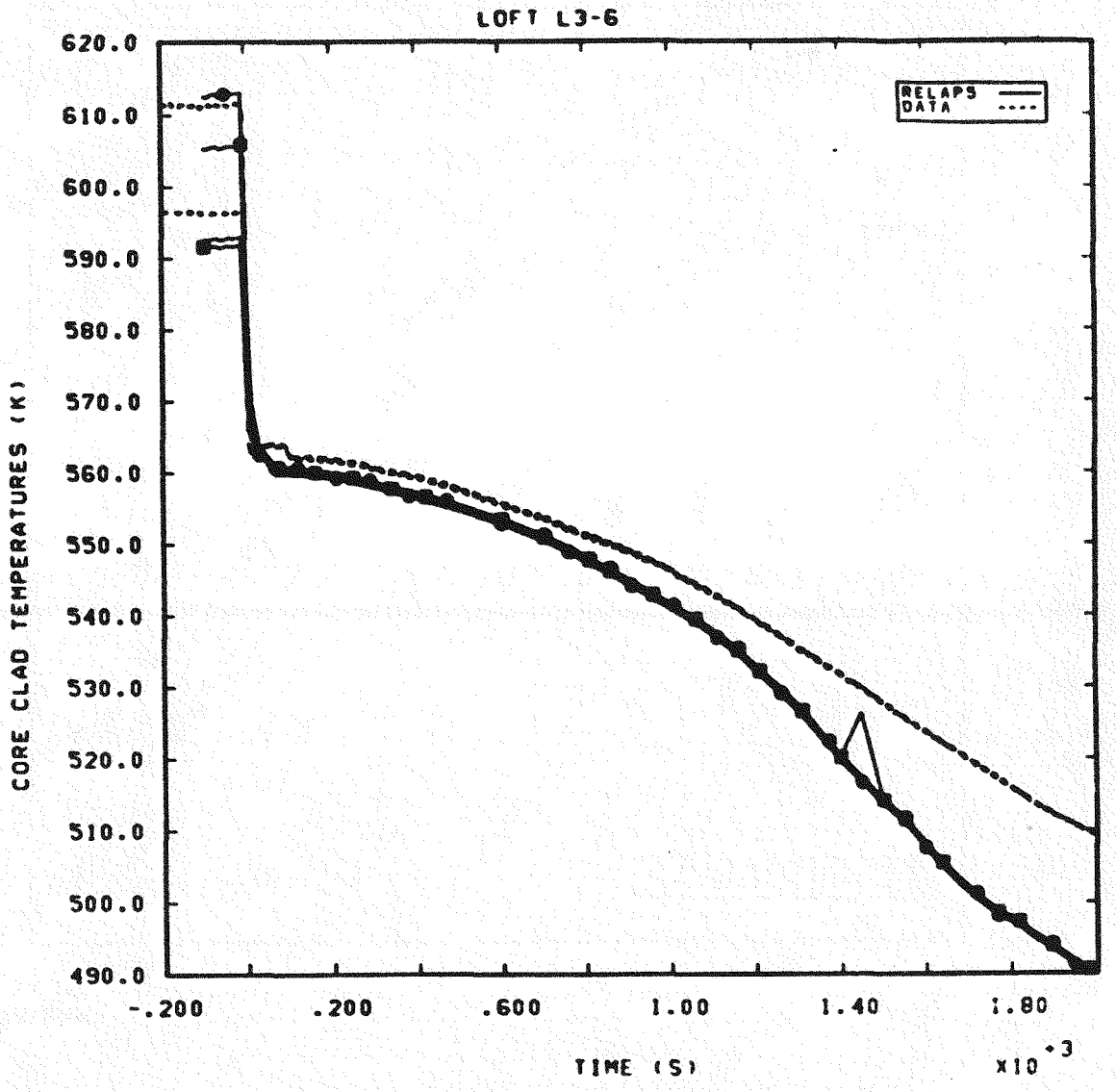

Figure 3.2.6 Calculated vs. Measured Core Clad Temperatures for L3-6

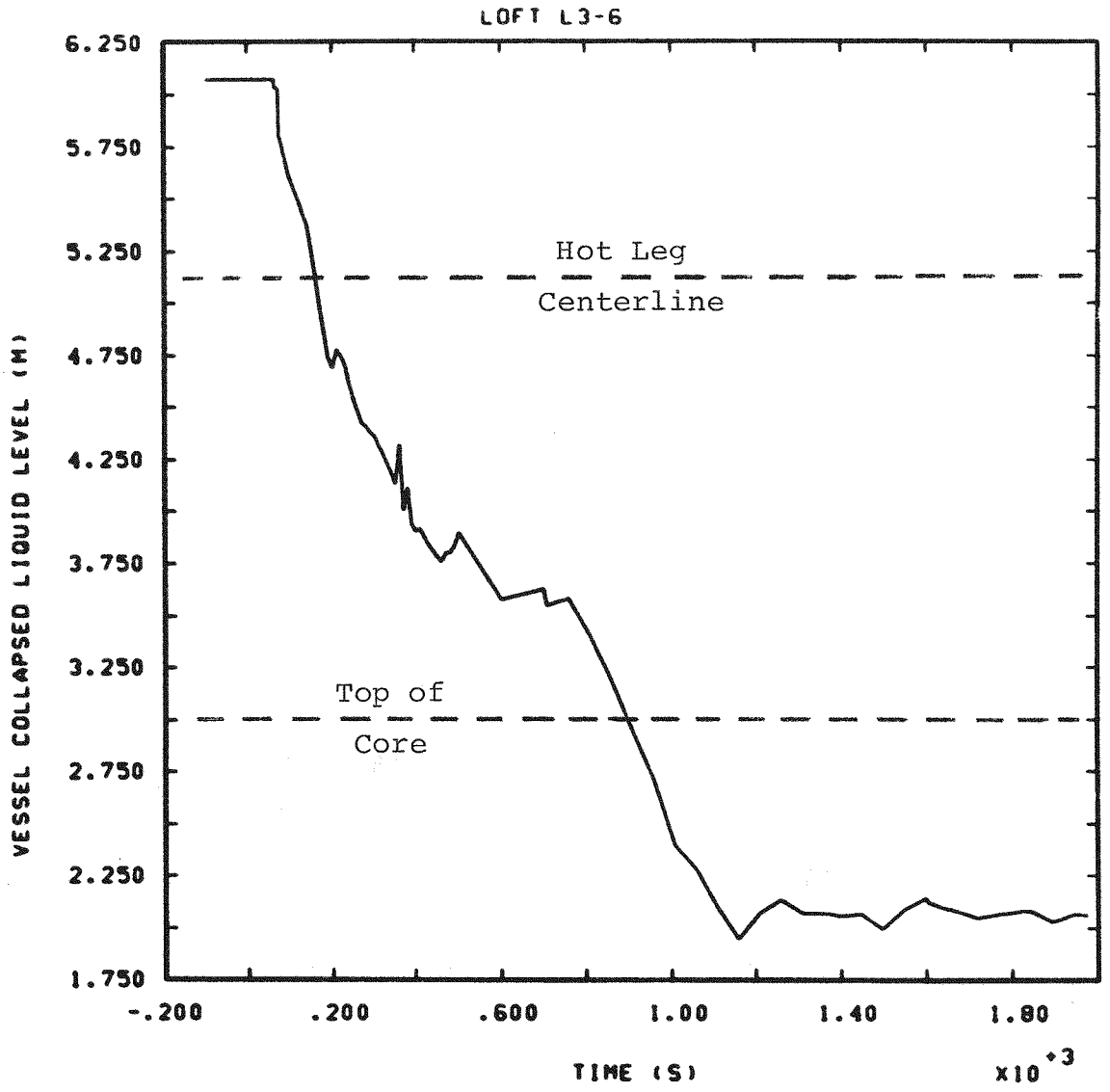

Figure 3.2.7 Calculated Vessel Collapsed Liquid Level for L3-6

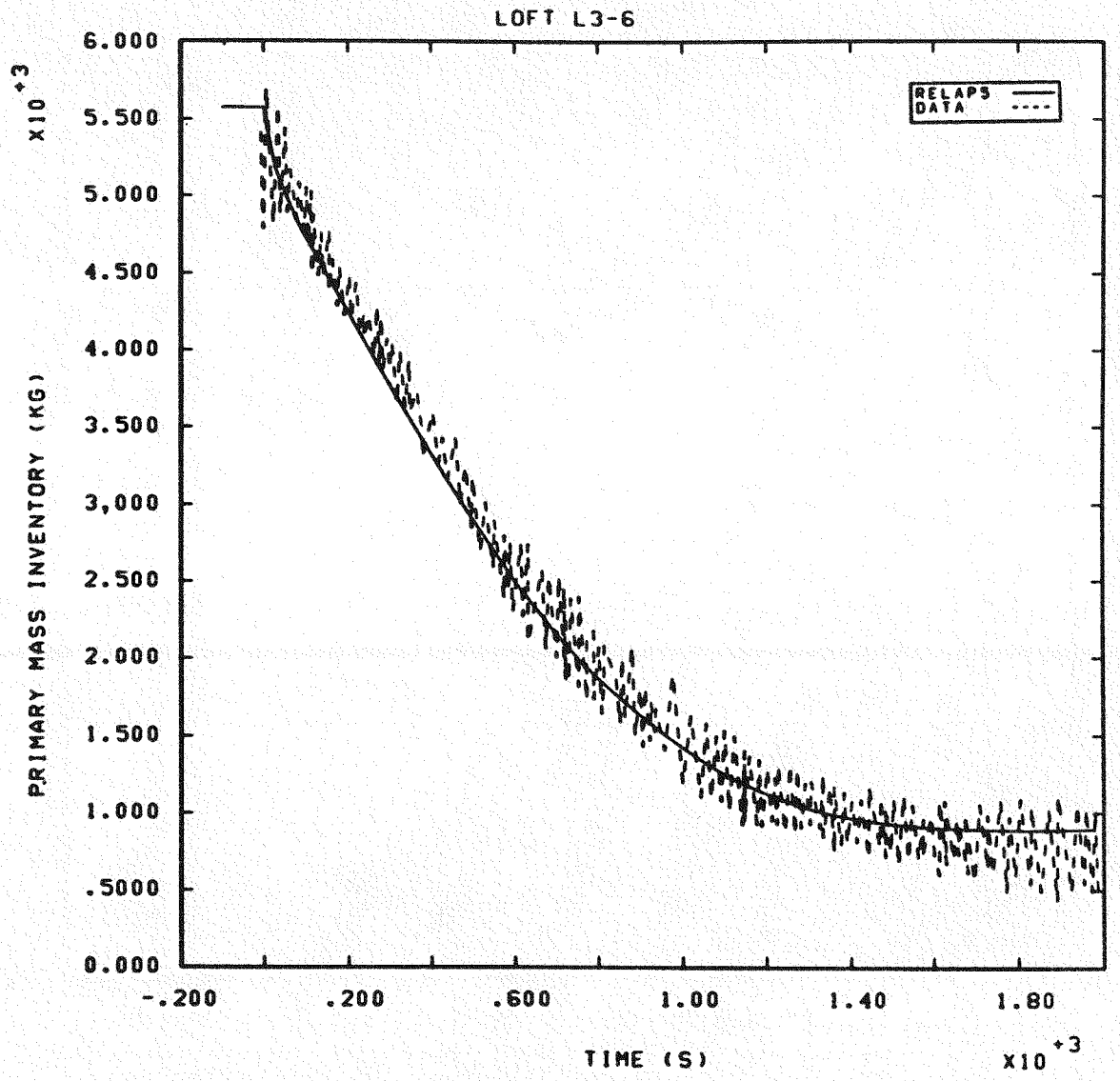

Figure 3.2.8 Calculated vs. Measured Primary System Mass Inventory for L3-6

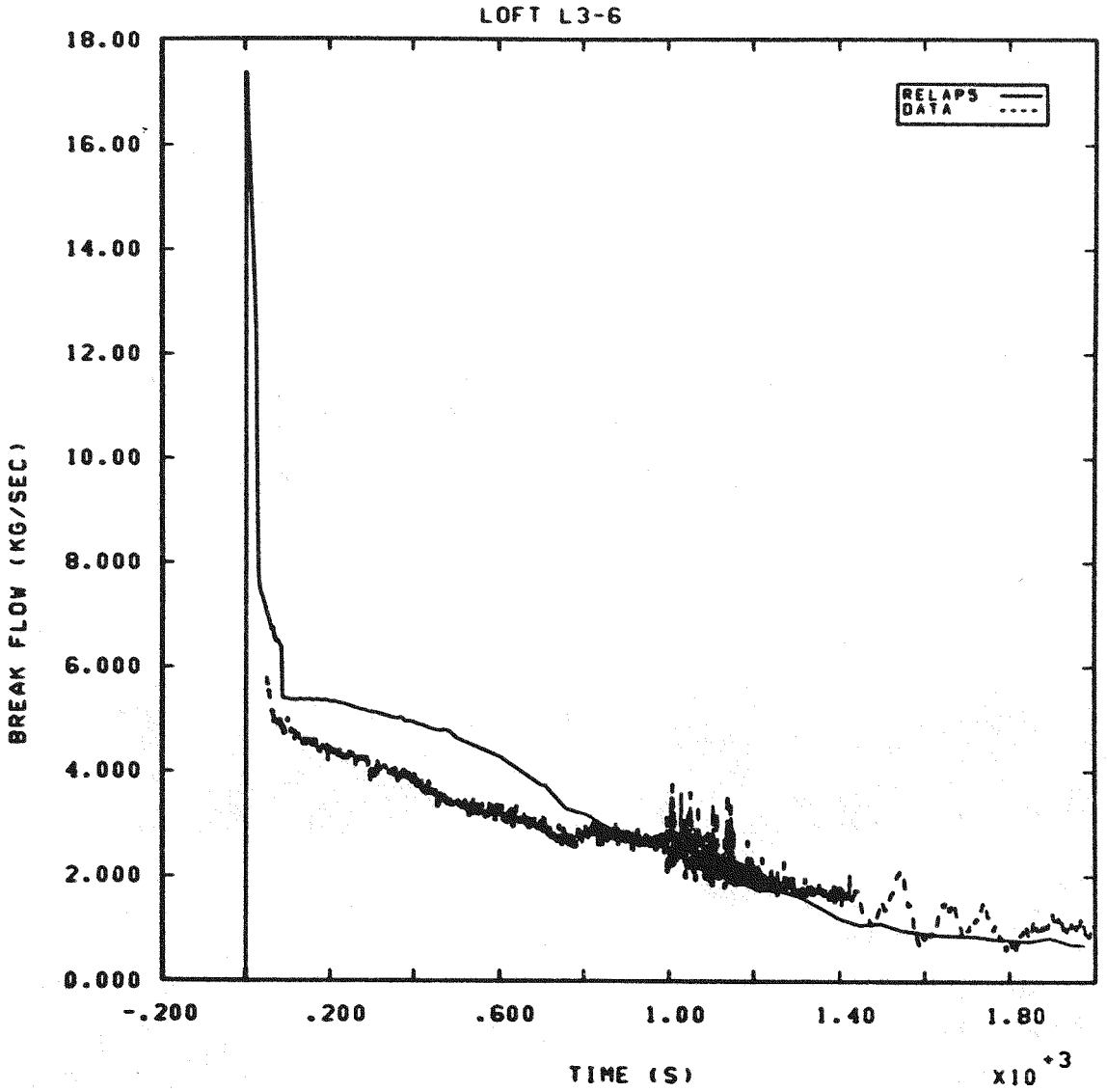

Figure 3.2.9 Calculated vs. Measured Break Flow for L3-6

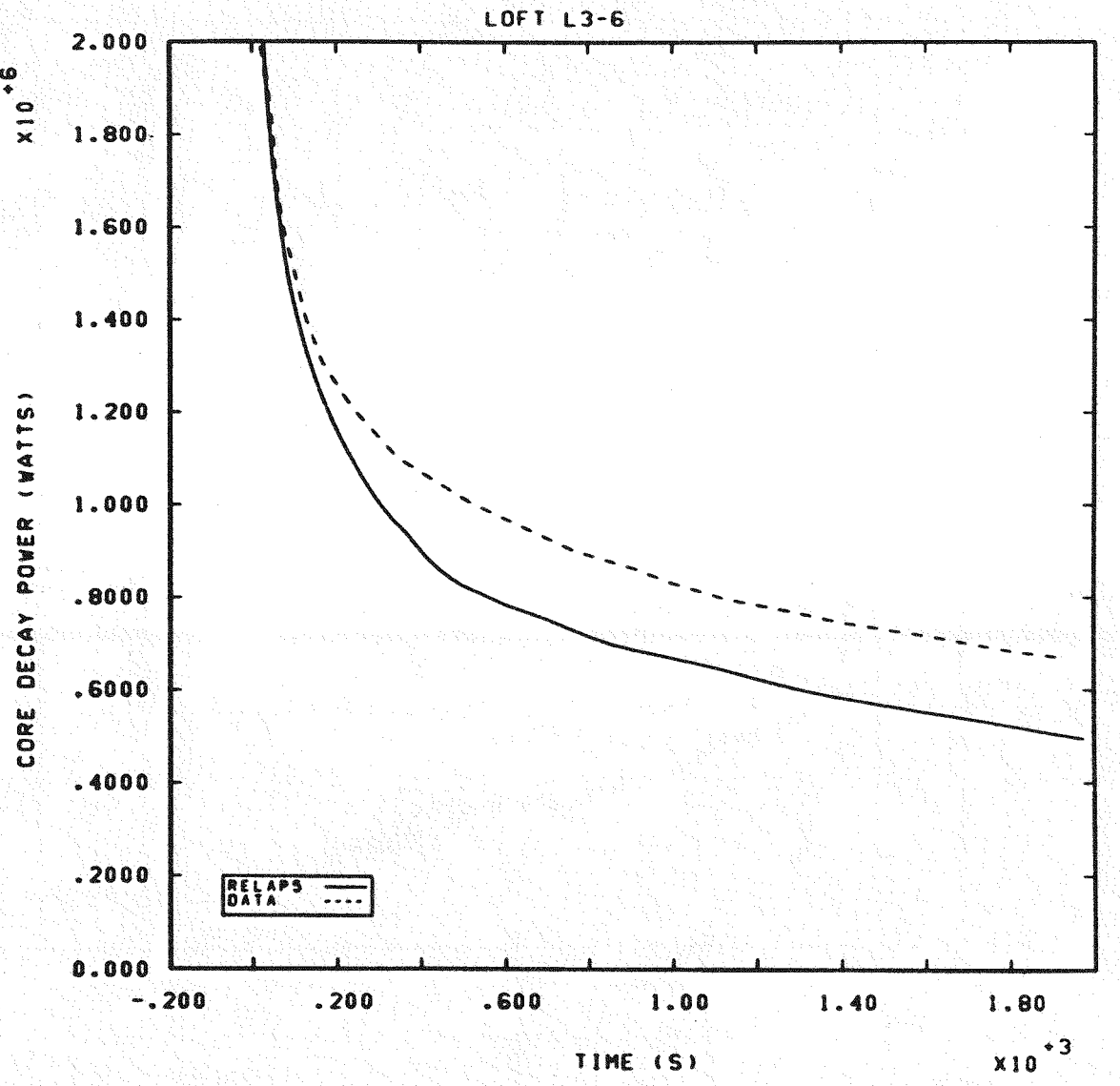

Figure 3.2.10 Calculated vs. Measured Core Decay Heat for L3-6

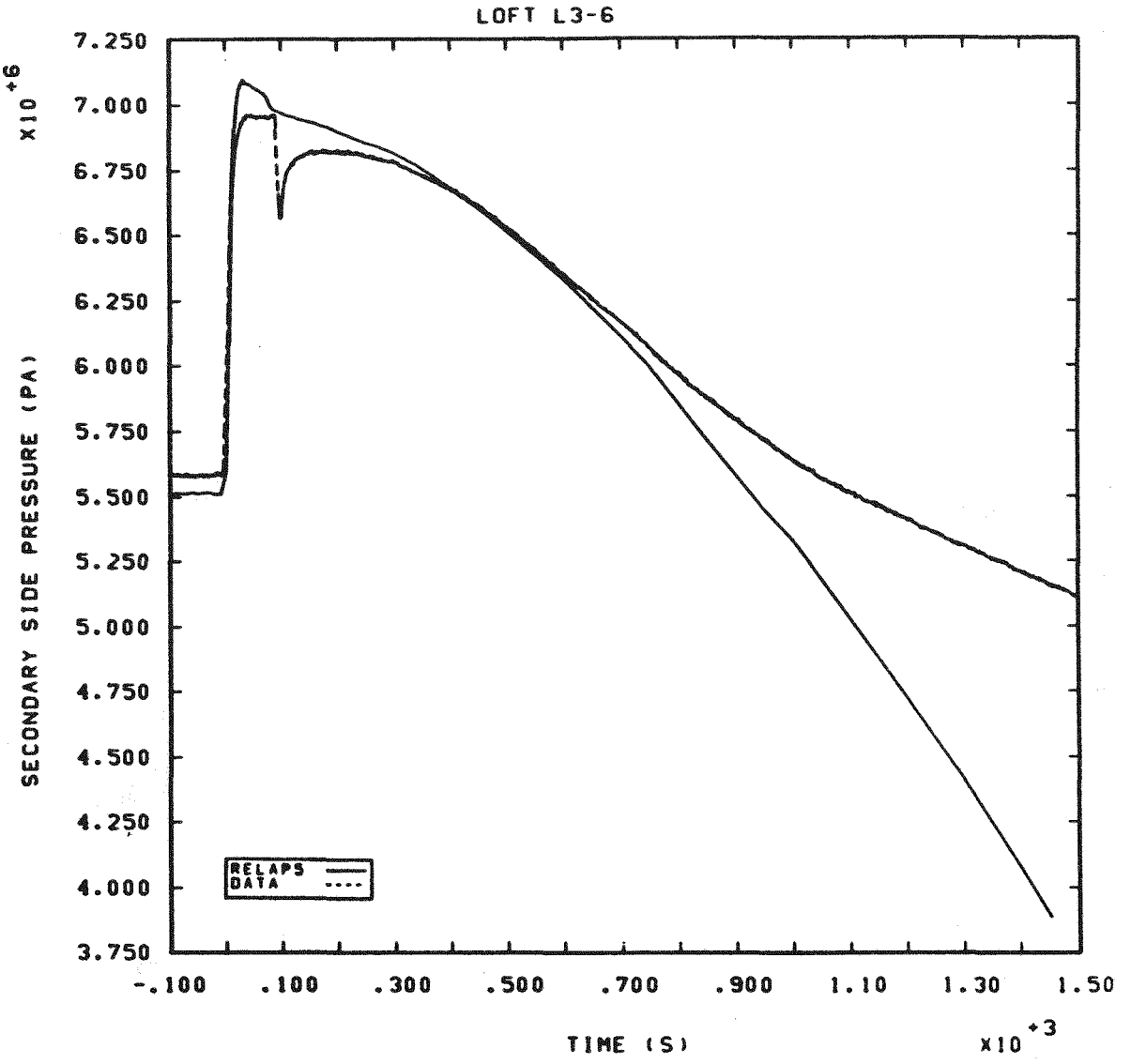

Figure 3.2.11 Calculated vs. Measured Secondary Side Pressure for L3-6 -- Turbine Trip Delayed

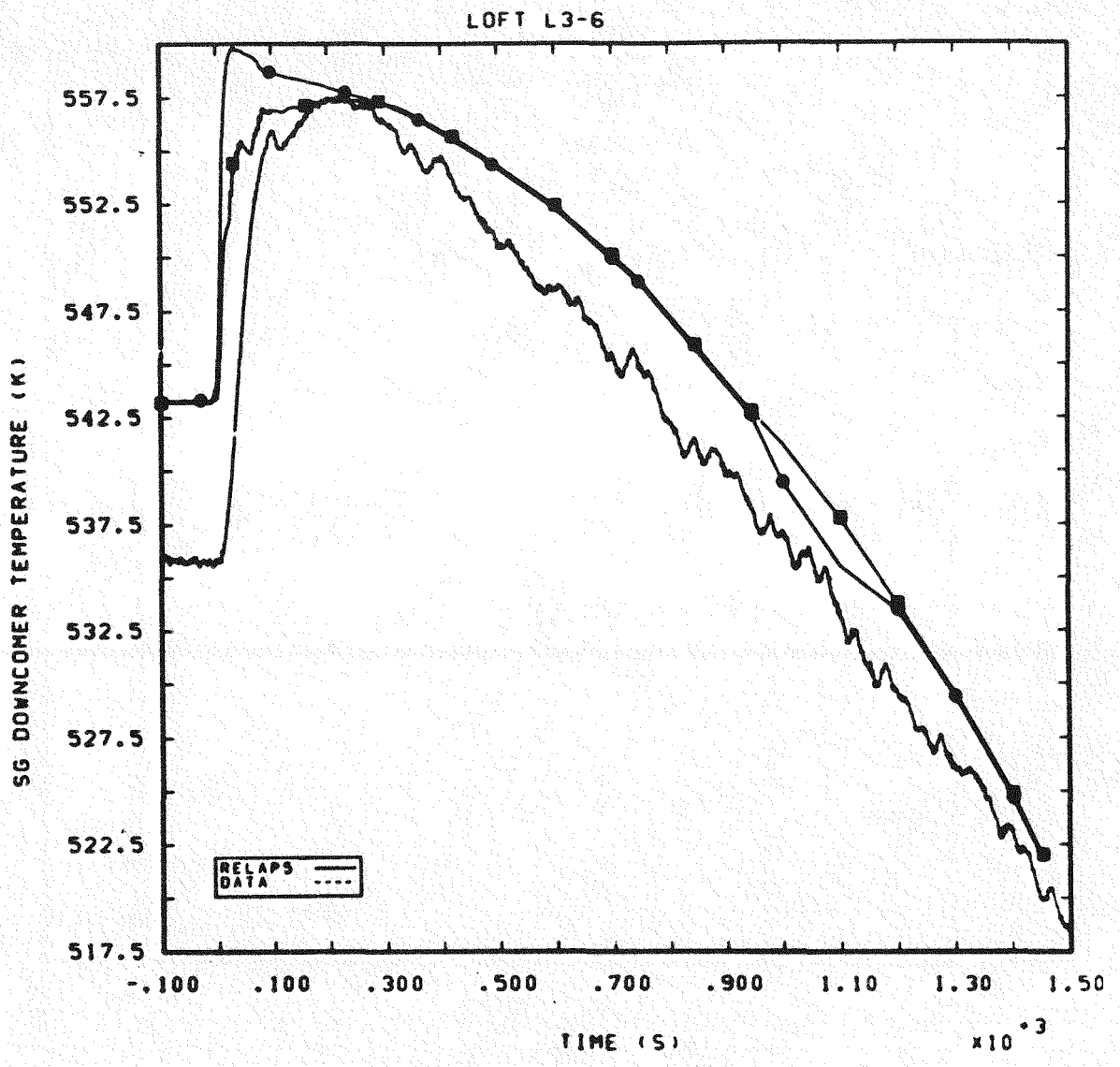

Figure 3.2.12 Calculated vs. Measured SG Downcomer Temperatures for L3-6 -- Turbine Trip Delayed

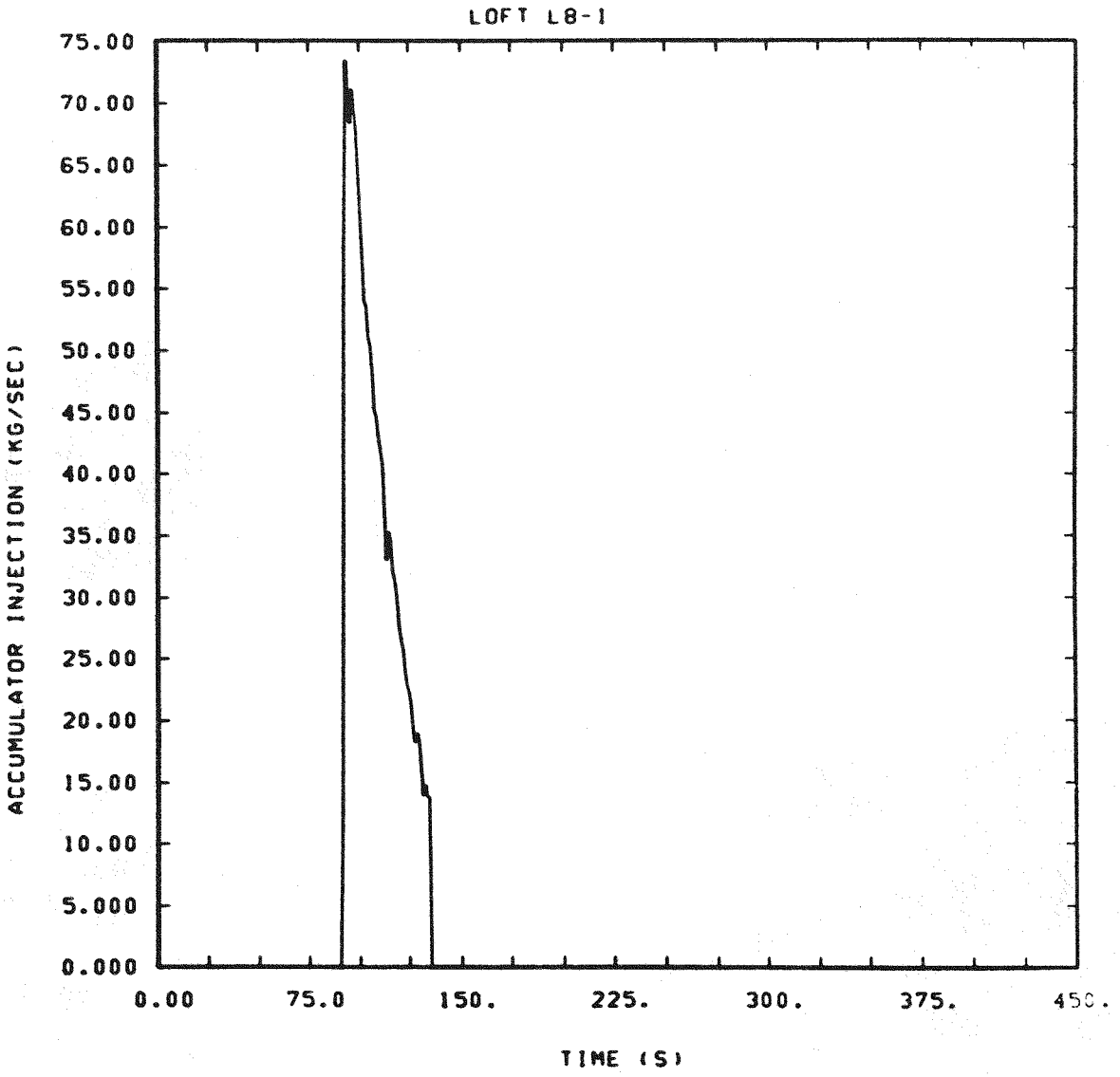

Figure 3.3.1 Estimated Accumulator Injection for L8-1

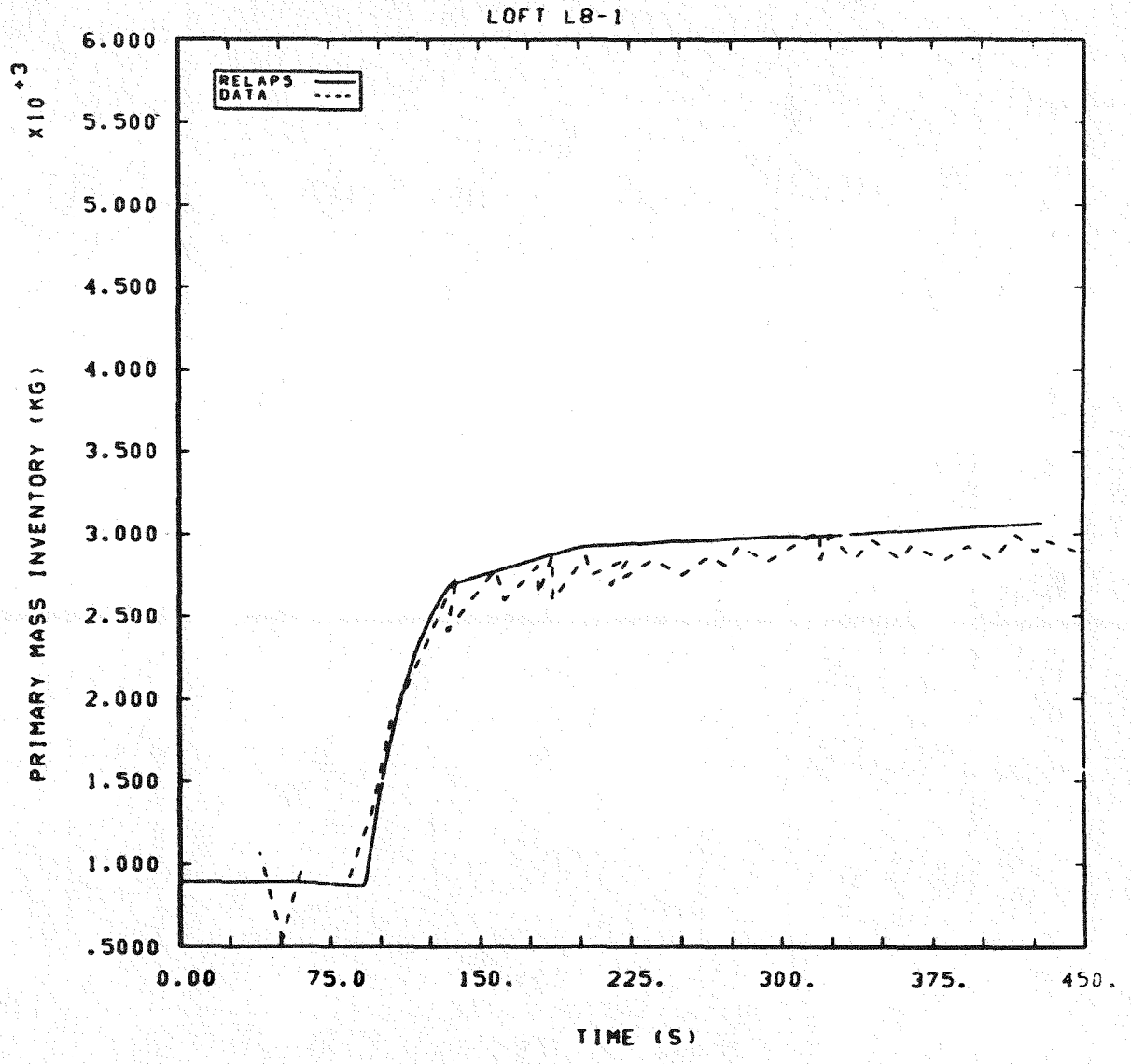

Figure 3.3.2 Calculated vs. Measured Primary System Mass Inventory for L8-1

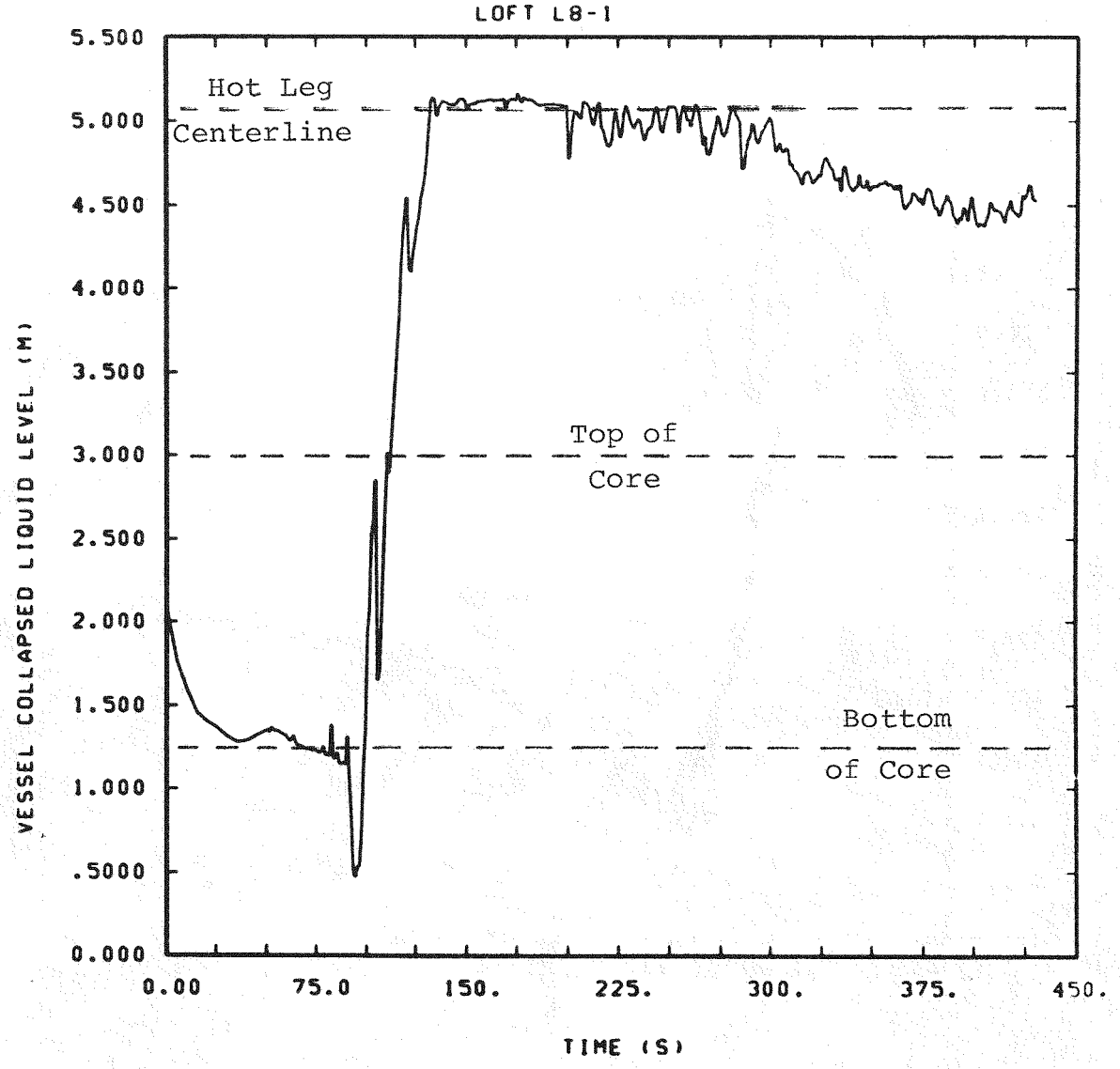

Figure 3.3.3 Calculated Core Collapsed Liquid Level for L8-1

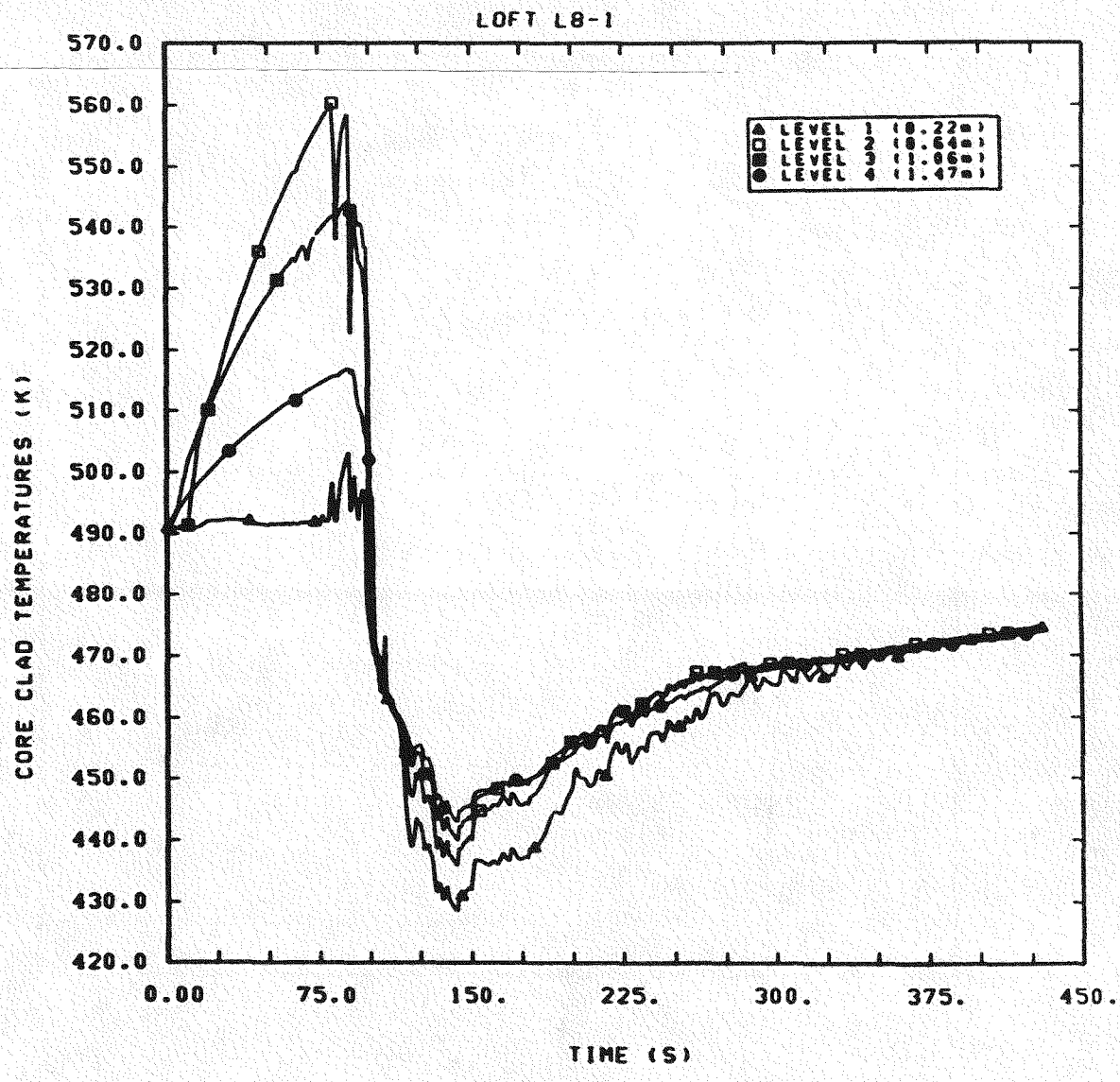

Figure 3.3.4 Calculated Core Clad Temperatures for L8-1

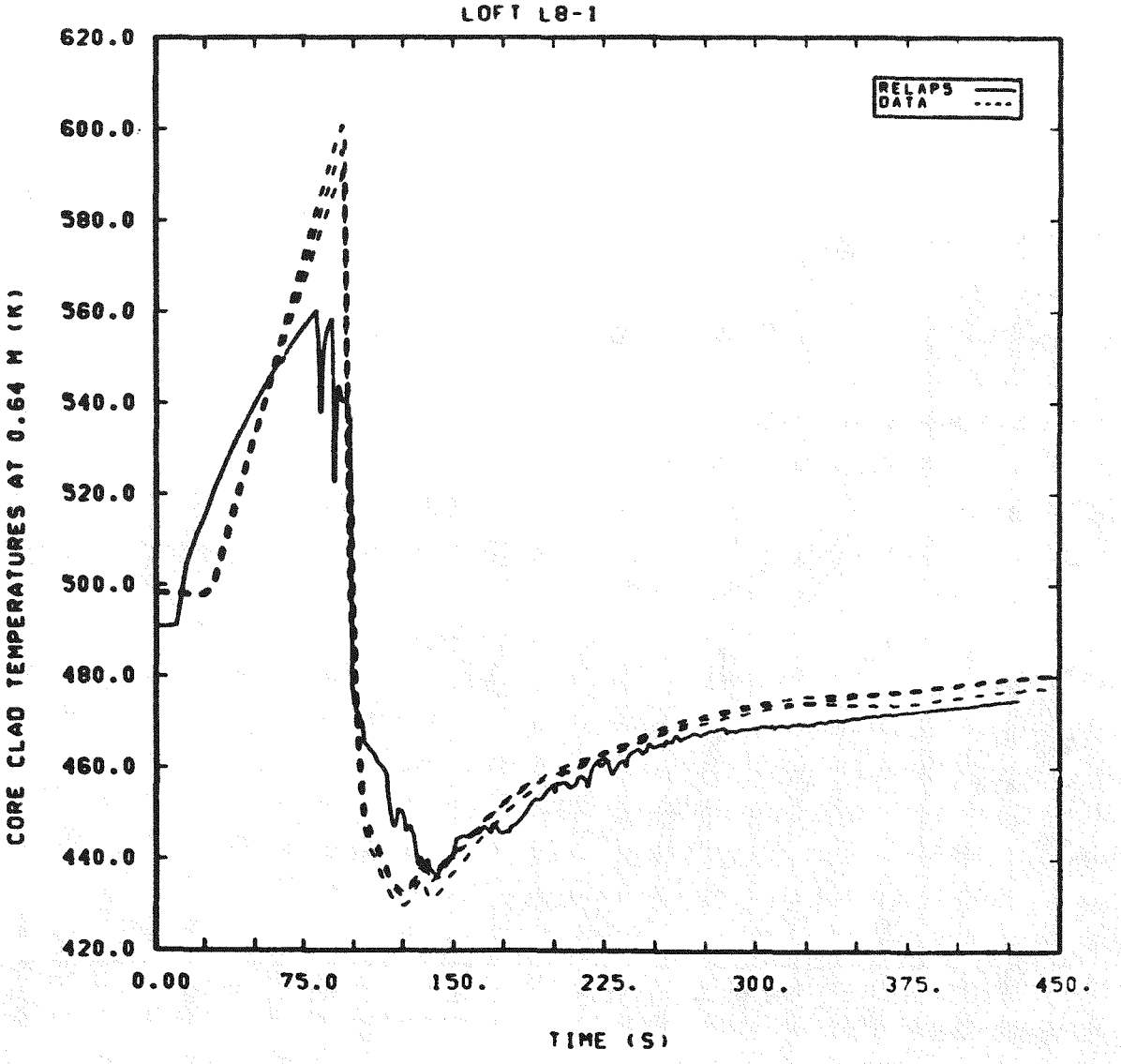

Figure 3.3.5 Calculated vs. Measured Core Clad Temperatures at 0.64 m Core Elevation for L8-1

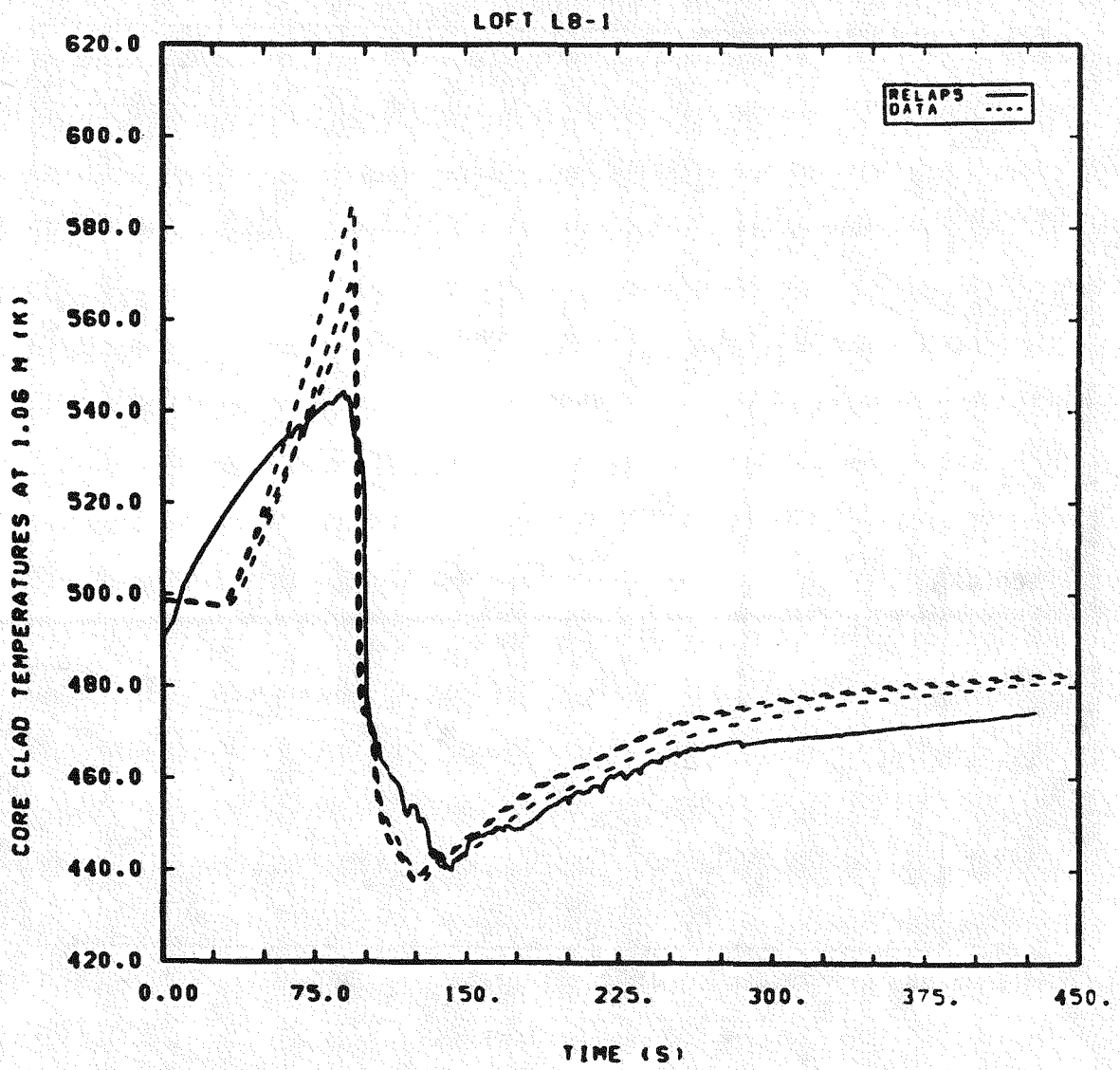

Figure 3.3.6 Calculated vs. Measured Core Clad Temperatures at 1.06 m Core Elevation for L8-1

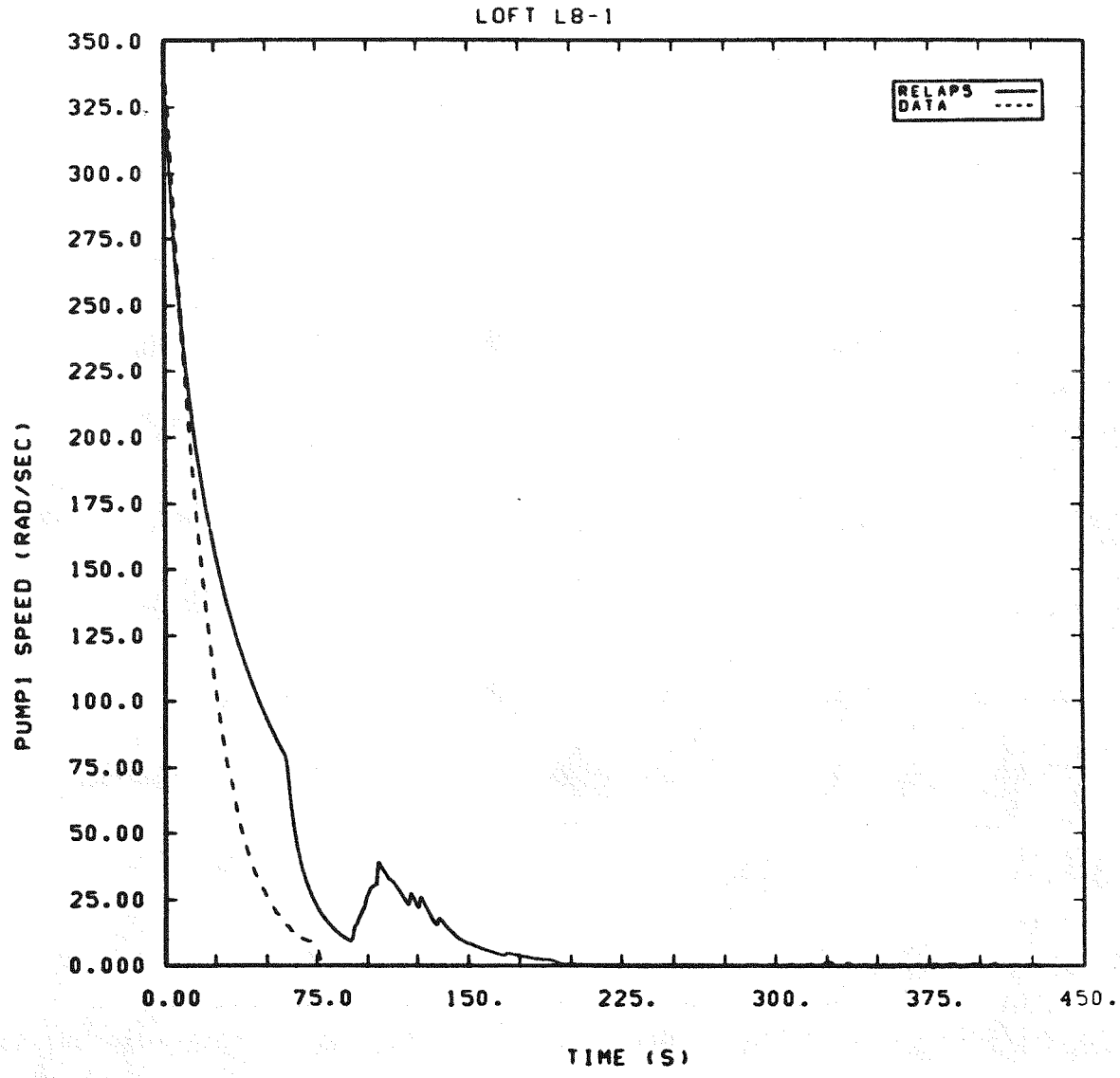

Figure 3.3.7 Calculated vs. Measured Pump Coastdown for L8-1

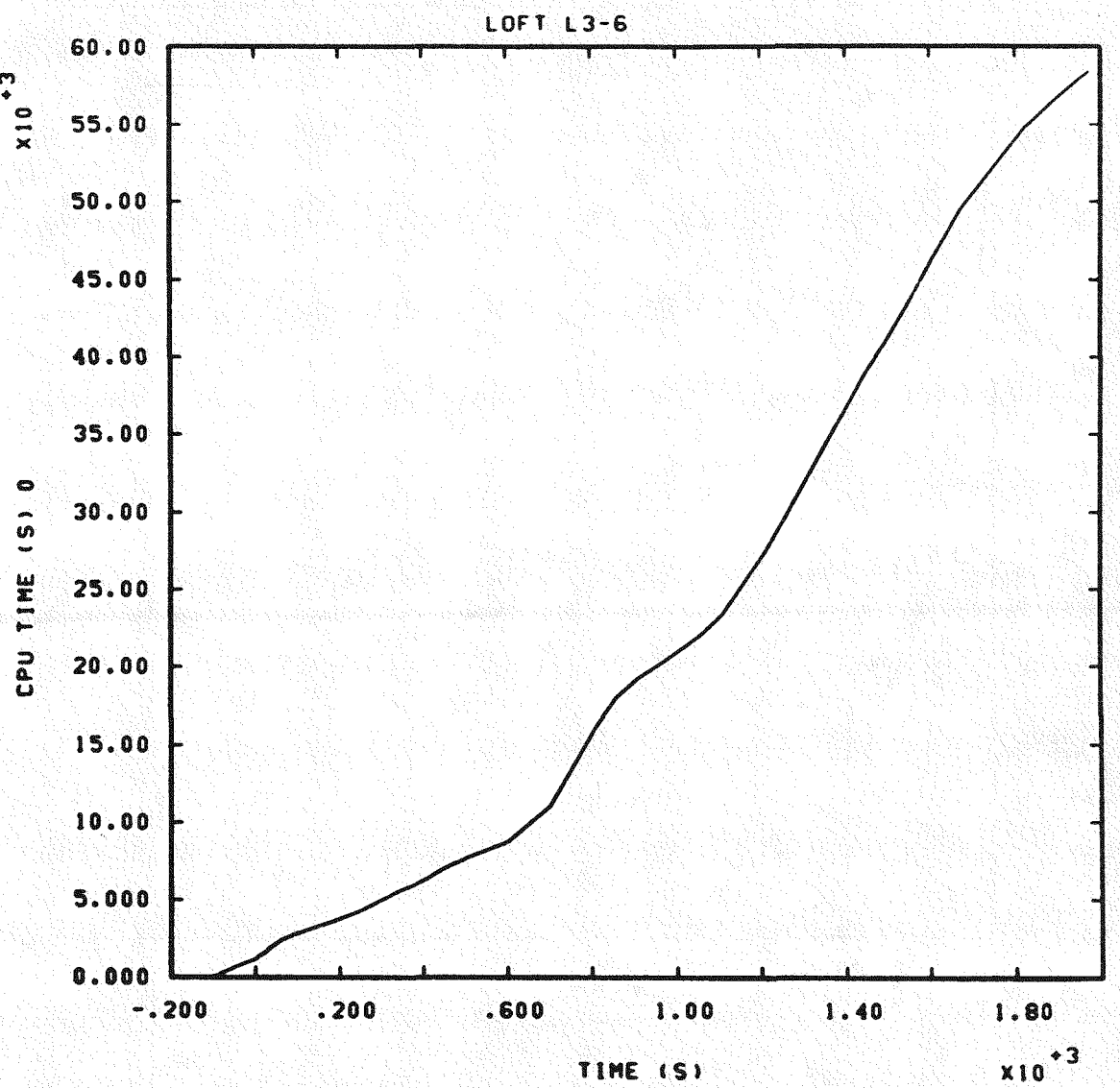

Figure 3.4.1 CPU Time Used for L3-6

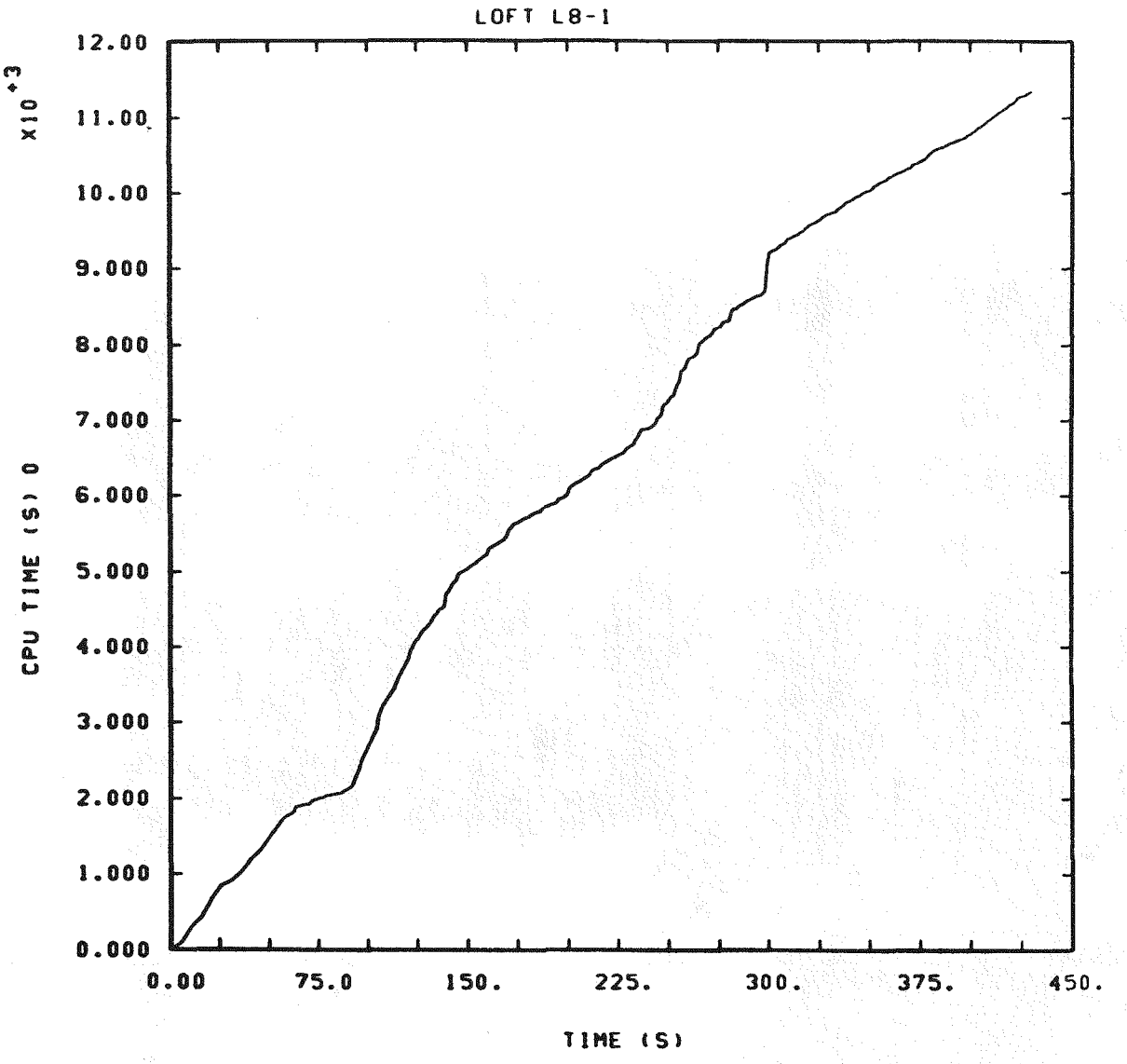

Figure 3.4.2 CPU Time Used for L8-1

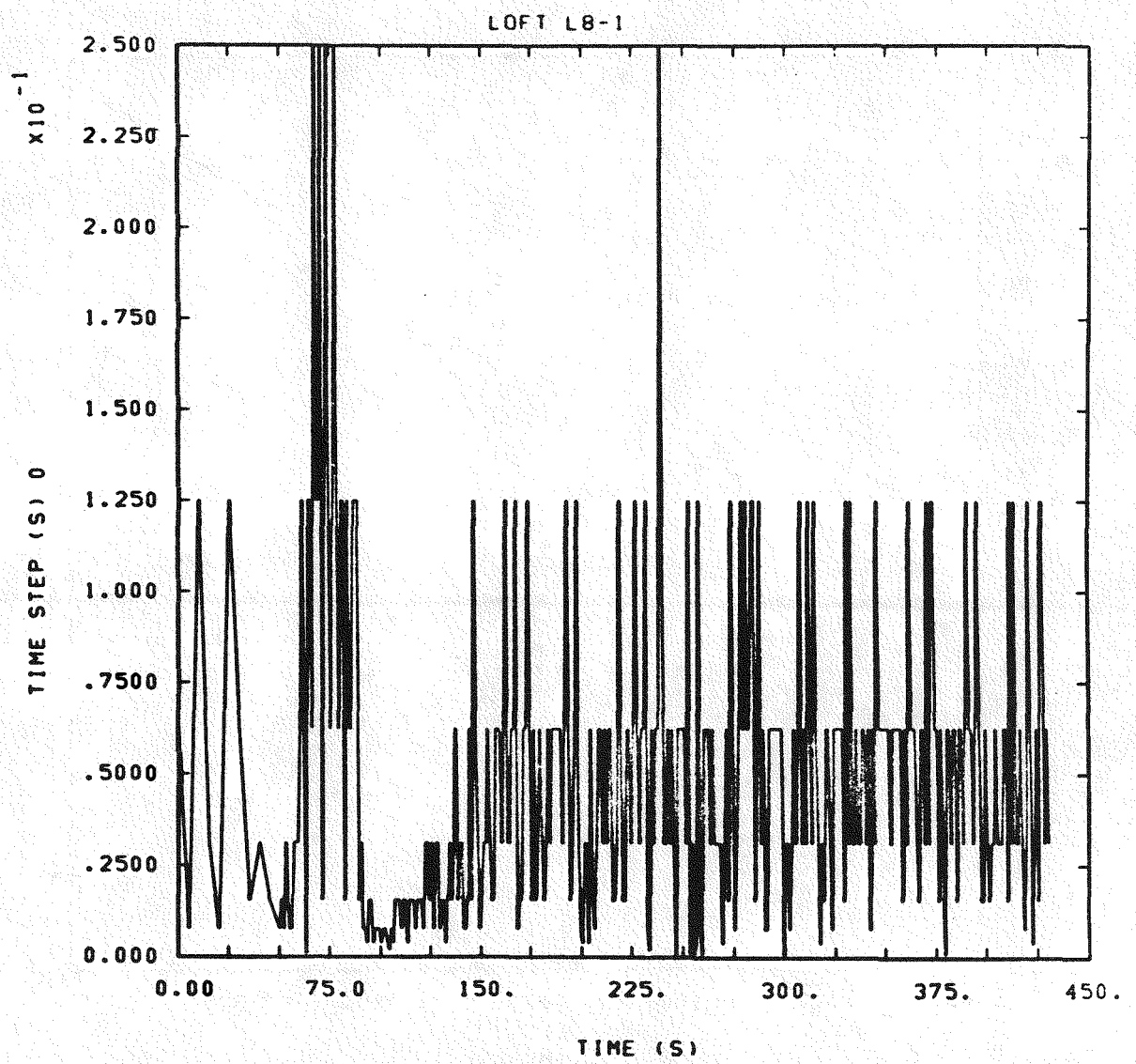

Figure 3.4.3 Time Step Used in L8-1

4.0 DISCUSSION AND CONCLUSIONS

RELAP5/MOD1 did a very good job of predicting all the overall qualitative features of these small break and subsequent core uncovery transients. The major quantitative discrepancy during the small break portion of the test (L3-6) was in the too-rapid primary depressurization, which in turn caused the transient (which ends on a pressure trip) to terminate too early and led to potentially different initial conditions for the follow-up core uncovery experiment. The discrepancy between calculated and measured primary depressurization could have been caused by any combination of: overprediction of steam generator heat transfer, overestimated break flow, overspecifying environmental heat loss, and underpredicting core decay heat. The excellent agreement in primary mass inventory throughout the transient would tend to preclude significant errors in break flow, although some disagreement is seen in predicted and observed break flow at early times. The behavior of the steam generator secondary side seems to indicate that the steam generator heat transfer is not correctly calculated during the latter parts of the transient, when the primary side depressurization deviates most from the data. The long run times required for this transient did not permit sensitivity studies on the effects of small variations in environmental heat loss, although given the quoted experimental value of 200 ± 100 kW the potential of improving agreement by varying this parameter is readily evident. The decay heat being calculated is low by ~20%, resulting in an error comparable to the total environmental heat loss estimated. A later version of MOD1 (cycle 18) does contain updates to "fix a reactor kinetics error that makes decay heat too low" [14], but we did not repeat this calculation with that version of the code due to cost constraints.

The discrepancy in the calculated and observed steam generator response during the reverse heat transfer regime in the later portions of the small break transient may or may not be related to the discrepancy in primary side depressurization during the same time period. The disagreement seen can easily be summarized -- the calculation shows the steam generator secondary behaving in an overall equilibrium and homogeneous manner at saturation conditions, while the admittedly limited data exhibits significant subcooling at the bottom of the secondary side after the onset of SG refill through aux feed injection. The subcooled auxiliary feedwater is in effect completely mixed with the saturated liquid inventory in the calculation, necessitating a simultaneous condensation of steam in order to maintain saturation conditions; the auxiliary feed thus has an overall depressurizing effect on the secondary side, contrary to data. The same behavior has been seen in other assessment calculations, both for other LOFT transients [10] and for a FLECHT SEASET steam generator separate effects test [12].

The latter in particular suggests that the nonequilibrium behavior on the secondary side of a steam generator in reverse heat transfer cannot be correctly calculated with MOD1. The presence of such a subcooled layer on the tube sheet in the separate effects test is closely associated with the propagation of a "quench front" up the insides of the U-tubes. This quench front cannot be calculated without a reflood model containing both a nonequilibrium heat transfer correlation package and a moving fine-mesh temperature grid, which will be available in RELAP5 in MOD1.5 and MOD2.

The discrepancy between calculated and measured primary side depressurization directly causes parallel discrepancies in various primary fluid temperatures, since after ~50 seconds saturation conditions prevail; the temperature discrepancy in turn causes a parallel discrepancy in core clad temperatures during the small break portion of the test. The code correctly predicts the presence of adequate core cooling until pump trip, although the core is certainly not liquid-full. (The code's hard-wired critical void fraction for dryout of 0.96 does cause a spurious dryout in one core level for a brief time.)

The code also correctly predicts the loss of core cooling immediately after pump trip. The clad temperatures after dryout are significantly below the experimentally observed values, with a calculated peak clad temperature of 561 K compared to a measured PCT of 637 K. The lower heatup observed is probably due mostly to the ~20% low decay heat being calculated, although lower starting temperatures, premature ECC injection, slower pump coastdown and higher primary side mass inventory may also be contributing factors. (The various discrepancies between calculation and experiment at the end of the small break transient L3-6 obviously preclude any significant quantitative comparison between calculation and experiment for the core uncovery transient L8-1.) Rapid core quench is observed at the correct time, but it is not clear in the calculation (with only four core levels) whether top-down quench is occurring, as in the test. (There is no significant downward flow of liquid during the quench time.) The calculation does show decreasing liquid subcooling with increasing core elevation after quench, indicating establishment of positive core flow.

The analysis was hampered by odd gaps in the experimental test description and data provided. The primary mass inventory, a key parameter in small break transients, was shown in the Quick-Look Report but not mentioned in the Experimental Data Report and not given on the data tape; the decay heat was shown in the Experimental Data Report but was not available on the data tape. The accumulator injection rate, an important boundary condition for L8-1, was not given anywhere (although the

appropriate instrumentation is listed as available), and the lack of any documentation on downcomer ECC injection piping geometry precluded any attempt to calculate the accumulator injection rate based on the RELAP5 accumulator model. The use of "unscaled" ECCS flow in L8-1 further complicated the issue. One major variable that could not be located in any of the experimental reports or on the data tape was the intact loop mass flow, although the required instrumentation certainly exists. The break mass flow is not given during the first ~50 seconds, the entire period of subcooled break flow. The steam generator response could be better analyzed if more instrumentation were available on the secondary side.

(Interpretation of the results obtained was also hampered by some lacks in the RELAP5 output variables available. In order to simplify the calculation of primary mass inventory, a variable called the component mass was added to our version of the code. Otherwise one would have to compute and then sum the average density times the geometric volume for every cell in the primary side nodalization. The analysis of the steam generator secondary side response would have been greatly simplified, in this and in other calculations, if the saturation temperature were available as an edit and plot variable.)

Finally (or rather, initially) we encountered various difficulties in trying to achieve a calculated steady state which matched all given the experimental initial conditions for the primary and secondary sides simultaneously, within the experimental uncertainties. The secondary pressure had to be reduced to its lowest possible experimental value to give good primary side cold leg temperature agreement, even after a substantial reduction in the secondary side equivalent diameter (which helps control the temperature gradient across the U-tubes). This problem has been encountered in the vast majority of our assessment calculations, but there are no documented changes or additions to future versions of RELAP5 which would alleviate the difficulty. The problem does not appear to be unique to RELAP5 since similar difficulties have been reported with TRAC [15], which suggests that it is inherent in the heat transfer correlation being used in the steam generator and its applicability to the outside of a tube bundle.

5.0 REFERENCES

1. V. H. Ransom, et al., RELAP5/MOD1 Code Manual Volume 1: System Model and Numerical Methods; Volume 2: Users Guide and Input Requirements, NUREG/CR-1826, EGG-2070, Idaho National Engineering Laboratory, March 1982.

2. D. L. Reeder, LOFT System and Test Description (5.5-ft Nuclear Core 1 LOCEs), NUREG/CR-0247, TREE-1208, Idaho National Engineering Laboratory, July 1978.

3. R. S. Semken, LOFT Small Experiment Operating Specification, Small Break Test Series L3, Severe Core Transient Test Series L8, Nuclear Experiment L3-6/L8-1, EGG-LOFT-5293, Idaho National Engineering Laboratory, December 1980.

4. G. E. McCreery, Quick-Look Report on LOFT Nuclear Experiment L3-6/L8-1, EGG-LOFT-5318, Idaho National Engineering Laboratory, December 1980.

5. P. B. Bayless and J. M. Carpenter, Experiment Data Report for LOFT Nuclear Small Break Experiment L3-6 and Severe Core Transient Experiment L8-1, NUREG/CR-1868, EGG-2075, Idaho National Engineering Laboratory, January 1981.

6. L6-7 Experiment Prediction Deck (LOFT L67-G07), private communication from D. Hall, INEL.

7. Handout at Joint LOFT/Semiscale Modelling Workshop, August 18-19, 1981, at Idaho Falls, ID.

8. W. H. Giedt, Principles of Engineering Heat Transfer, Van Nostrand, Princeton NJ, 1957.

9. S. L. Thompson and L. N. Kmetyk, RELAP5 Assessment: LOFT Turbine Trip L6-7/L9-2, NUREG/CR-3257, SAND83-0832, to be published.

10. R. K. Byers and L. N. Kmetyk, RELAP5 Assessment: LOFT L9-1/L3-3 Anticipated Transient with Multiple Failures, to be published.

11. R. M. Summers, RELAP5 Assessment: Semiscale Mod-3 S-SB-P Small Break Tests, to be published.

12. L. N. Kmetyk, RELAP5 Assessment: FLECHT SEASET Steam Generator Test 23402, NUREG/CR-2887, SAND82-2894, Sandia National Laboratories, January 1983.

13. T. K. Knight to L. N. Kmetyk, private communication.

14. R. J. Wagner, "RELAP5/MOD1 Update Synopsis and Listing of Updates to Create Cycle 19", RELAP5 News No. 2, Idaho National Engineering Laboratory, November 1982.

15. T. K. Knight, "U-Tube Steam Generator Modelling", TRAC Newsletter No. 7, Los Alamos Scientific Laboratory, May 1982.

APPENDIX I FACILITY DESCRIPTION

The Loss-of-Fluid Test (LOFT) facility [2] is located at the Idaho National Engineering Laboratory and supported by the NRC. The facility is a 50 MWt pressurized water reactor (PWR) with instrumentation to measure and provide data on the thermal/hydraulic conditions during a postulated accident. The experimental assembly includes five major subsystems: the reactor vessel, the intact loop (scaled to represent three operational loops), the broken loop, the blowdown suppression system and the emergency core cooling system (ECCS). The general philosophy in scaling coolant volumes and flow areas was to use the ratio of the LOFT core power (50 MWt) to a typical PWR core (3000 MWt). A summary of the LOFT primary volume distribution is given in Table AI.1. The LOFT configuration for test L3-6/L8-1 is shown in Figure AI.1.

The intact loop, shown in Figure AI.2, simulates three loops of a commercial four-loop PWR and contains a steam generator, two primary coolant pumps in parallel, a pressurizer, a venturi flowmeter and connecting piping (and, for L3-6/L8-1, the break assembly).

The coolant leaves the reactor vessel outlet nozzle through 14-in. Schedule 160 piping and proceeds to the steam generator inlet through a venturi flowmeter. The steam generator inlet is slightly higher than the reactor vessel outlet nozzle. The piping entering and leaving the steam generator is 16-in. Schedule 160. After dropping to the level of the reactor vessel nozzles, it proceeds into a 14-in. reducer and then down into a tee. At this point, the piping branches into two 10-in. Schedule 160 lines and proceeds to the pump inlets. A 10-in. Schedule 160 pipe connects the pump outlets to a tee, at which point the loop becomes 14-in. Schedule 160 piping joining the reactor vessel inlet. A brief summary of the intact loop piping is given in Figure AI.3 and Table AI.2.

The pressurizer includes a vertical cylindrical pressure vessel, immersion-type electrical heaters, a surge nozzle, pressure relief and spray nozzles. The surge line connects to the primary coolant loop between the flow venturi and the reactor vessel. The spray line connects to the primary coolant system downstream of the pump discharge. Pressure is increased by energizing the electric immersion heaters and decreased by spray flow of relatively cool primary coolant into the steam space. The pressurizer is described in Figure AI.4, while the surge line piping is summarized in Figure AI.5 and Table AI.3.

The steam generator is a vertical shell and U-tube recirculation-type heat exchanger with primary coolant flow in the tube side and secondary coolant in the shell side. The steam generator, located between the reactor outlet and primary coolant pump suction, is elevated such that its entire primary volume will tend to drain into the reactor vessel. Orifices are installed in the inlet and outlet plena to scale primary flow through the intact loop for simulation of PWR response to a LOCA. Penetrations in the shell are provided for the steam outlet, feedwater inlet, top and bottom blowdown, level control, draining, and primary coolant inlet and outlet. The steam generator is shown in Figure AI.6 and some steam generator design parameters are given in Tables AI.4 and AI.5.

The broken loop, shown in Figure AI.7, consists of a hot leg and a cold leg that are connected to the reactor vessel and the blowdown suppression tank header. Each leg consists of a break plane orifice, a quick-opening blowdown valve, an isolation valve, and connecting piping. Recirculation lines (not shown) establish a small flow from the broken loop to the intact loop and are used to warm up the broken loop prior to experiment initiation. The broken loop hot leg also contains a simulated steam generator and a simulated pump; these simulators have hydraulic orifice plate assemblies which have similar (passive) resistances to flow as an active steam generator and pump. A brief summary of the broken loop piping is given in Figure AI.8 and Table AI.6.

The break location for L3-6/L8-1 is not in the broken loop, but is instead in the cold leg of the intact loop between the primary coolant pumps and the reactor vessel. The break orifice is in a pipe that connects the intact loop cold leg to the blowdown suppression tank (BST). The two new spool pieces and small break orifice installed for L3-5 and also used in L3-6 are shown in Figure AI.9; the small break orifice has a diameter of 1.619 cm (0.6374-in).

The blowdown suppression system consists of the blowdown suppression tank (BST) itself, the BST header, the nitrogen pressurization system and the BST spray system. The blowdown header is connected to the suppression tank downcomers which extend inside the tank below the water level. The header is also directly connected to the BST vapor space to allow pressure equilibration. The nitrogen pressurization system is supplied by the LOFT inert gas system and uses a remote-controlled pressure regulator to establish and maintain the specified BST initial pressure. The spray system consists of a centrifugal pump that discharges through a heatup heat exchanger and any of three spray headers or a pump recirculation line that contains a cooldown heat exchanger. The spray pump suction can be aligned

to either the BST or the borated water storage tank. The three spray headers have flow rate capacities of 1.3, 3.8 and 13.9 l/s, respectively, and are located in the BST along the upper centerline. For L3-6/L8-1, the BST header was not used to carry flow. Break flow entered the BST via a 4-in. pipe which was connected to the end of the BST and discharged below the water level. The BST spray pump suction was connected to the BST and the liquid in the tank was recirculated at full spray pump capacity.

The LOFT ECCS simulates the ECCS of a commercial PWR. It consists of two accumulators, a high-pressure injection system and a low-pressure injection system. Each system is normally arranged to inject scaled-down flow rates of emergency core coolant directly into the primary coolant system intact loop cold leg. Typical flow rates for accumulator injection might be 10-15 kg/sec and for HPIS flow would be 0.4-0.7 kg/sec. During L3-6, the accumulators were not used and scaled-down HPIS flow was directed into the reactor downcomer. During the reflood portion of L8-1, both HPIS pumps and one accumulator injected full-scale flow into the reactor downcomer. The accumulator flow was estimeted to be as high as ~70 kg/sec, and the HPIS flow was about 1.8 kg/sec for each of the two pumps. (The LPIS pumps were not used during this set of experiments.)

The LOFT reactor vessel, shown in Figure AI.10, has an annular downcomer, a lower plenum, upper and lower core support plates, a nuclear core and an upper plenum. The vessel volume distribution is given in Table AI.7, and the metal mass present is summarized in Table AI.8. The station numbers in Figure AI.10 are explained in Table AI.9.

The reactor vessel itself is a vertical stainless steel clad, low alloy steel cylinder with a semi-elliptical bottom head and a flanged, bolted two-piece top head. The vessel has two primary coolant inlet and outlet nozzles in the same plane above the core; they are diametrically opposite and provide the interface between the primary coolant and the reactor systems. The core support barrel, a single stainless steel structure, is a cylindrical barrel with a heavy top flange whose shoulder rests on the reactor vessel; the flange is also counterbored to accept the upper core support plate assembly. The cylindrical section of the core barrel has approximately a 0.76 m (30-in) ID, 4.6 m (15.1-ft) length and 0.04 m (1.5-in) wall thickness. Outlet nozzles in the core barrel are aligned with the reactor vessel outlet nozzles. An interior shoulder at the lower end of the barrel supports the lower core support structure. The core support barrel forms the inside of the annular downcomer, separates the inlet from the outlet coolant, and also serves as the outside of the cylindrical outlet plenum above the core.

The core support structure consists of three assemblies: the upper core support plate, the upper core support tubes and the lower core support structure. The upper core support plate is a 0.99 m (39-in) diameter, 0.18 m (7-in) thick plate made of Type 304 stainless steel, bolted to a ledge in the core support barrel. It has a 0.23 m (9-in) square hole in the center (which provides access for the replacement of the center fuel module) and four circular holes (for passage of control rod shafts). The lower core support structure, seated on the interior ledge of the core support barrel, is made of Type 304 stainless steel. It is basically a three-plate assembly surrounded by a cylindrical shell with an outside diameter approximately the same as the inside diameter of the core support barrel (the lower core support skirt). Support for the three plates is provided by the cylinder and inner structural columns. The upper (core mounting) plate is 38 mm (1-1/2-in) thick and has 24 round flow distribution holes. The intermediate (diffuser) plate acts as a diffuser to improve coolant distribution to the core; it is 0.025 m (1-in) thick and is supported only by the interior structure (columns). The flow paths for the coolant are through 1543 holes in the diffuser plate and 154 holes through the lower core support skirt. The bottom core support plate has a 0.76 m (29.96-in) outside diameter and a 0.11 m (4.22-in) thickness; coolant flow through this plate is through five 0.15 m (6-in) square holes and four 0.1 m (3.9-in) circular holes.

The flow skirt and core filler assembly are considered as one assembly due to the similarity of purpose and design. The core filler is fabricated by bolting relatively small sections to the flow skirt. The flow skirt and core filler assemblies consist of three subassemblies which stack vertically to form a structure that lines the length of the core support barrel above the lower core support structure. Core filler subassemblies have the same length as the flow skirt sections and are permanently attached to them. The fillers occupy the volume between the flow skirt and the fuel assembly envelope. Coolant bypass channels (discussed below) are provided through and around the flow skirt core filler to limit the temperature rise in this assembly due to nuclear heating.

The purpose of the reactor vessel fillers is to displace excess coolant in the inlet and downcomer regions to maintain a ratio of water in the inlet and downcomer to that in the core and primary system similar to the ratio found in a PWR; the fillers also serve to distribute inlet coolant and ECC downcomer flow. The filler assemblies form the outer edge of the annular downcomer regions. A 0.05 m (2-in) thick annulus is formed with the core support barrel except in the nozzle region where a 0.089 m (3.5-in) thick by 0.69 m (27-in) high annulus is formed. This larger annulus links the two inlet nozzles and acts as a main flow distribution channel. A thin [6.4 mm (0.25-in)] secondary annular downcomer is formed by the clearance between the filler assembly and the reactor vessel.

The flow has several paths available when it enters the reactor vessel. The main flow path is around the distributor annulus, down the downcomer, through the core, and out the outlet nozzles. There are several alternate paths available which do not direct the coolant through the core; these are termed core bypass paths. Figure AI.11 shows the reactor flow paths schematically. There are five possible core bypass flow paths (paths 1 through 5) and one path (path 6) which allows communication between the core and a bypass path. These are shown and numbered in Figure AI.10 and detailed in Figure AI.12. Path 1 allows coolant to flow between the lip at the bottom of the core support barrel and the lower core support plate. From there it travels between the lower core support structure and the core barrel upwards to the bottom of the flow skirt, then travels in the annulus between the core barrel and support skirt to the top of the support skirt and into the hot leg nozzle region. Path 2 allows coolant which has gone through the lower core support structure to flow underneath the core filler blocks and in the gap between the filler blocks and the flow skirt or in the gaps between the filler blocks. This path has the opportunity to communicate with the core at station 173.236. The coolant entering path 2 will either flow in the flow skirt-filler block gaps to the top of the upper flow skirt or communicate with the core flow at the lower to intermediate flow skirt mating or the intermediate to upper flow skirt mating. Path 3 allows coolant to flow from the downcomer directly into the core support barrel-flow skirt annulus. After the coolant enters the core support barrel-flow skirt annulus, it flows upward to the top of the flow skirt and into the hot leg nozzle region. Path 4 allows coolant to flow from the cold leg nozzle region directly to the hot leg nozzle region. The coolant flows in the gap between the reactor vessel filler blocks and the reactor vessel and then through the gap between the core support barrel hot leg nozzle and the reactor vessel into the hot leg nozzle area. Path 5 allows coolant to flow from the cold leg nozzle region into the upper plenum. The controlling flow areas and their equivalent diameters, as well as the nominal flow rates in each bypass, are given in Table AI.10.

The 1.68 m (5.5-ft) core used in LOFT is designed to have the same physical, chemical and metallurgical properties as those in PWRs. It is also designed to provide thermal/hydraulic relationships, mechanical response, and fission product release behavior during the LOCEs and ECC recovery which are representative of PWRs during a LOCA. The core contains 1300 unpressurized nuclear fuel rods arranged in five square (15 x 15) assemblies and four triangular (corner) assemblies, shown in Figure AI.13. The center assembly is highly instrumented. Two of the corner and one of the square assemblies are not instrumented. The fuel rods have an active length of 1.67 m and

an outside diameter of 10.72 mm. The fuel consists of UO-2 sintered pellets with an average enrichment of 4.0 wt% fissile uranium (U-235) and with a density that is 93% of theoretical density. The fuel pellet diameter and length are 9.29 and 15.24 mm, respectively. Both ends of the pellets are dished with the total dish volume equal to 2% of the pellet volume. The cladding material is Zircaloy-4. The cladding inside and outside diameters are 9.48 and 10.72 mm, respectively.

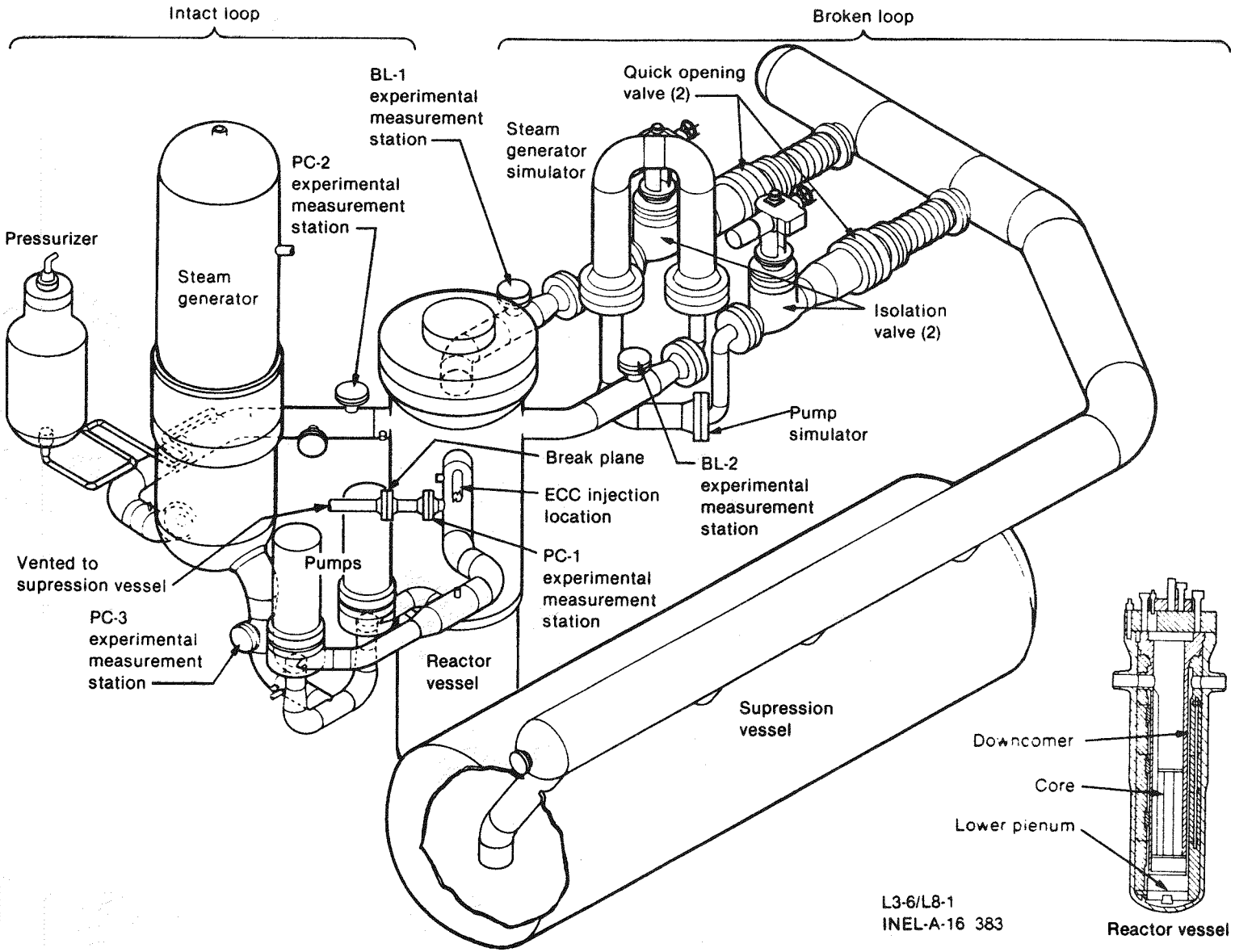

Figure AI.1 LOFT Configuration for L3-6/L8-1

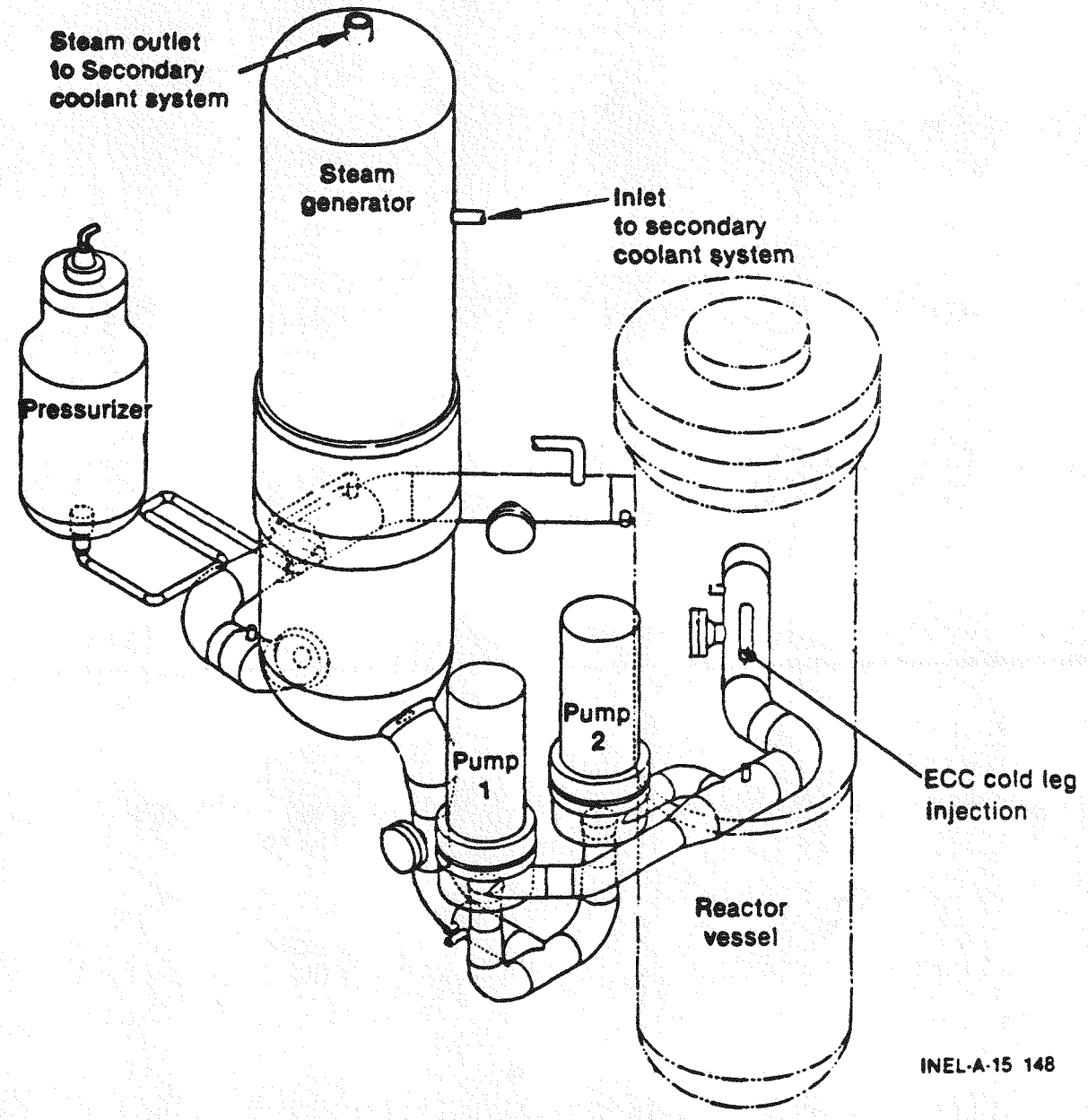

Figure AI.2 LOFT System -- Intact Loop

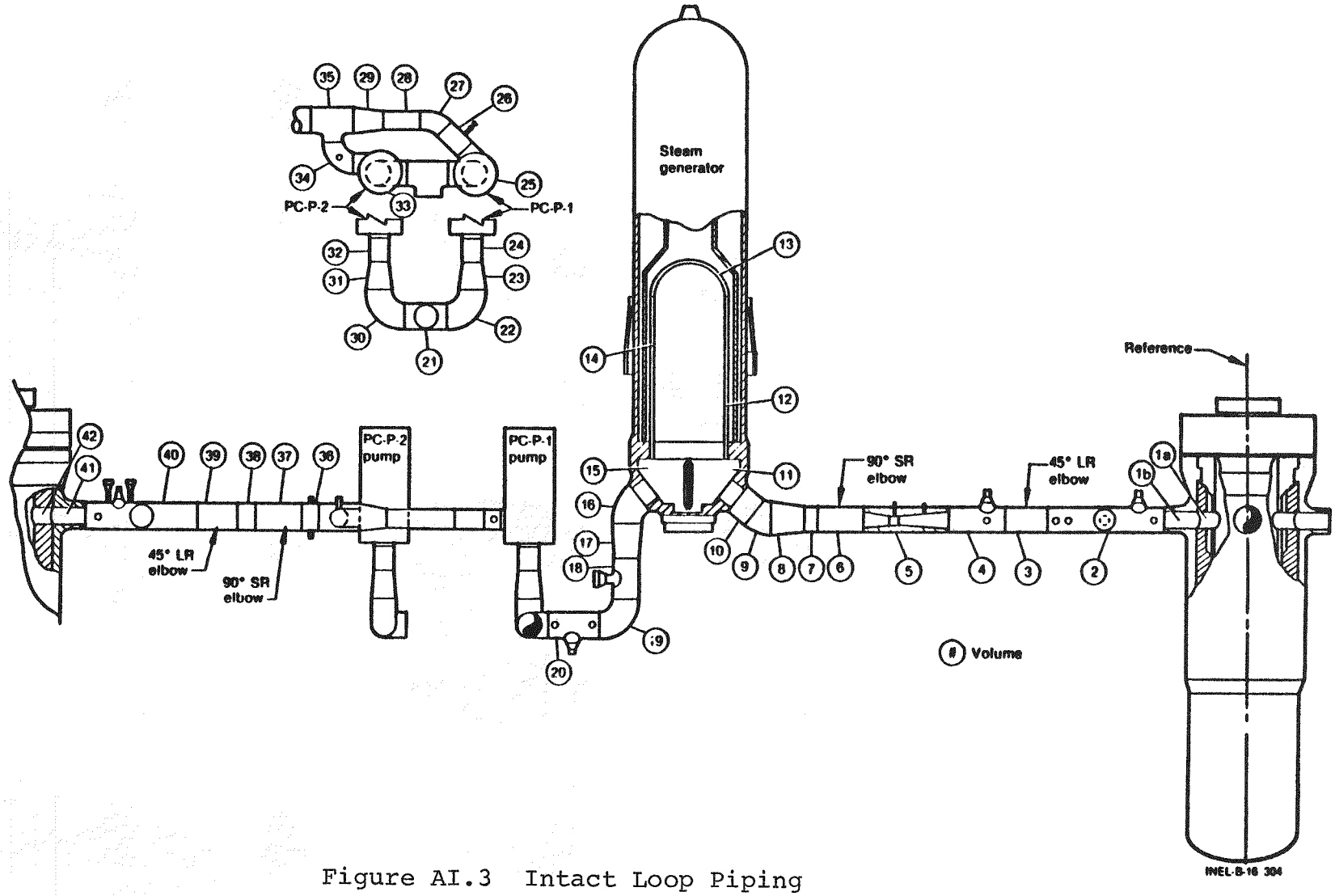

Figure AI.3 Intact Loop Piping

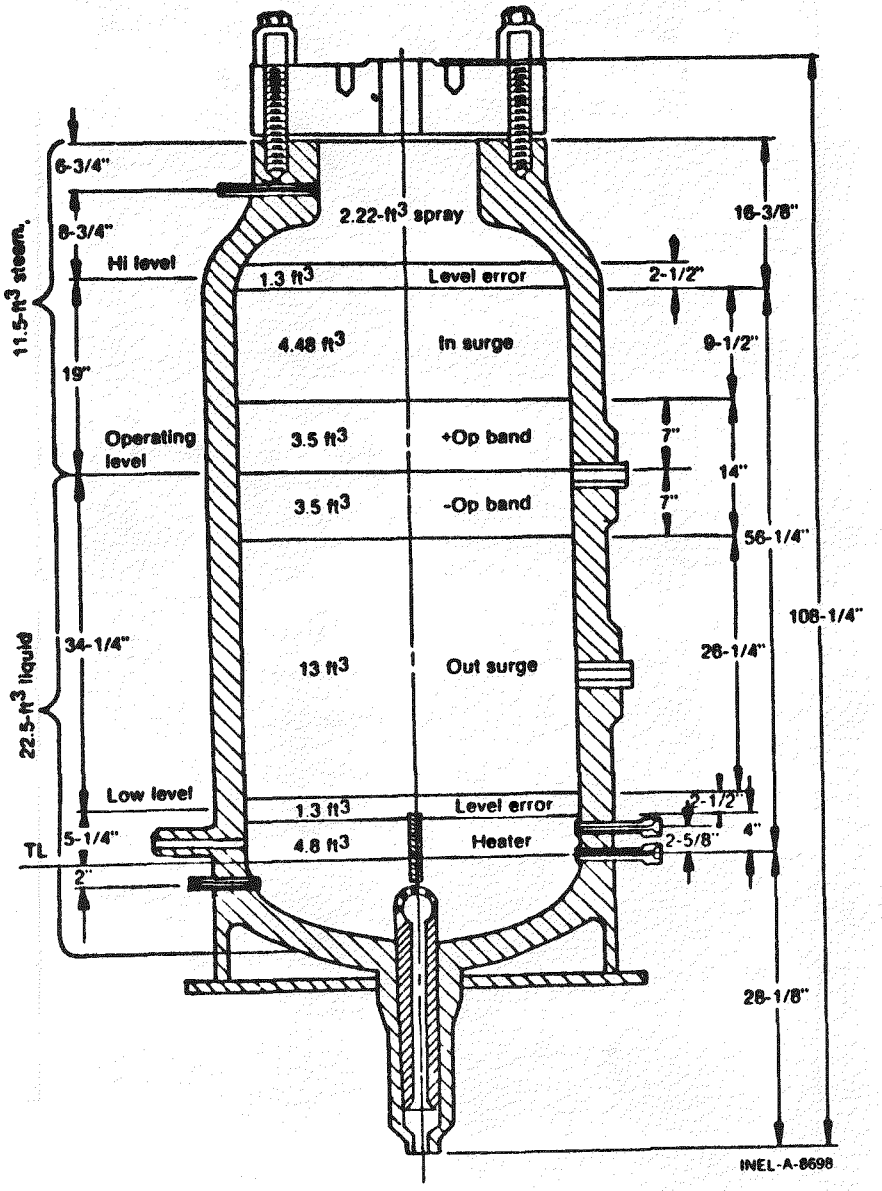

Figure AI.4 Pressurizer Geometry

THERMAL-HYDRAULIC DATA -- PRESSURIZER

Parameter	Value
Normal operating pressure	15.51 MPa (2250 psig)
Normal operating temperature	617 K (650°F)
Normal variation in pressure	
Operating[a]	±0.10 MPa (±15 psia)
Accuracy[a]	±0.31 MPa (±45 psia)
Pressurizer volume	0.96 m^3 (34 ft^3)
Steam volume	0.33 m^3 (11.5 ft^3)
Liquid volume	0.64 m^3 (22.5 ft^3)
Volume/MW(t)	0.0175 m^3/MW(t) [0.618 ft^3/MW(t)]
Maximum heater input by heaters	48 kW
Continuous spray flow	0.03 l/s (0.5 gpm)
Spray rate (maximum)	1.26 l/s (20 gpm)
Spray nozzle differential pressure at maximum spray rate and 555 K (540°F)	0.13 MPa (20 psid)

[a] The error band of the pressure transducers is ±0.310 MPa (±45 psia); however, the transducers are repeatable within 0.103 MPa (±15 psia).

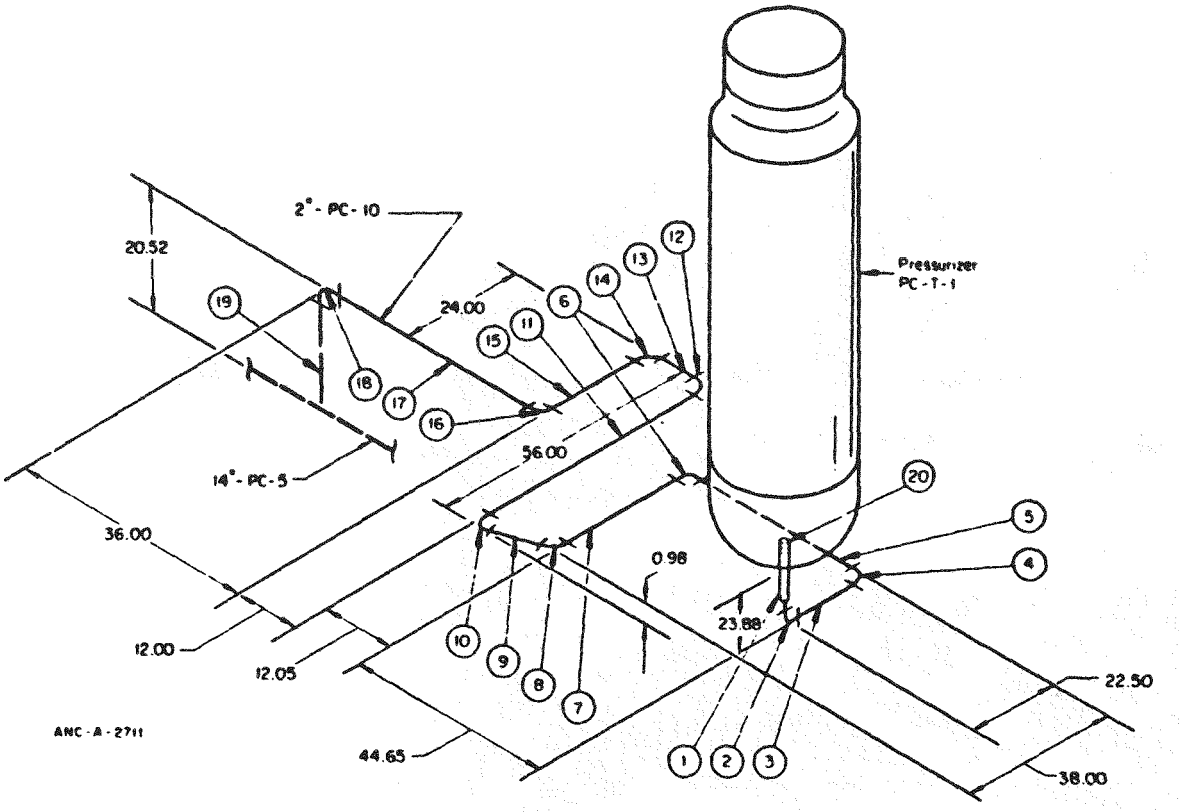

Figure AI.5 Pressurizer Surge Line Routing

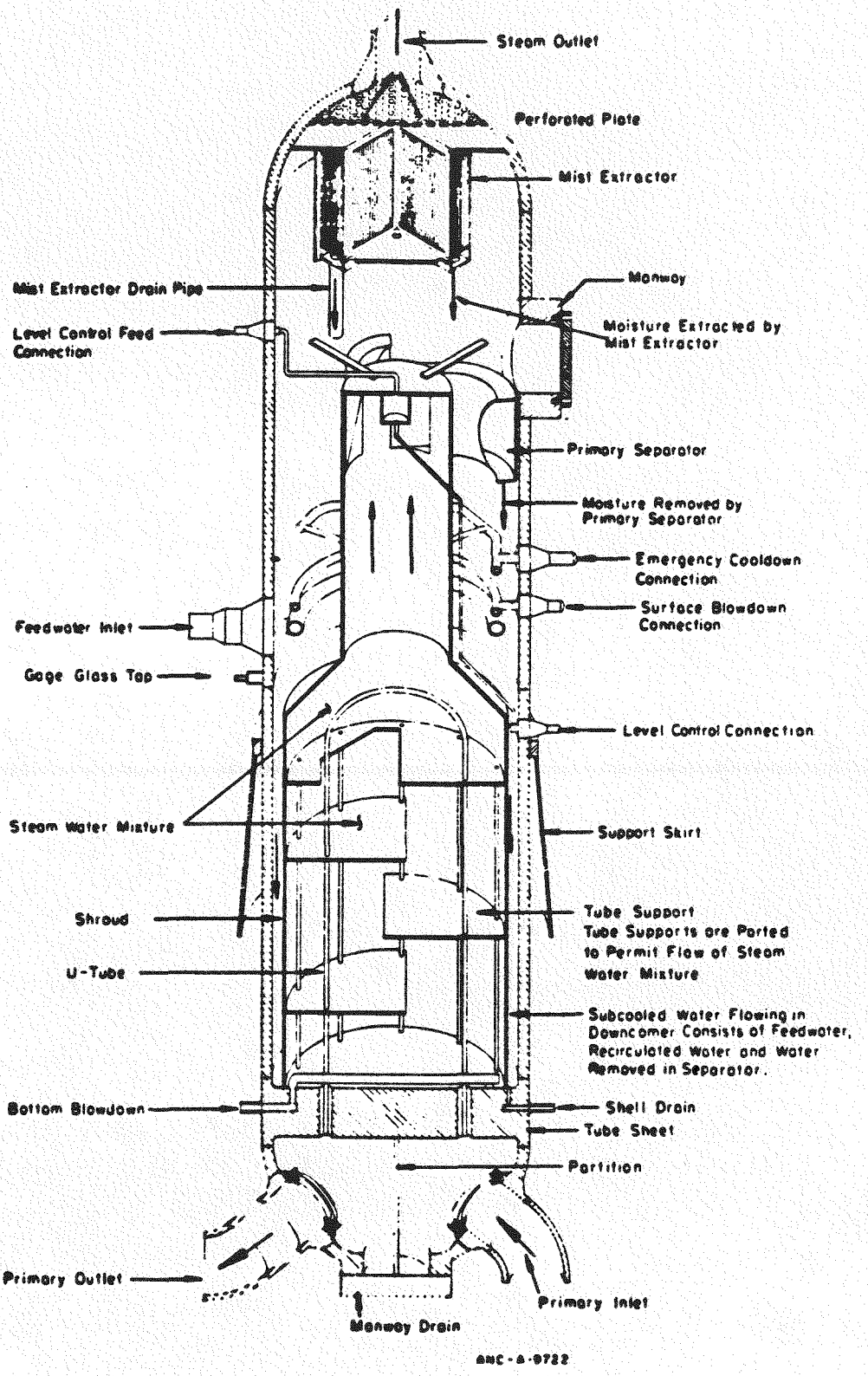

Figure AI.6 Steam Generator Schematic

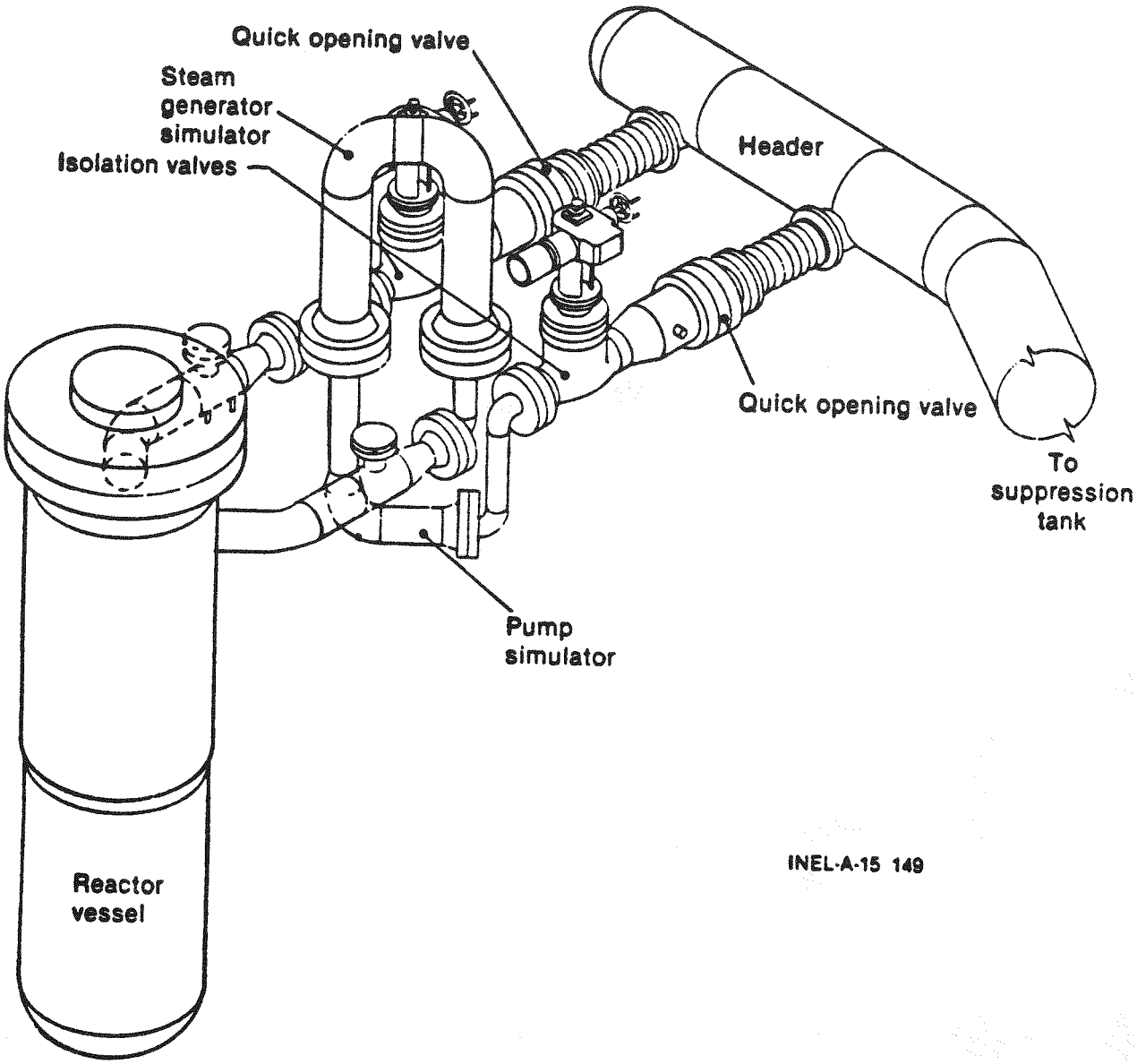

Figure AI.7 LOFT System -- Broken Loop

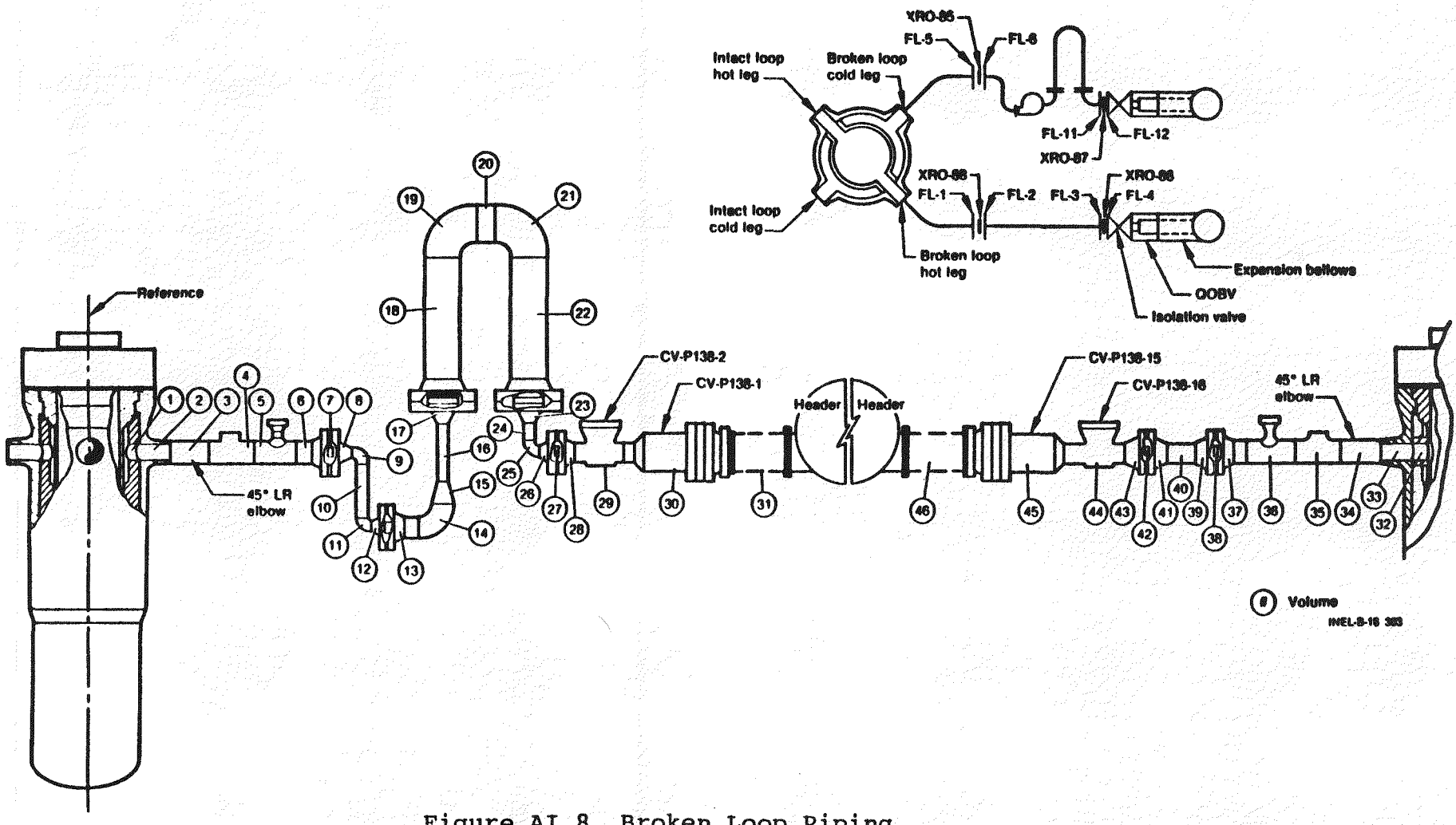

Figure AI.8 Broken Loop Piping

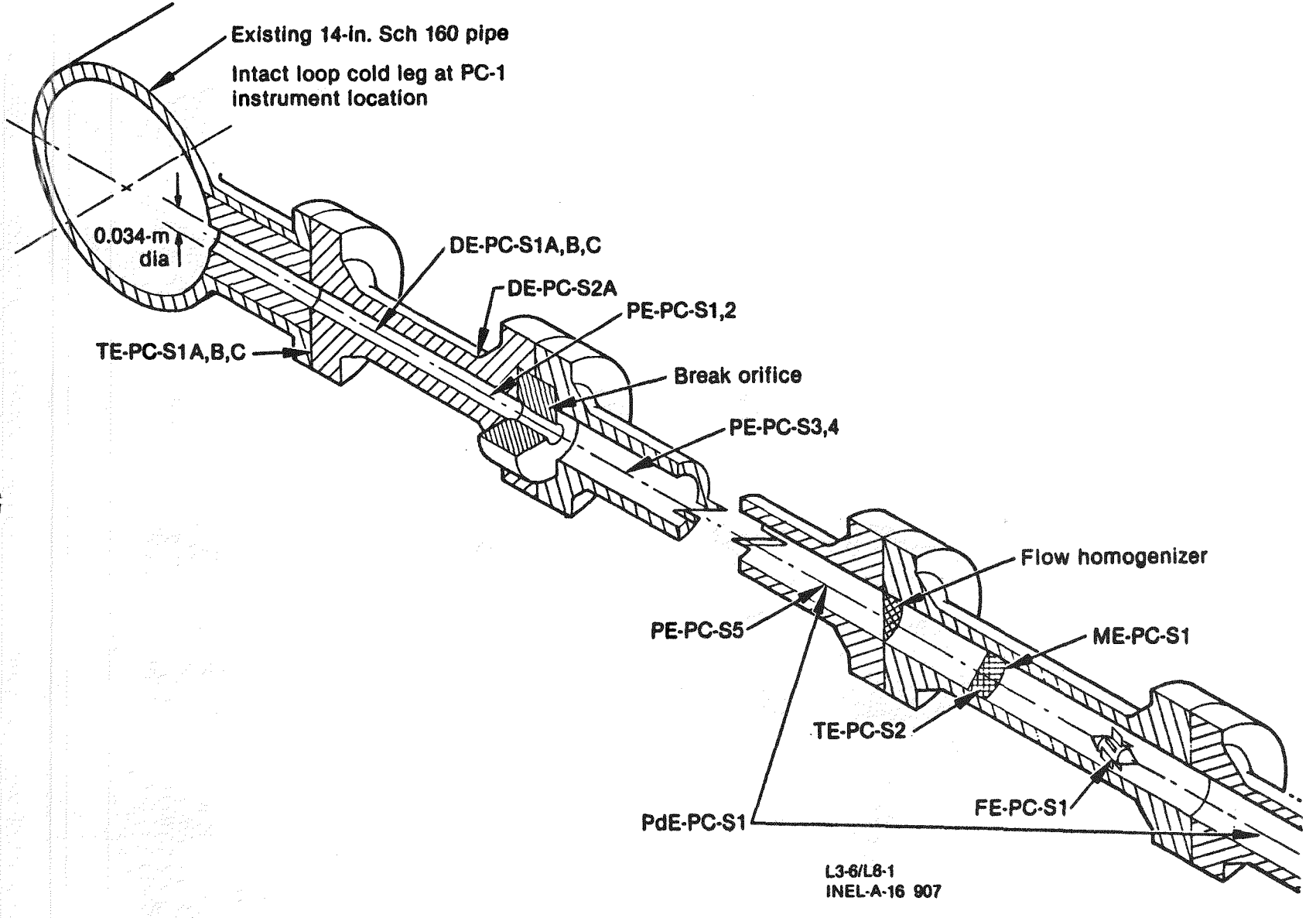

Figure AI.9 LOFT Spool Piece and Small Break Orifice Configuration

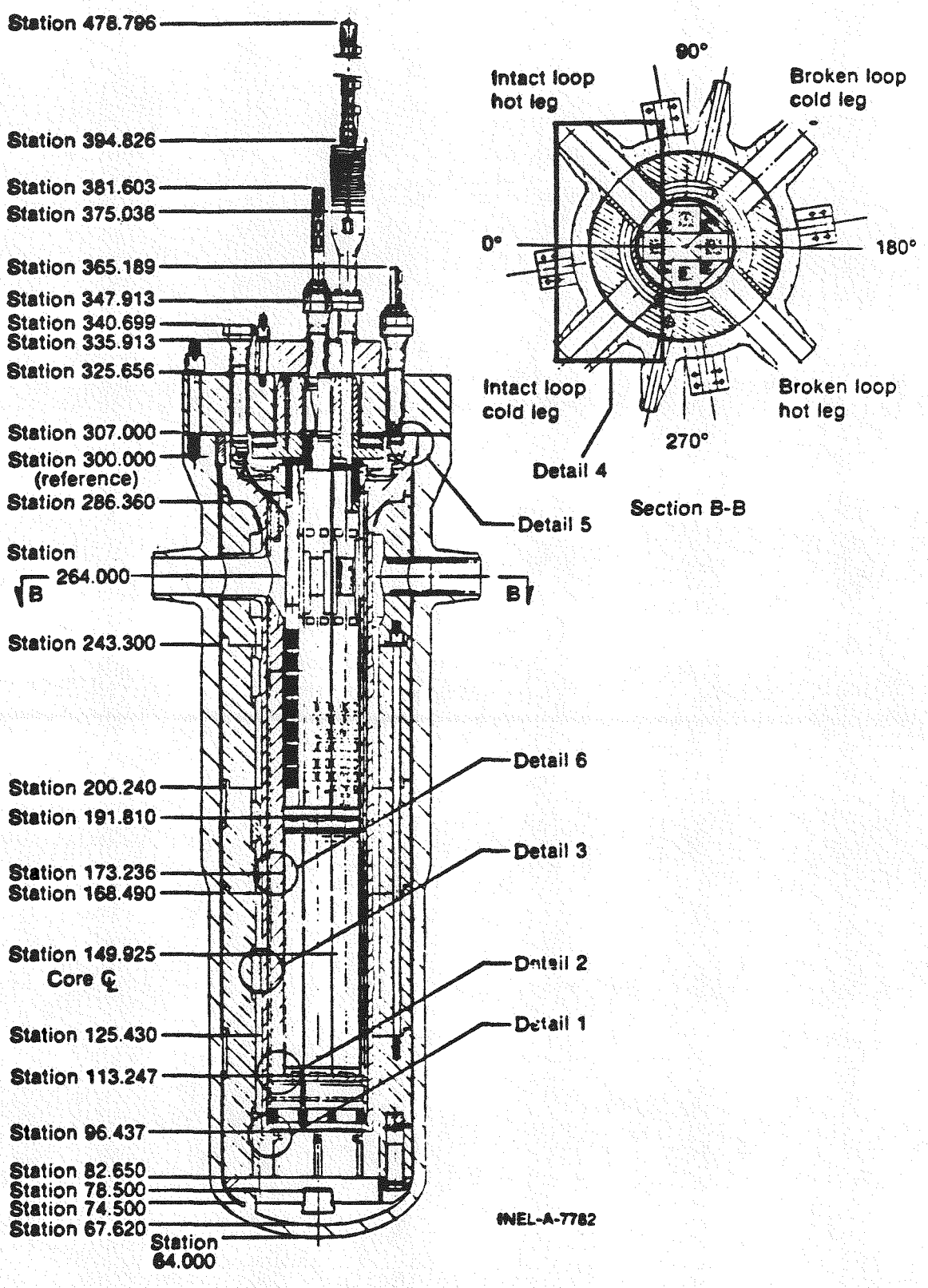

Figure AI.10 Reactor Vessel Showing Core Bypass Paths

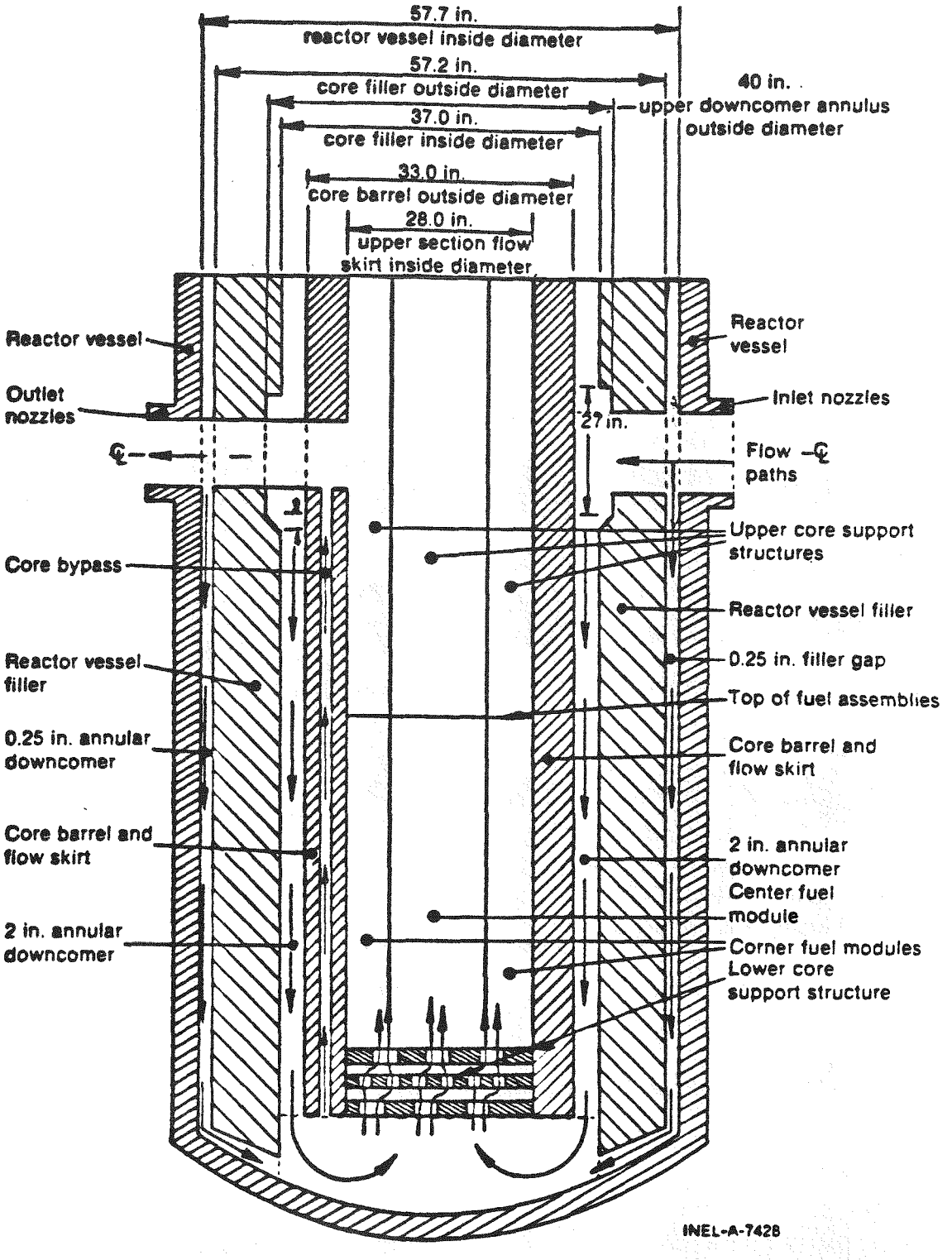

Figure AI.11 Reactor Vessel Schematic With Flow Paths

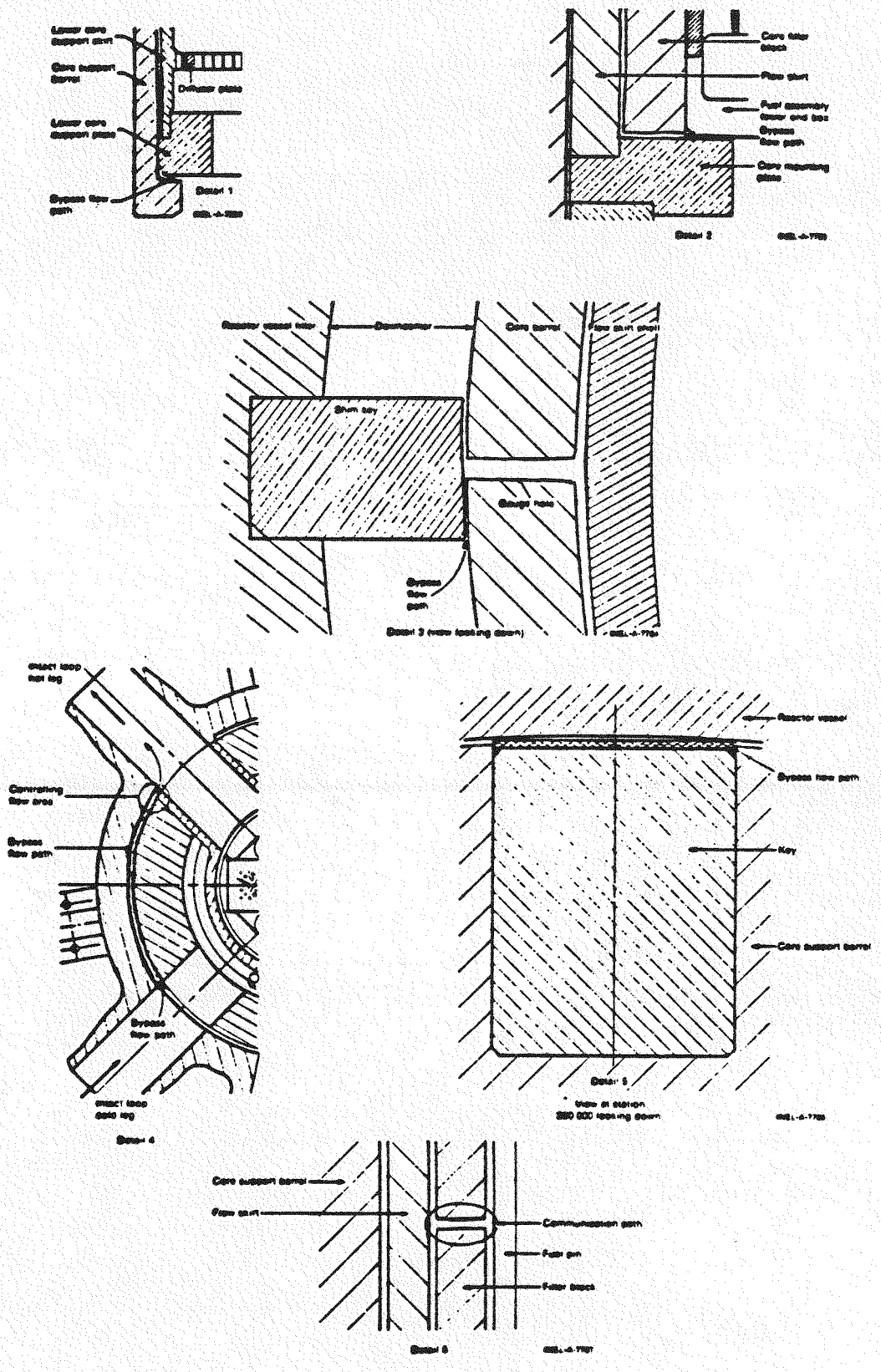

Figure AI.12 Core Bypass Details

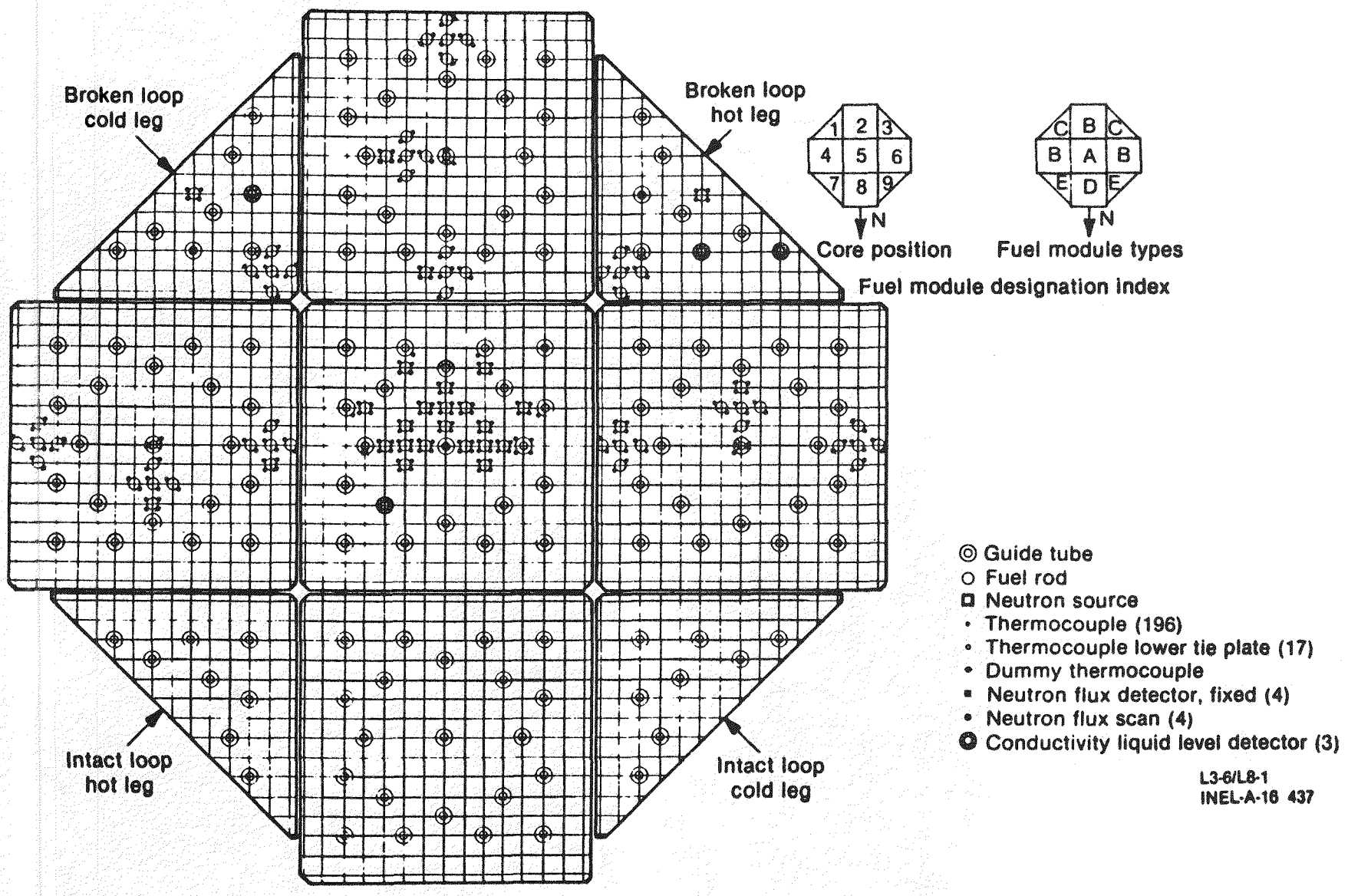

Figure AI.13 LOFT Core Configuration and Instrumentation

Table AI.1

LOFT VOLUME DISTRIBUTION [a]

Parameter	Value [m^3 (ft^3)]	
Reactor Vessel		
Downcomer region		
Vessel to filler gap	0.285	(10.05)
Distribution annulus		
Above bottom of nozzles	0.104	(3.67)
Below bottom of nozzles	0.068	(2.41)
Downcomer annulus	0.564	(19.91)
Lower plenum		
Below core support structure	0.564	(19.92)
Within lower core support	0.096	(3.39)
Above lower core support to active core	0.020	(0.71)
Core	0.293	(10.36)
Core bypass	0.053	(1.89)
Upper plenum	0.896	(31.63)
Reactor vessel total	2.943	(103.94)
Intact loop		
Hot leg from reactor vessel to steam generator inlet	0.384	(13.56)
Steam generator plenums and tubes	1.452	(51.27)
Pump suction piping	0.337	(11.89)
Pumps	0.198	(7.00)
Cold leg from pump outlet to reactor vessel	0.333	(11.75)
Pressurizer	0.928	(32.88)
Pressurizer surge line	0.012	(0.44)
Intact loop total	3.647	(128.79)

Table AI.1 (Continued)

Parameter	Value [m^3 (ft^3)]	
Broken loop		
From reactor vessel to centerline of joint A including hot leg side of reflood assist bypass system	0.332	(11.74)
From reactor vessel to centerline of joint C including cold leg side of reflood assist bypass system	0.358	(12.64)
Spool piece	0.023	(0.80)
Simulator section	0.617	(21.77)
From joint F to isolation valve	0.013	(0.47)
From joint B to isolation valve	0.014	(0.48)
Broken loop total	1.356	(47.90)
Total system liquid volume [b]	7.566	(267.20)
Total system volume [c]	7.896	(278.86)
Suppression system		
Tank (w/downcomers)	85.23	(3010)
Header	19.40	(685)
Downcomers inside tank (4)	2.61 (0.65 each)	92 (23 each)
Downcomers between tank and headers (4)	0.99 (0.24 each)	34.8 (8.7 each)
Accumulator A line volumes		
Accumulator A to cold leg	0.36	(12.8)
Accumulator A to lower plenum	0.37	(12.9)
Accumulator A to downcomer	0.56	(19.7)
Borated water storage tank	102.22	(3610)

[a] These volumes represent the best knowledge of the system at this time (September 1980).

[b] The system is defined as the intact loop piping and components, the reactor vessel, and the broken loop piping and components up to the break planes.

[c] Includes pressurizer gas volume of 0.33 m^3 (11.7 ft^3).

Table AI.2 Intact Loop Piping Geometry

Volume No.[a]	Description	Flow Length (m)		Elevation (Station)		Diameter (m)		Area (m^2)		Volume (m^3)
		Piece	Ref.[b] to Exit	Entry	Exit	Entry	Exit	Entry	Exit	
1a	Core barrel nozzle	0.351	0.736	264.00	264.00	0.292	0.292	0.0670	0.0670	0.0239
1b	Vessel nozzle	0.526	1.262	264.00	264.00	0.284	0.284	0.0634	0.0634	0.0336
2	14-in. Sch 160	1.322	2.584	264.00	264.00	0.284	0.284	0.0634	0.0634	0.0869
3	14-in. Sch 160 45° LR elbow	0.419	3.003	264.00	264.00	0.284	0.284	0.0634	0.0634	0.0266
4	14-in. Sch 160	0.719	3.722	264.00	264.00	0.284	0.284	0.0634	0.0634	0.0461
5	Venturi	0.965	4.688	264.00	264.00	0.284	0.290	0.0634	0.0659	0.0490
	Throat	—	—	—	—	0.206	—	0.0333	—	—
6	14-in. Sch 160 90° SR elbow	0.559	5.246	264.00	264.00	0.284	0.284	0.0634	0.0634	0.0354
7	14-in. Sch 160	0.195	5.441	264.00	264.00	0.284	0.284	0.0634	0.0634	0.0124
8	16 x 14-in. Sch 160 reducer	0.356	5.797	264.00	264.00	0.284	0.325	0.0634	0.0832	0.0260
9	16-in. Sch 160 38° elbow	0.270	6.066	264.00	267.39	0.325	0.325	0.0832	0.0832	0.0224
10	16-in. Sch 160	0.260	6.327	267.39	273.70	0.325	0.325	0.0832	0.0832	0.0217
11	SG[c] inlet plenum	0.630	6.956	273.70	293.89	0.325	0.439	0.0832	0.1512	0.3353
12	SG straight tube	2.135	9.091	293.89	377.93	0.439	0.439	0.1512	0.1512	0.3226
13	SG curved tube	0.899	9.990	377.93	377.93	0.439	0.439	0.1512	0.1512	0.1359
14	SG straight tube	2.135	12.125	377.93	293.89	0.439	0.439	0.1512	0.1512	0.3226
15	SG outlet plenum	0.630	12.754	293.89	273.70	0.439	0.325	0.1512	0.0832	0.3353
16	16-in. Sch 160 52° elbow	0.369	13.123	273.70	261.09	0.325	0.325	0.0832	0.0832	0.0307
17	16 x 14-in. Sch 160 reducer	0.356	13.479	261.09	247.09	0.325	0.284	0.0832	0.0634	0.0260
18	14-in. Sch 160	0.511	13.990	247.09	226.98	0.284	0.284	0.0634	0.0634	0.0332
19	14-in. Sch 160 90° SR elbow	0.559	14.548	226.98	212.98	0.284	0.284	0.0634	0.0634	0.0354
20	14-in. Sch 160	0.622	15.171	212.98	212.98	0.284	0.284	0.0634	0.0634	0.0401
21	14-in. Sch 160 tee Main run (pump 1)	0.439	15.609	212.98	212.98	0.284	0.284	0.0634	0.0634	0.0464
	Branch run (pump 2)	0.439	0.439	212.98	212.98	0.284	0.284	0.0634	0.0634	
22	14-in. Sch 160 90° SR elbow	0.559	16.168	212.98	226.98	0.284	0.284	0.0634	0.0634	0.0354

Table AI.2 (continued)

Volume No.[a]	Description	Flow Length (m)		Elevation (Station)		Diameter (m)		Area (m^2)		Volume (m^3)
		Piece	Ref.[b] to Exit	Entry	Exit	Entry	Exit	Entry	Exit	
23	14 x 10-in. Sch 160 reducer	0.330	16.498	226.98	239.98	0.284	0.216	0.0634	0.0366	0.0163
24	10-in. Sch 160	0.292	16.790	239.98	251.48	0.216	0.216	0.0366	0.0366	0.0107
25	Pump 1	0.457	17.247	251.48	264.00	0.216	0.216	0.0366	0.0366	0.0991
26	10-in. Sch 160	0.203	17.450	264.00	264.00	0.216	0.216	0.0366	0.0366	0.0074
27	10-in. Sch 160 45° LR elbow	0.299	17.750	264.00	264.00	0.216	0.216	0.0366	0.0366	0.0110
28	10-in. Sch 160	0.799	18.549	264.00	264.00	0.216	0.216	0.0366	0.0366	0.0292
29	10 x 14-in. Sch 160 reducer	0.330	18.879	264.00	264.00	0.216	0.284	0.0366	0.0634	0.0163
30	14-in. Sch 160 90° SR elbow	0.559	0.997	212.98	226.98	0.284	0.284	0.0634	0.0634	0.0354
31	14 x 10-in. Sch 160 reducer	0.330	1.328	226.98	239.98	0.284	0.216	0.0634	0.0366	0.0163
32	10-in. Sch 160	0.292	1.620	239.98	251.48	0.216	0.216	0.0366	0.0366	0.0107
33	Pump 2	0.457	2.077	251.48	264.00	0.216	0.216	0.0366	0.0366	0.0991
34	10-in. Sch 160 90° SR elbow	0.399	2.476	264.00	264.00	0.216	0.216	0.0366	0.0366	0.0146
35	14 x 10-in. Sch 160 tee									
	Main run (pump 1)	0.559	19.438	264.00	264.00	0.284	0.284	0.0634	0.0634	0.0408
	Branch run (pump 2)	0.424	2.900	264.00	264.00	0.216	0.284	0.0366	0.0634	
36	14-in. Sch 160	0.217	19.655	264.00	264.00	0.284	0.284	0.0634	0.0634	0.0138
37	14-in. Sch 160 90° SR elbow	0.559	20.213	264.00	264.00	0.284	0.284	0.0634	0.0634	0.0354
38	14-in. Sch 160	0.194	20.408	264.00	264.00	0.284	0.284	0.0634	0.0634	0.0123
39	14-in. Sch 160 45° LR elbow	0.419	20.827	264.00	264.00	0.284	0.284	0.0634	0.0634	0.0266
40	14-in. Sch 160	1.412	22.239	264.00	264.00	0.284	0.284	0.0634	0.0634	0.0917
41	Vessel nozzle	0.526	22.765	264.00	264.00	0.284	0.284	0.0634	0.0634	0.0336
42	Vessel filler	0.224	22.988	264.00	264.00	0.286	0.286	0.0641	0.0641	0.0143

a. The volume numbers correspond to the circled numbers in Figure AI.3.

b. Ref. - Reference at centerline of reactor vessel, see Figure AI.3.

c. SG - steam generator.

Table AI.3 Pressurizer Surge Line Component Identification

Location[a]	Description	Centerline Length [m (ft)]	Metal Weight [kg (lb)]	Cross-Section Flow Area [m^2 (ft^2)]	Fluid Volume [m^3 (ft^3)]	ID Surface Area [m^2 (ft^2)]	Equivalent[b] Length [m (ft)]	L/D
1	4-in. pressurizer stub	0.581 (1.9062)	0.835 (1.84)	0.006 (0.0167)	0.003 (0.1176)	0.157 (1.686)	0.581 (1.906)	6.6
2	2-in. Sch 160 LR EL[c]	0.120 (0.3932)	1.361 (3.0)	0.001 (0.0156)	0.0002 (0.0061)	0.016 (0.174)	0.858 (2.815)	20.0
3	2-in. Sch 160 pipe	0.419 (1.3750)	4.627 (10.2)	0.001 (0.0156)	0.001 (0.0214)	0.056 (0.608)	0.419 (1.375)	9.8
4	2-in. Sch 160 LR EL	0.120 (0.3932)	1.361 (3.0)	0.001 (0.0156)	0.0002 (0.0061)	0.016 (0.174)	0.858 (2.815)	20.0
5	2-in. Sch 160 pipe	0.982 (3.2214)	10.886 (24.0)	0.001 (0.0156)	0.001 (0.0503)	0.132 (1.425)	0.982 (3.221)	22.9
6	2-in. Sch 160 LR EL	0.120 (0.3932)	1.361 (3.0)	0.001 (0.0156)	0.0002 (0.0061)	0.016 (0.174)	0.858 (2.815)	20.0
7	2-in. Sch 160 pipe	0.838 (2.7500)	9.299 (20.5)	0.001 (0.0156)	0.001 (0.0382)	0.113 (1.215)	0.838 (2.750)	19.5
8	2-in. Sch 160 SR EL	0.080 (0.2617)	0.907 (2.0)	0.001 (0.0156)	0.0001 (0.0041)	0.011 (0.115)	1.287 (4.221)	30.0
9	2-in. Sch 160 pipe	0.204 (0.6706)	2.268 (5.0)	0.001 (0.0156)	0.0003 (0.0105)	0.027 (0.296)	0.205 (0.671)	4.8
10	2-in. Sch 160 SR EL	0.080 (0.2617)	0.907 (2.0)	0.001 (0.0156)	0.0001 (0.0041)	0.011 (0.115)	1.287 (4.221)	30.0
11	2-in. Sch 160 pipe	1.321 (4.333)	14.606 (32.2)	0.001 (0.0156)	0.0002 (0.0676)	0.178 (1.915)	1.321 (4.333)	30.8
12	2-in. Sch 160 SR EL	0.080 (0.2617)	0.907 (2.0)	0.001 (0.0156)	0.0001 (0.0041)	0.011 (0.115)	1.287 (4.221)	30.0
13	2-in. Sch 160 pipe	0.203 (0.6667)	2.268 (5.0)	0.001 (0.0156)	0.0003 (0.0104)	0.027 (0.295)	0.203 (0.667)	4.7
14	2-in. Sch 160 SR EL	0.080 (0.2617)	0.907 (2.0)	0.001 (0.0156)	0.0001 (0.0041)	0.011 (0.115)	1.287 (4.221)	30.0
15	2-in. Sch 160 pipe	0.483 (1.5833)	5.352 (11.8)	0.001 (0.0156)	0.001 (0.0247)	0.065 (0.700)	0.483 (1.584)	11.2
16	2-in. Sch 160 LR EL	0.0120 (0.3932)	1.361 (3.0)	0.001 (0.0156)	0.0002 (0.0061)	0.016 (0.174)	0.858 (2.815)	20.0
17	2-in. Sch 160 pipe	0.762 (2.5000)	8.437 (18.6)	0.001 (0.0156)	0.001 (0.039)	0.103 (1.104)	0.762 (2.500)	17.8
18	2-in. Sch 160 LR EL	0.120 (0.3932)	1.361 (3.0)	0.001 (0.0156)	0.0002 (0.0061)	0.016 (0.174)	0.858 (2.815)	20.0
19	2-in. Sch 160 pipe	0.303 (0.9935)	3.357 (7.4)	0.001 (0.0156)	0.0004 (0.0155)	0.041 (0.439)	0.303 (0.994)	7.1
20	Screen	----- -----	----- -----	----- -----	------ ------	----- -----	----- -----	24.7

[a] Location numbers correspond to circled numbers on Figure AI.5.

[b] Equivalent length is the length of pipe that will give the same pressure drop as the piping section described.

[c] EL - elbow.

Table AI.4 Steam Generator Design Parameters

Parameter	Value
Tubes	
Minimum length including tube sheet	4.27 m (14.0 ft)
Maximum length including tube sheet	6.19 m (20.3 ft)
Average length including tube sheet	5.17 m (16.95 ft)
External surface area of tubes less tube sheet	335 m^2 (3610 ft^2)
Surface area of tubes inside tube sheet	43 m^2 (463 ft^2)
Internal cross-sectional area of tubes	82 mm^2 (0.127 $in.^2$)
Outside diameter of tubes	12.7 mm (0.50 in.)
Average wall thickness	1.24 mm (0.049 in.)
Number of tubes	1845
Thickness of tube sheet	0.292 m (11.5 in.)
Tube arrangement	Equilateral triangular pitch on 19-mm (0.75-in.) centers
Material	Inconel-600
Maximum height from bottom of tube sheet	2.73 m (107.5 in.)
Minimum height from bottom of tube sheet	2.15 m (84.5 in.)
Tube bundle diameter	1.22 m (48 in.)
Internal volume of tubes including tube sheet	0.781 m^3 (27.6 ft^3)
Internal volume of tubes inside tube sheet	0.088 m^3 (3.12 ft^3)
Primary plenums	
Inlet plenum volume	0.223 m^3 (7.887 ft^3)
Outlet plenum volume	0.223 m^3 (7.887 ft^3)
Secondary side	
Secondary shell volume	6.654 m^3 (235 ft^3)
Secondary shell material	Carbon steel MIL-QQ-S691a, Grade C
Normal operating pressure	15.51 MPa (2250 psig)

Table AI.5 Steam Generator Data

STEAM GENERATOR INFORMATION

NUMBER OF TUBES	1845
TUBE INSIDE DIAMETER	0.402 IN.
TUBE OUTSIDE DIAMETER	0.500 IN.
AVERAGE TUBE LENGTH INCLUDING TUBE SHEET	16.957 FT
TUBE SHEET THICKNESS	11.5 IN.
DOWNCOMER OUTSIDE DIAMETER	56.00 IN.
DOWNCOMER INSIDE DIAMETER	51.75 IN.
SHROUD INSIDE DIAMETER	50.75 IN.
BAFFLES	
NUMBER	4
SPACING	17.375 IN.
AREA OF 3 LOWER BAFFLES	4.867 SQ FT
AREA OF TOP BAFFLES	4.314 SQ FT
COOLANT MASS	
50 MW OPERATION	4130 LBM
37 MW OPERATION	4505 LBM

STEAM GENERATOR ELEVATIONS ABOVE TUBE SHEET

	ELEVATION* INCHES
TUBE BEND LINE	72.50
LOW TUBE SPILLOVER	73.00
BOTTOM OF FRUSTRUM	88.125
HIGH TUBE SPILLOVER	96.00
TOP OF FRUSTRUM	101.22
NORMAL WATER LEVEL	126.00 **
BOTTOM OF SEPARATOR	144.63
TOP OF RISER	161.75

* TUBE SHEET TOP IS 41.39 INCHES ABOVE THE COLD LEG CENTERLINE

** OPERATING LEVEL IS 116 + 1 INCH FOR EVERY 10% POWER

Table AI.6 Broken Loop Piping Geometry

Volume No.[a]	Description	Flow Length (m)		Elevation (Station)		Diameter (m)		Area (m^2)		Volume (m^3)
		Piece	Ref.[b] to Exit	Entry	Exit	Entry	Exit	Entry	Exit	
1	Vessel filler	0.224	0.736	264.00	264.00	0.286	0.286	0.0641	0.0641	0.0143
2	Vessel nozzle	0.526	1.262	264.00	264.00	0.284	0.284	0.0634	0.0634	0.0336
3	14-in. Sch 160 45° LR elbow	0.419	1.681	264.00	264.00	0.284	0.284	0.0634	0.0634	0.0266
4	14 x 14 x 10-in. Sch 160 tee	0.559	2.240	264.00	264.00	0.284	0.284	0.0634	0.0634	0.0403
	10-in. branch	—	—	—	—	—	0.216	—	0.0366	—
5	14-in. Sch 160	0.695	2.935	264.00	264.00	0.284	0.284	0.0634	0.0634	0.0449
6	Flange	0.450	3.385	264.00	264.00	0.284	0.103	0.0634	0.0084	0.0050
7	Orifice plate	0.076	3.461	264.00	264.00	0.103	0.103	0.0084	0.0084	0.0006
8	Flange	0.168	3.629	264.00	264.00	0.103	0.103	0.0084	0.0084	0.0014
9	5-in. Sch XX 90° LR elbow	0.299	3.928	264.00	256.50	0.103	0.103	0.0084	0.0084	0.0025
10	6-in. Sch 160	0.832	4.760	256.50	223.75	0.132	0.132	0.0136	0.0136	0.0114
11	5-in. Sch XX 90° LR elbow	0.299	5.059	223.75	216.25	0.103	0.103	0.0084	0.0084	0.0025
12	Flange	0.168	5.228	216.25	216.25	0.103	0.103	0.0084	0.0084	0.0014
13	Pump simulator	0.473	5.701	216.25	216.25	0.103	0.287	0.0084	0.0645	0.0102
	Orifice plate	—	—	—	—	—	0.008	—	0.0101	—
	Support plate	—	—	—	—	—	0.152	—	—	—
14	14-in. Sch 160 90° SR elbow	0.559	6.259	216.25	230.25	0.284	0.284	0.0634	0.0634	0.0354
15	14 x 5-in. Sch 160 reducer	0.330	6.590	230.25	243.25	0.284	0.110	0.0634	0.0094	0.0107
16	5-in. Sch 160	0.937	7.526	243.25	280.12	0.110	0.110	0.0094	0.0094	0.0088
17	Flange	0.206	7.732	280.12	288.24	0.103	0.103	0.0084	0.0084	0.0008
18	SG simulator	2.051	9.784	288.24	369.00	0.103	0.371	0.0084	0.1079	0.1725
	Support plate	—	—	—	—	—	0.119	—	0.0112	—
	Orifice plate	—	—	—	—	—	0.124	—	0.0326	—
19	18-in. Sch 160 90° SR elbow	0.718	10.502	369.00	387.00	0.367	0.367	0.1056	0.1056	0.0759
20	18-in. Sch 160	0.263	10.765	387.00	387.00	0.367	0.367	0.1056	0.1056	0.0278
21	18-in. Sch 160 90° SR elbow	0.718	11.483	387.00	369.00	0.367	0.367	0.1056	0.1056	0.0759
22	SG simulator	2.051	13.535	369.00	288.24	0.371	0.103	0.1079	0.0084	0.1725
	Support plate	—	—	—	—	0.119	—	0.0112	—	—
	Orifice plate	—	—	—	—	—	0.123	—	0.0326	—
23	Flange	0.206	13.741	288.24	280.12	0.103	0.103	0.0084	0.0084	0.0008

Table AI.6 (continued)

Volume No.[a]	Description	Flow Length (m) Piece	Flow Length (m) Ref.[b] to Exit	Elevation (Station) Entry	Elevation (Station) Exit	Diameter (m) Entry	Diameter (m) Exit	Area (m^2) Entry	Area (m^2) Exit	Volume (m^3)
24	5-in. Sch XX	0.282	14.023	280.12	269.00	0.103	0.103	0.0084	0.0084	0.0024
25	5-in. oversize 90° elbow	0.199	14.223	269.00	264.00	0.103	0.103	0.0084	0.0084	0.0017
26	Flange	0.168	14.391	264.00	264.00	0.103	0.103	0.0084	0.0084	0.0014
27	Orifice	0.076	14.467	264.00	264.00	0.077	0.114	0.0046	0.0108	0.0005
28	Flange	0.244	14.712	264.00	264.00	0.257	0.257	0.0520	0.0520	0.0127
29	Isolation valve	0.762	15.474	264.00	264.00	0.257	0.257	0.0519	0.0519	0.0838
30	QOBV[c]	1.651	17.125	264.00	264.00	0.257	0.273	0.0520	0.0520	0.1050
31	Expansion joint	0.991	18.115	264.00	264.00	0.273	0.298	0.0586	0.0700	0.0972
32	Core barrel nozzle	0.351	0.736	264.00	264.00	0.292	0.292	0.0670	0.0670	0.0239
33	Vessel nozzle	0.526	1.262	264.00	264.00	0.284	0.284	0.0634	0.0634	0.0336
34	14-in. Sch 160 45° LR elbow	0.419	1.681	264.00	264.00	0.284	0.284	0.0634	0.0634	0.0266
35	14 x 14 x 10-in. Sch 160 tee	0.559	2.240	264.00	264.00	0.284	0.284	0.0634	0.0634	0.0403
	Branch	—	—	—	—	—	0.216	—	0.0366	—
36	14-in. Sch 160	0.695	2.935	264.00	264.00	0.284	0.284	0.0634	0.0634	0.0449
37	Flange	0.450	3.385	264.00	264.00	0.284	0.110	0.0634	0.0309	0.0054
38	Orifice plate	0.076	3.461	264.00	264.00	0.114	0.077	0.0102	0.0046	0.0005
39	Flange	0.206	3.667	264.00	264.00	0.173	0.173	0.0235	0.0235	0.0049
40	8-in. Sch 160	0.494	4.161	264.00	264.00	0.173	0.173	0.0235	0.0235	0.0116
41	Flange	0.206	4.368	264.00	264.00	0.173	0.173	0.0235	0.0235	0.0049
42	Orifice plate	0.076	4.444	264.00	264.00	0.173	0.173	0.0235	0.0235	0.0018
43	Flange	0.244	4.688	264.00	264.00	0.257	0.257	0.0520	0.0520	0.0127
44	Isolation valve	0.762	5.450	264.00	264.00	0.257	0.257	0.0519	0.0519	0.0838
45	QOBV	1.651	7.101	264.00	264.00	0.257	0.273	0.0520	0.0520	0.1050
46	Expansion joint	0.991	8.092	264.00	264.00	0.273	0.298	0.0586	0.0700	0.0972

a. The volume numbers correspond to the circled numbers in Figure AI.8

b. Ref. - Reference at centerline of reactor vessel, see Figure AI.8

c. QOBV - quick-opening blowdown valve.

Table AI.7

LOFT REACTOR VESSEL VOLUME DISTRIBUTION [a]

Parameter	Value [m^3 (ft^3)]	
Downcomer region		
Vessel to filler gap	0.285	(10.05)
Distribution annulus		
Above bottom of nozzles	0.104	(3.67)
Below bottom of nozzles	0.068	(2.41)
Downcomer annulus lower plenum	0.564	(19.91)
Below core support structure	0.564	(19.92)
Within lower core support	0.096	(3.39)
Above lower core support to active core	0.020	(0.71)
Core	0.293	(10.36)
Core bypass	0.053	(1.89)
Upper plenum	0.896	(31.63)
Total	2.943	(103.94)

[a] These volumes represent the best knowledge of the system at this time (September 1980).

Table AI.8

REACTOR VESSEL MATERIAL

Component	Estimate Weight [kg (lb)]	Material
Reactor vessel closure heads		
Instrumentation head	11 000 (24,000)	ASME SA 336, modified to Code Case 1332-1, clad with Type 308L SS
Closure plate	2300 (5000)	ASME SB 166 (Inconel-600)
Pressure vessel	34 000 (75,000)	ASME SA 336, modified to Code Case 1332-1, clad with Type 308L SS
Core support barrel	10 000 (22,200)	Type 304L SS
Upper core support plate	800 (1800)	Type 304 SS
Upper reactor vessel filler	6600 (14,600)	Type 304L SS
Lower reactor vessel filler	25 000 (55,200)	Type 304L SS
Flow skirt	640 (1400)	Type 304L SS
Lower core support structure	550 (1200)	Type 304L SS
Upper core support structure	2100 (4706)	Type 304L SS
Fuel assembly end boxes	200 (430)	Type 304L SS
Fuel pins (cladding only)	155 (340)	Zr-4
Fuel pellets	1470 (3240)	UO_2

Table AI.9

DIMENSIONAL DATA--REACTOR VESSEL

Elevation Points	Station [a]	Height Above Reactor Vessel Bottom [m (in.)]
Bottom (inside) of reactor vessel	67.80	0.00 (0.0) [b]
Bottom of downcomer annulus	96.44	0.727 (28.64)
Top of lower core support structure	113.25	1.154 (45.45)
Top of lower grid plate	116.24	1.230 (48.44)
Bottom of uninstrumented fuel	116.93	1.248 (49.13)
Bottom of instrumented fuel pins	117.24	1.256 (49.44)
Bottom of spacer grid 1	117.74	1.268 (49.94)
Bottom of instrumented fuel	117.93	1.273 (50.13)
Bottom of spacer grid 2	134.34	1.690 (66.54)
Bottom of spacer grid 3	150.94	2.112 (83.14)
Bottom of spacer grid 4	167.44	2.531 (99.64)
Top of uninstrumented fuel	182.93	2.924 (115.13)
Top of instrumented fuel	183.93	2.950 (116.13)
Bottom of spacer grid 5	184.04	2.953 (116.24)
Top of uninstrumented fuel pins	186.62	3.018 (118.82)
Bottom of upper grid plate	187.62	3.043 (119.82)
Top of fuel module	191.82	3.150 (124.02)
Top of downcomer annulus	247.33	4.560 (179.53)
Vessel nozzle centerline	264.00	4.983 (196.20)
Top of distributor annulus	277.05	5.315 (209.25)
Internals support ledge in vessel	300.00 [b]	5.898 (232.20)
Inside surface of vessel flange	307.0	6.076 (239.20)

[a] The station numbers shown in this table are elevations in inches, with reference station 300.0 at the internals support ledge of the pressure vessel.

[b] Reference point.

Table AI.10

CORE BYPASS CHANNELS

Core Bypass Path[a]	Controlling Flow Area [mm^2 ($in.^2$)]	Equivalent Diameter [mm (in.)]
1	874 (1.356)	3.13 (0.123)
2	3703 (5.740)	3.48 (0.137)
3	65 (0.100)	0.64 (0.025)
4	309 (0.479)	0.30 (0.012)
5	286 (0.443)	2.76 (0.109)
6	4162 (6.452)	3.91 (0.154)

[a] Numbers correspond to "Detail" numbers on Figure A.IO.

CORE BYPASS

PATH*	% LOOP FLOW
1	1.31 - 1.34
2	1.02 - 1.04
3	0.96 - 1.01
** 4	4.38 - 6.58
** 5	0.04
6	0.27 - 0.28
**RABV	1.42 - 1.43
	9.40 - 11.72
	10.56 ± 1.16

* NUMBERS REFER TO DETAILS ON FIGURE AI.10

** STEAM VENTING PATHS

APPENDIX II

INPUT LISTING

An input listing for the L3-6/L8-1 transient calculation run is given on attached microfiche.

DISTRIBUTION:

U. S. NRC Distribution Contractor (CDSI) (360)
7300 Pearl Street
Bethesda, MD 20014
360 copies for R4

List available from Author (8)

8214 M. A. Pound
9400 A. W. Snyder
9410 D. J. McCloskey
9412 J. W. Hickman
9420 J. V. Walker
9421 R. L. Coats
9422 D. A. Powers
9423 P. S. Pickard
9424 M. J. Clauser
9425 W. J. Camp
9440 D. A. Dahlgren
9441 M. Berman
9441 J. C. Cummings
9441 R. K. Cole, Jr.
9442 W. A. von Riesemann
9443 D. D. Carlson
9444 S. L. Thompson
9444 L. D. Buxton
9444 R. K. Byers
9444 D. Dobranich
9444 M. G. Elrick
9444 L. N. Kmetyk
9444 R. Knight
9444 K. McFadden
9444 J. M. McGlaun
9444 J. Orman
9444 G. C. Padilla
9444 A. C. Peterson
9444 W. R. Schmidt
9444 R. M. Summers
9444 G. G. Weigand
9444 C. C. Wong
3141 L. J. Erickson (5)
3151 W. L. Garner (3)

NRC FORM 335 (11-81) U.S. NUCLEAR REGULATORY COMMISSION

BIBLIOGRAPHIC DATA SHEET

1. REPORT NUMBER *(Assigned by DDC)*
NUREG/CR-3163
SAND83-0245

4. TITLE AND SUBTITLE *(Add Volume No., if appropriate)*
RELAP5 ASSESSMENT: LOFT SMALL BREAK L3-6/L8-1

2. *(Leave blank)*

3. RECIPIENT'S ACCESSION NO.

7. AUTHOR(S)
L. N. Kmetyk

5. DATE REPORT COMPLETED
MONTH: February YEAR: 1983

9. PERFORMING ORGANIZATION NAME AND MAILING ADDRESS *(Include Zip Code)*
Organization 9444
Sandia National Laboratories
P. O. Box 5800
Albuquerque, NM 87185

DATE REPORT ISSUED
MONTH: March YEAR: 1983

6. *(Leave blank)*

8. *(Leave blank)*

12. SPONSORING ORGANIZATION NAME AND MAILING ADDRESS *(Include Zip Code)*
U. S. Nuclear Regulatory Commission
Office of Nuclear Regulatory Research
Analytical Models Branch
Division of Accident Evaluation
Washington, DC 20555

10. PROJECT/TASK/WORK UNIT NO.

11. FIN NO.
A-1205

13. TYPE OF REPORT
Technical

PERIOD COVERED *(Inclusive dates)*

15. SUPPLEMENTARY NOTES

14. *(Leave blank)*

16. ABSTRACT *(200 words or less)*

The RELAP5 independent assessment project at Sandia National Laboratories is part of an overall effort funded by the NRC to determine the ability of various systems codes to predict the detailed thermal/ hydraulic response of LWR's during accident and off-normal conditions. The RELAP5 code is being assessed at SNLA against test data from various integral and separate effects test facilities. As part of this assessment matrix, a small break transient and subsequent partial core uncovery transient performed at the LOFT facility have been analyzed.

The results show that RELAP5 does very well on predicting the qualitative behavior for this small break experiment, although there are a number of quantitative disagreements. The primary mass inventory and core clad response during the first transient are in excellent agreement with data; however, the calculated break flow is ~25% high at early times and the overall primary side depressurization is ~18% overestimated. (The primary depressurization rate is very sensistive to small errors in break flow, environmental heat loss and steam generator heat transfer.) The steam generator response during reverse heat transfer is not predicted accurately. After delayed pump trip, the core does experience a sustained dryout, but the predicted peak clad temperature (561 K) is lower than was observed experimentally (637 K) in the second transient, largely because the decay power then is ~20% low compared to data and because of premature core quench, but also because pump coastdown is significantly slower than was measured. A subsequent rapid core quench is observed after substantial ECC injection. Some difficulties were encountered in obtaining a good steady state which matched all the experimental initial conditions, and the transient calculations were very slow-running, precluding any sensitivity studies on the results obtained.

17. KEY WORDS AND DOCUMENT AN

17b. IDENTIFIERS/OPEN-ENDED TERMS

18. AVAILABILITY STATEMENT

19. SECURITY CLASS *(This report)*: Uncl

21. NO. OF PAGES: 88

20. SECURITY CLASS *(This page)*: Uncl

22. PRICE: S

NRC FORM 335 (11-81)

☆U.S. GOVERNMENT PRINTING OFFICE: 1983-0-676-027/541